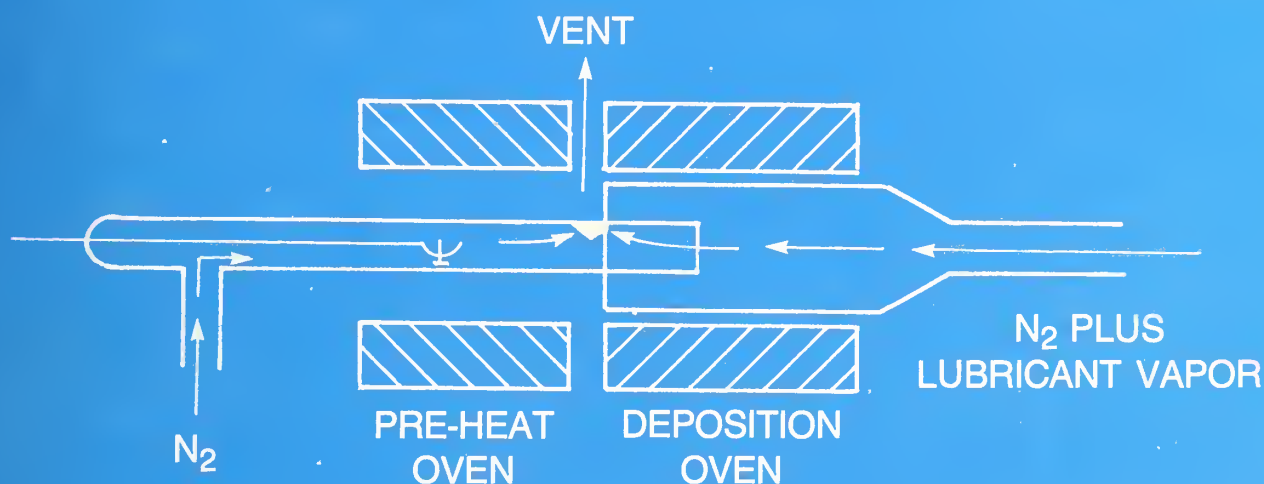U.S. DEPARTMENT OF COMMERCE
National Institute of Standards and Technology
(formerly National Bureau of Standards)

NIST Special Publication 744

Formation of Lubricating Films at Elevated Temperatures From the Gas Phase

E. E. Klaus, J. L. Duda, and S. K. Naidu

NIST Special Publication 744

Formation of Lubricating Films at Elevated Temperatures From the Gas Phase

E. E. Klaus, J. L. Duda, and S. K. Naidu

Department of Chemical Engineering
The Pennsylvania State University
University Park, PA 16802

R. G. Munro and S. M. Hsu, Editors and Project Leaders

National Institute of Standards and Technology
(formerly National Bureau of Standards)
Gaithersburg, MD 20899

NOTE: As of 23 August 1988, the National Bureau of Standards (NBS) became the National Institute of Standards and Technology (NIST) when President Reagan signed into law the Omnibus Trade and Competitiveness Act.

September 1988

CONTENTS

PREFACE

The U.S. government and industrial enterprises pay a high cost, on the order of $100 billion annually, as a result of losses to friction and wear. These losses are incurred in many forms including energy expended by friction, direct and indirect losses due to discarded materials, and lost productivity. Efforts to understand and reduce these losses require an interdisciplinary research effort involving chemistry, physics, materials science, mechanical engineering, and a wide range of chemical and materials property characterization capabilities. These capabilities are blended in the rapidly evolving field of tribology, the science of friction and wear and the control of those phenomena through lubrication.

In 1980, the U.S. Department of Energy (DOE) began a new program, the Energy Conversion and Utilization Technologies (ECUT) program, that included tribology as one of its principal activities. The ECUT program as a whole was designed to improve the rate at which technological advances made in basic research are transferred to industry or other end-use applications. In developing this new program, DOE had perceived that there was a significant conceptual barrier between basic science and its end-use applications. Basic science is exploratory and often deals with highly constrained systems. Its objective is to understand fundamental principles. End-use applications, in contrast, are devoted to specific products and have economic gain as their primary objective. The emphasis on different objectives caused communications between the two activities to be cumbersome and slow. The ECUT program was established to reduce this barrier by providing an interface between the two objectives in the form of a new concept of "directed basic research." Within this concept, developments in basic science would be utilized and supplemented by additional research, conducted selectively, with the objective of developing the new technology into a form that could be readily adapted to specific industries.

Within the context of directed basic research, the ECUT Tribology program was established to address the critical research issues relating to reducing the enormous energy and economic losses promulgated by friction and wear processes. The initial guidance for the program was provided by two studies, conducted by the American Society of Mechanical Engineers, entitled "Strategy for Energy Conservation through Tribology" and published in two parts (1977 and 1981). These works were followed by several DOE-sponsored studies that investigated and analyzed the specific tribological losses in 11 different industries. It was estimated that about three quadrillion BTU's of energy could be saved within these industries with modest, feasible reductions in friction and wear. Most of those reducible losses were concentrated in the transportation industry and focused on engine technology. In that area, it was quickly found that the dominant critical issue was lubrication.

Lubricants serve several purposes in engines. By forming a medium between moving surfaces, such as between piston rings and cylinder liners, friction between the moving parts can be reduced and efficiency enhanced. The lubricating film also reduces the damage to the surfaces and thus enhances the durability and wear life of the components. Further, a liquid lubricant can remove wear debris from the tribocontact and thereby prevent or reduce the three-body type of abrasion on the surfaces. All of these functions are important to the successful operation of engines.

Advances in engine technology are mostly directed towards a more efficient use of the energy developed in the engine cycle. A prime target for improving efficiency is the reduction of the energy loss that occurs by way of thermal diffusion to the engine coolants and other engine parts. Approximately one-third of the energy released in combustion is lost in this manner. Designs for low heat rejection engines that would reduce this energy loss, therefore, could achieve significant gains in efficiency.

As with conventional engines, a critical issue for these new engine designs is lubrication. By losing less energy through diffusion, the low heat rejection engines must operate at higher temperatures than occur in conventional engines. Temperatures in the range 300°C to 600°C are expected in the near-term designs, and in the more distant future temperatures as high as 1200°C are envisioned. Such temperatures are beyond the useful range of conventional lubricants. Indeed, conventional lubricants have upper operating limits of only about 250°C. Consequently, the technology base for lubrication must be expanded dramatically if the advantages of the new engine designs are to be realized in practice. The ECUT Tribology program is addressing this challenge on several fronts. It is clear that the small incremental refinements of lubricants traditionally produced by the trial-and-error approach will not be adequate for developing the new generation of high temperature lubricants. Thus, the ECUT Tribology program is conducting fundamental studies of lubricating mechanisms, particularly as they apply to the high temperatures of low heat rejection engines. New measurement capabilities and methodologies are being developed to enable laboratory studies of mechanisms to be conducted and to provide a means for testing and screening potential high temperature basestocks and additives. Data acquired from these efforts are being used to gain insights into the role of tribochemical interactions that occur between lubricants and substrates. These data are also forming the basis for assessing the progress made towards achieving high temperature lubricants.

New concepts in lubrication and lubricant delivery systems are also being investigated. The following report discusses one of the more exciting alternatives to using liquid or solid lubricants: gas phase lubrication. This new approach is being explored, in part, under ECUT sponsorship via an NBS subcontract to Pennsylvania State University. This report represents the results of the first phase of that research effort. The accomplishments to date are very encouraging and currently are being extended in a joint PSU-NBS study of gas phase lubrication of advanced structural ceramics at high temperatures.

R. G. Munro
S. M. Hsu
DOE/ECUT Project Leaders
NBS Contract Officers

EXECUTIVE SUMMARY

Conventional liquid lubricants, when subjected to temperatures of 250°C and above for extended time in an air atmosphere, degrade rapidly to make large amounts of solid sludge and deposits. Based on boundary lubrication of bearings, these same lubricants, when subjected to temperatures from 250°C to the melting point of the bearing metal, produce in the micro- to milli-second residence time in the bearing contact enough "friction polymer" to result in good lubrication. This report describes the use of these conventional liquid lubricants delivered in a homogeneous vapor phase where the carrier gas is nitrogen, air, or mixtures of these two gases. The lubricants studied include alkyl and aryl phosphate esters, organic acid esters, polyphenyl ethers, and mineral oil.

A static deposition test was conducted in a tubular ceramic oven where the lubricant-containing carrier gas contacted the metal substrate resulting in a deposit resulting from a chemical reaction of the lubricant vapor on the surface of the metal. The lubricant was introduced into the carrier gas in an evaporation chamber where the pre-heated gas passed over a fiberglass packing wet with the desired amount of liquid lubricant. The temperature in the evaporation chamber was kept somewhat above that required to maintain the desired concentration of the liquid in the carrier gas. This temperature was determined by the vapor-pressure temperature curve for the lubricant. Reactions of the lubricant in the gas phase during delivery were minimized until contact was made with the solid surface of the target metal or the bearing. Even under oxidizing conditions, it has been shown with hydrocarbon vapors and oxygen that the formation of complex gaseous or solid reaction products take place primarily in the liquid phase or on a solid surface but not in the gas phase.

A second target for the gas phase lubricant was a dynamic four-ball wear tester utilizing M50 tool-steel balls. These tests were conducted at 371°C which was limited by the steel machine elements in the wear tester. The static deposition tests were run over the range of 500 to 850°C using stainless steel, iron, copper, and nickel as the metal targets with quartz as a non-reactive control specimen.

The specimen coatings applied by the vapor-delivered lubrication techniques are very uniform as measured by radio tracer techniques or the use of an SEM with a microprobe attachment. Photomicrographs taken with the SEM also show uniform coatings. For convenience, the coatings are measured quantitatively with a seven-place electrobalance or a six-place microbalance. The two-oven system used for static coating consists of one oven which is continuously swept with nitrogen gas for pre-heating or high-temperature soak of the coated specimen. The second oven contains a constant flow of lubricant vapor in the carrier gas at the desired test temperature. The specimens to be coated can be transferred from one oven to the other in less than a second. In this manner, coating times of as small as a few seconds can be achieved while specimens to be coated or after coating can be stored under nitrogen at the desired test temperature

for as long as desired. Coatings are given in micrograms per square
centimeter which can be translated approximately into molecular layers of
coating thickness by multiplying the $\mu g/cm^2$ by 10. Coatings of up to
several hundred molecular layers (50 $\mu g/cm^2$) adhere well to the wire
specimen. When the coating thickness reaches a value of several thousand
molecular layers, the deposit develops sufficient thickness and integrity
so that differences in properties, such as coefficient of thermal
expansion, between the wire and the thick coating causes the coating to
crack on cooling to ambient temperatures. The coatings formed appear to be
solid at the temperature of application. The effect of the metal substrate
on the coating rate can best be demonstrated by a tabulation of the coating
achieved during the first 1 minute of deposition by tricresyl phosphate
(TCP), diphenyl-ditertiarybutyl phenyl phosphate (DPDTPP), poly phenyl
ether (PPE), and trimethylol propane triheptanoate (TMPTH). These coatings
were all applied at 700°C from a nitrogen carrier gas containing between
1.0 and 1.75 mol percent of the lubricant.

	Lubricant			
	TCP	DPDTPP	PPE	TMPTH
Substrate(a)				
Iron	290	430	19	127
Copper	210	280	6	1
Stainless Steel	110	45	0	8
Nickel	15	10	16	24
Quartz	15	10	2	1

(a) Coating thickness in the first minute is given in $\mu g/cm^2$. To convert
this value to molecular layers the multiplication factor is
approximately 10.

These data show that the deposited lubrication coatings are strongly
influenced by the nature of the surface in contact with the gaseous
lubricant. The phosphate esters generally show a low energy path
decomposition in the presence of transition metals. The PPE and TMPTH with
more of a hydrocarbon-like structure appear to be more sensitive to metals
that provide hydrogenation or dehydrogenation catalysts to the system.

Long time tests show that the initial catalytic effect of the metal
surface will diminish with increasing thickness of the coating. Finally,
at some coating thickness the catalytic effect will disappear and a common
coating rate similar to that on a non-catalytic surface like quartz will be
achieved. The rate of disappearance of this catalytic effect appears to be
related to a diffusion-like process which differs with both lubricant types
and metal substrate.

The deposition rate for a given lubricant will increase with
increasing lubricant in the vapor phase over a lubricant concentration
change of 0.1 to 2.0 mol percent. The rate of deposit will increase
substantially for a given concentration of lubricant over the temperature
range of 600 to 850°C. The magnitudes of these concentration and
temperature changes are shown in detail in the body of this report.

In addition to the static deposition tests, dynamic wear tests in a four-ball wear tester have also been conducted on vapor-delivered lubrication. In this case, M50 tool-steel balls have been used for their hot hardness characteristics. The wear specimens and the metallurgy of the tester limited the temperature of this system to 371°C. The standard duration of the test was 30 minutes, and the lubricant was delivered to the four-ball wear tester below the level of the sliding contact in the ball pot using the same vapor-delivery system used for the static tests. In all cases, the amount of lubricant in the carrier gas was below the vapor pressure of the lubricant component for the delivery temperature which in turn was well below the 371°C test temperature. This delivery system precludes the possibility of lubricant condensation on the balls in the bearing area. An extrapolation of the deposit rate of lubricant on the balls, by chemical reaction on the ball surface, indicates that the maximum rate of lubricant application is of the order of a few molecular layers per second. All of the lubricant types illustrated in the static deposit mode were also run at 371°C in the four-ball wear tester. The results in the wear tester are excellent. For example, it can be shown that TCP at 0.5 mol percent in nitrogen shows wear properties over a load range of 5 to 50 kg that are better than those shown by a well-refined mineral oil at 75°C in the liquid form over the same load range. A study of wear versus TCP concentration, at 10 kg load and 371°C, shows a minimum wear rate at 0.5% TCP in nitrogen with higher wear rates at higher TCP concentrations. In the latter cases, the wear scars show evidence of too much film formation at the higher concentrations leading to three-body wear from the wear debris trapped in the lubricant coating. These studies show significant wear protection below the 0.5% optimum concentration which suggests that significant coating rates occur at concentrations as low as 0.1% TCP. It appears that the optimal wear condition occurs when the rate of film formation is equal to the rate of film removal.

Vapor-phase PPE lubrication at 1.0% concentration produced less wear in the four-ball wear tester than did liquid-phase PPE lubrication tested at the same load at 75°C.

These results show that vapor-phase lubricants at low deposition rates can be effective lubricants in dynamic wear tests at loadings typical of those found in many operational bearing systems. Specific data on the four-ball wear tester run at 371°C are shown in the body of the report.

The study of overall lubricant deposit rate and stability at high temperature suggests that adequate lubricant can be delivered at the temperatures studied. The results with the four-ball wear tester show that the amount of lubricant delivered is important in wear control. These data show that a balance of deposition rate and removal rate in a dynamic system can be controlled. This control is necessary to minimize wear.

Wear tests at higher temperatures are needed to extend these results from 371°C to the temperature range where static tests have been evaluated. At these higher temperatures, data from the static tests will improve our ability to demonstrate and to understand delivery rate versus removal rate in dynamic testing.

I.   INTRODUCTION

The purpose of this project was to investigate the feasibility of a new vapor phase lubricant-delivery system and its associated lubricants for high-temperature applications. This work was initiated in response to the need for advances in lubrication technology to achieve energy conservation in the metal-fabricating and transportation industries. The Research Committee on Lubrication of the ASME identified these two areas in an assessment conducted for the Department of Energy [1].

Better metal-forming capabilities to minimize machining and grinding requires lubrication techniques and lubricants that can be used effectively at temperatures approaching the melting points of the metals involved. In transportation, one of the most productive areas for increasing energy efficiencies is referred to as the adiabatic engine [2]. This trend means that lubricants and lubricant delivery systems must be designed to accommodate temperatures much higher than those used in conventional high-performance engines. Problems are already evident in current high-performance engines where lubricant life and, in some cases, engine performance are limited by the amount of lubricant degradation at operating conditions.

Recent studies have begun to define the temperatures encountered in conventional lubrication systems [3-9]. Temperatures range from those in the bulk system (75-150°C) to boundary lubrication temperatures of 315 to 340°C. Conventional lubrication under these temperatures is delivered as a liquid saturated with air. Studies of lubrication chemistry over the temperature range covered by bulk systems, elastohydrodynamic bearings and boundary lubrication systems show that oxidation reactions modified by metal catalytic systems predominate [10-16]. An extension of these reactions to higher temperatures results in excessive sludge and deposits. Thus, successful lubrication at the high temperatures of interest (350-1600°C) requires new concepts of lubrication and/or lubricant delivery systems.

The primary goal of this study is to investigate a new high-temperature vapor phase lubricant delivery system and the associated lubricant materials. In this system, a lubricating film is formed on a hot metal surface from a homogeneous vapor phase exposed to the surface. Molecules from the vapor are adsorbed on the metal and react to form the lubricant film. This process involves high-temperature thermal reactions and thermal-oxidative combinations in the appropriate temperature region. The vapor in these reactions consists of essentially two components: a carrier gas and the intended lubricant. The major ingredient of the gas-phase mixture is the carrier gas, a chemically inert material such as nitrogen. In some cases, the thermal reactions will be enhanced by the addition of oxygen to the carrier gas. The lubricant component is a volatile substance such as organic phosphate ester, polyphenyl ether, organic acid esters, or a hydrocarbon.

1

II. EXPERIMENTAL EQUIPMENT AND TEST PROCEDURES

A. Vapor Deposition Apparatus

The apparatus used for producing the lubricant vapor and depositing it on a substrate surface is shown schematically in figure 1. The equipment consists of three sections: vaporization, deposition, and preheating. The main criteria for the design and associated operating procedure are:

a)   The lubricant should be vaporized quickly to eliminate reactions at elevated temperatures in the liquid state.

b)   The metal substrate should be preheated to avoid condensation and liquid phase reactions.

c)   The procedure should have the capability of making precise measurements of the amount of deposit for precisely measured periods of time.

d)   The techniques should incorporate the means to control and vary the following parameters: metal surface temperature, vapor temperature, lubricant concentration, vapor flow rate, and carrier gas composition.

The vaporization apparatus is shown in more detail in figure 2. It consists of three stainless steel tubes (0.794 cm o.d.) fitted with a T joint. The joint is filled with a glass packing to increase the surface area available for lubricant vaporization. In this section lubricant vapor is produced and then transported to the deposition section by a carrier gas. The carrier is either an inert gas (nitrogen) or a reactant gas (air or a mixture of air and nitrogen). The carrier gas is fed through the system at a rate of 200 ml/min. The vaporization apparatus is heated to the required temperature using heating tape regulated by a variable transformer. The temperature is selected to give the desired lubricant vapor pressure, while keeping the temperature below the thermal decomposition temperature of the lubricant being evaluated.

The deposition and preheating sections consist of two ovens. In the preheating oven (fig. 1), the substrate to be coated is heated to the deposition temperature under an inert atmosphere (nitrogen). When the substrate reaches the desired test temperature, it is guided into the deposition oven. In the deposition oven, the substrate is exposed to the lubricant vapor in the carrier gas. The flow rates of gases in both preheating and deposition ovens is maintained at 200 ml/min. The gases from both ovens exit through a vent located between the two ovens. The deposition oven and preheating oven are connected by a stainless steel tube that can be removed for substrate loading and unloading. A stainless steel rod with a hook on one end is mounted inside the tube. This rod can be slid across the preheating and deposition ovens. The substrates are wire specimens of about 0.025 to 0.05 cm in diameter. A hook on the stainless steel rod acts as a sample holder for the substrate. The deposition oven

is connected to the vaporization apparatus by a ceramic tube that is cemented at the joint between the vaporization apparatus and the deposition oven.

The operating procedure for the vapor deposition tests consists of three stages: cleaning and drying the substrate, preheating, and deposition. The substrate is washed successively with naphtha and tetrahydrofuran and then dried in a high velocity stream of air. The substrate is then held in the preheating oven for 5 minutes to vaporize any residual solvent. The substrate is then weighed using an electrobalance or a six-place microbalance. Stainless steel, copper, and quartz substrates are weighed using the electrobalance, whereas magnetic substrates such as iron and nickel are weighed using a six-place microbalance. The substrate is then placed on the sample holder and preheated to the desired deposition temperature under a nitrogen blanket in the preheating oven. After it reaches the desired deposition temperature, the substrate holder is slid across to the deposition oven, where the substrate contacts the lubricant vapor for the duration of the test. After deposition is completed, the substrate is pulled back to the preheating oven. The substrate is cooled for 10 minutes under a steady flow of nitrogen and then weighed. The weight gain of the substrate is reported as the amount of deposit formed. It should be noted that while the substrate is being preheated in nitrogen, oxygen impurities in nitrogen may cause oxide coatings to form on the substrate surface. This weight gain due to formation of oxide coatings in the preheating section is subtracted from the total weight gain reported.

After the completion of a deposition test, the deposit is examined using the Scanning Electron Microscopy (SEM) and Energy Dispersive Analytical X-Ray Spectroscopy (EDAX). The SEM is used to examine the surface of the substrates and the morphology of the vapor deposited films. EDAX is used to determine the relative elemental composition of the deposits.

An earlier version of the vapor deposition apparatus, figure 3, was used with some of the lubricants discussed in this report. That preliminary technique was replaced because the exact concentration of the lubricant in the vapor was not known or controlled, and the liquid-phase reactions could modify the lubricant which was kept as a liquid at elevated temperature for the duration of the experiment.

The earlier apparatus consists of a ceramic tube 0.76 m long and 0.025 m i.d., with three sections, each heated by a separate tubular oven. In the first section, a stainless steel boat or crucible (0.0095 m x 0.0064 m x 0.076 m) filled with lubricant is heated to produce the desired vapor pressure of the lubricant. In the second section, the temperature is increased and the gas stream containing the lubricant vapor is brought into contact with the specimen surface where the solid lubricant film is to be formed. The last section is used to preheat the specimen while the boat is being heated to the desired temperature. The direction of flow of the carrier gas is controlled by the three-way valve. At the beginning of an experiment, the flow of carrier gas is directed away from the specimen to be coated while the boat and specimen are heated to the desired

3

temperature. When the desired system temperature is reached, the direction
of the carrier gas is reversed to carry the lubricant vapor to the specimen
which is then positioned in the middle section. The specimen is then
exposed to the vaporized lubricant for a specified time during which a
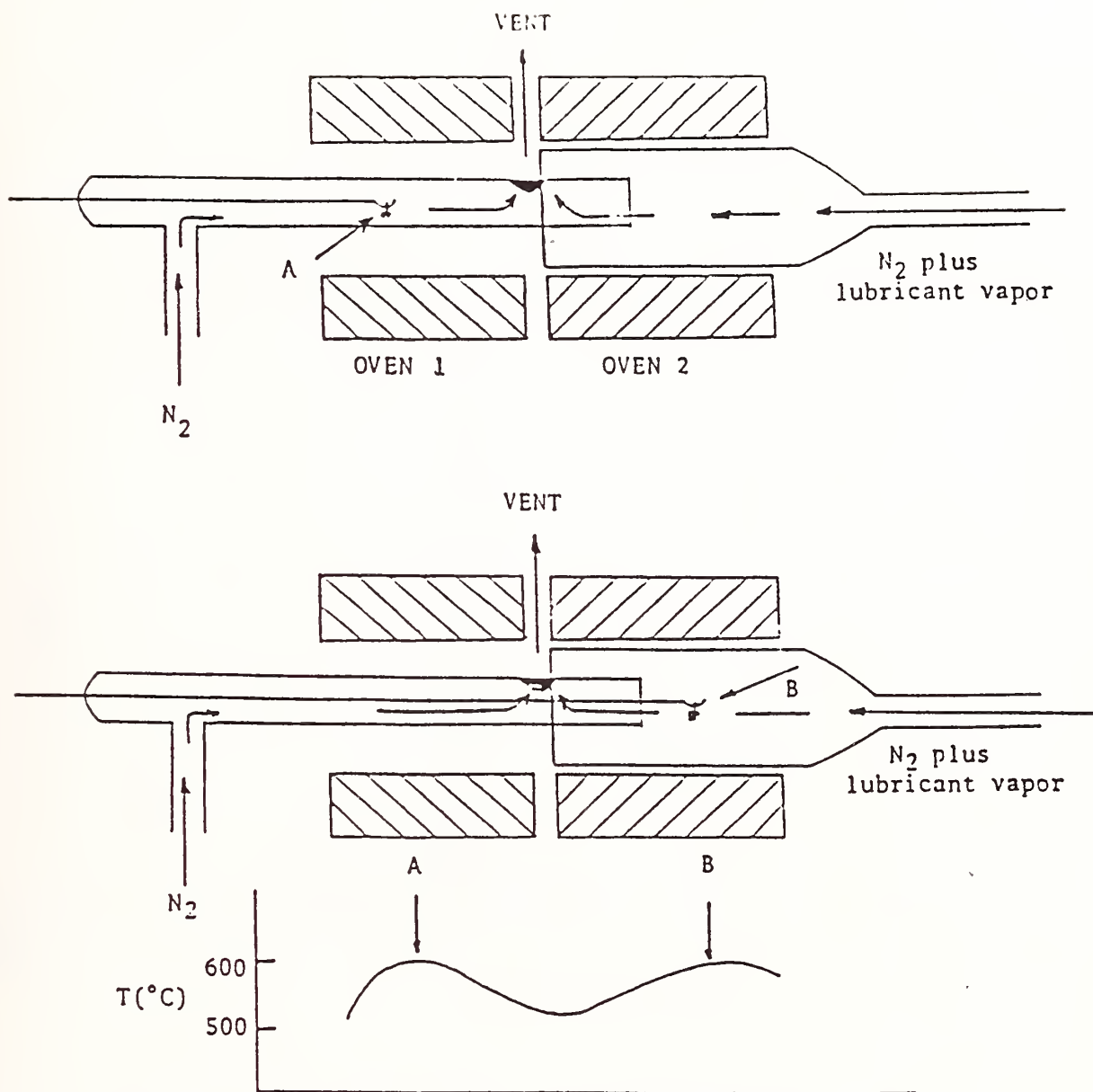solid lubricant film is deposited on the specimen.

Figure 1. Apparatus for vapor phase lubrication of stationary samples and temperature profile in apparatus.

(A)   Position of sample during preheating cycle.
(B)   Position of sample during deposition.
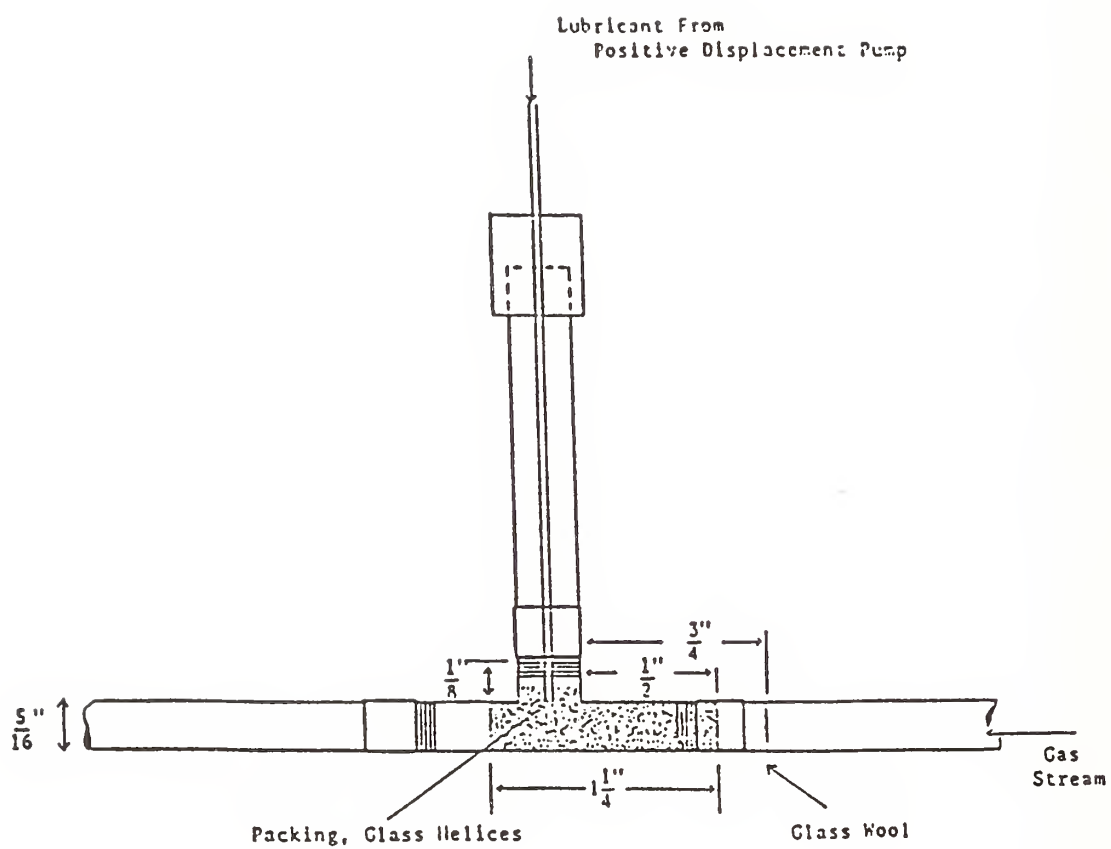
Figure 2. Lubricant vaporization apparatus.
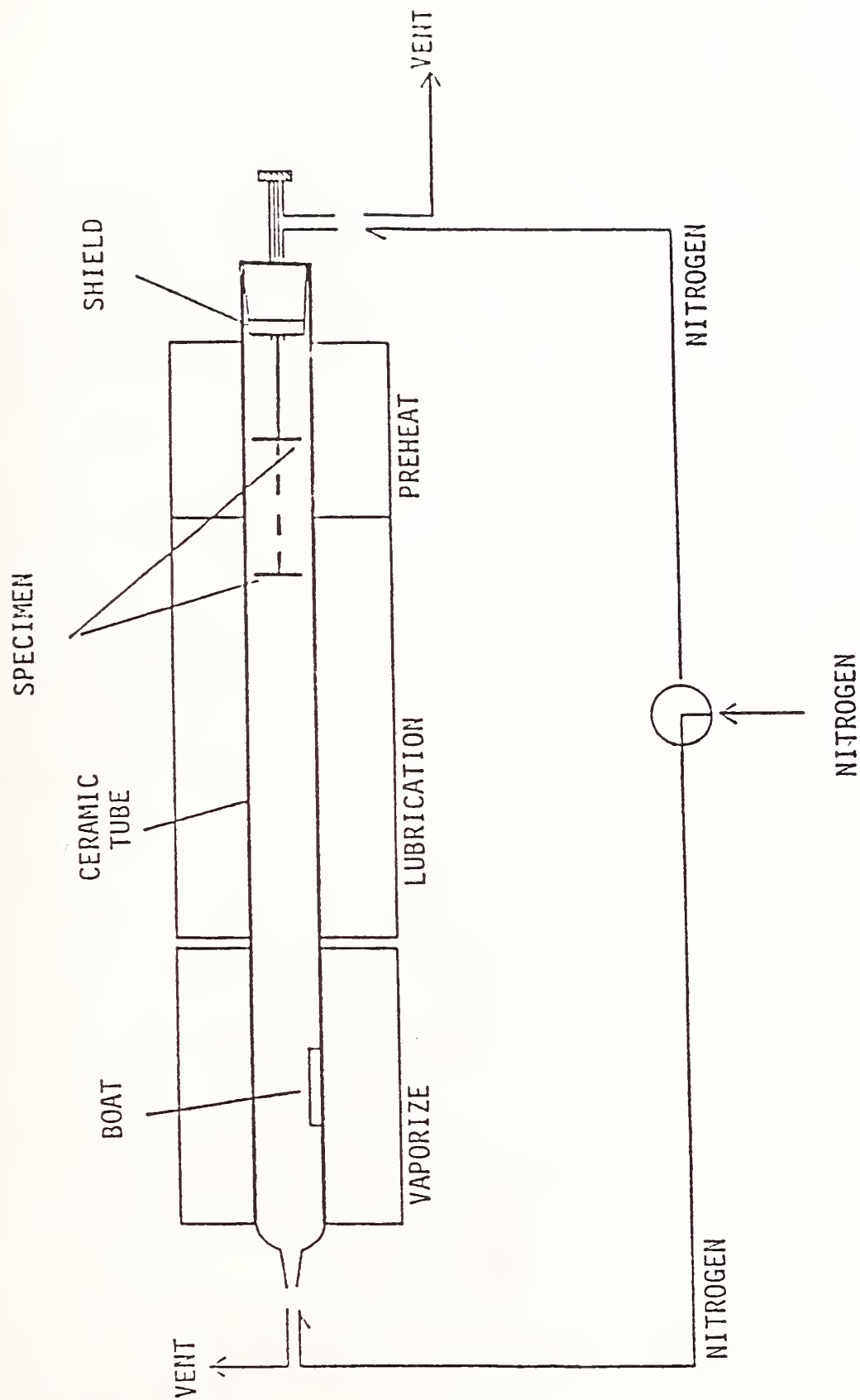
Figure 3. Equipment for coating specimens with lubricant vapor.

B. Dynamic Wear Testing with a Four-Ball Wear Tester

    A modified four-ball wear tester was used to study the anti-wear
characteristics of vapor deposited lubricating films. A schematic of the
test apparatus is shown in figure 4. The wear tester consisted of three
contacting balls held in place in a ball pot and a top rotating ball that
impinges onto the stationary balls with an adjustable load. The wear
tester was modified to accommodate a lubricant vapor delivery system. The
design allows for control of both the temperature and the environment
surrounding the ball pot and spindle. The lubricant vapor was produced in
a vaporization apparatus similar to that described earlier. Lubricant
vapors were carried to the ball pot by a carrier gas (nitrogen, air, or
mixtures of nitrogen and air) at a rate of 200 ml/min. The ball pot was
brought up to the desired test temperature, usually 371°C, with a
continuous purge of nitrogen gas. To initiate a test, liquid lubricant
from a syringe pump was fed into the vaporization column where it was
vaporized and delivered into the preheated ball pot for 2 minutes. Next,
the wear tester was started using a set speed of 600 rpm. Then, the load
was applied bringing the rotating upper ball bearing into contact with the
three stationary ball bearings. Loads from 5 to 60 kg were studied. Each
test was run for 30 min with a continuous supply of lubricant vapor. After
30 min, the load was removed and the balls were disassembled from the ball
pot. The wear scars on the lower three balls were measured using a
calibrated microscope. The diameters of these scars were taken as a good
measure of the wear behavior of the lubricant. The wear scars were
dependent on the type of lubricant, load, speed, test time, and temperature
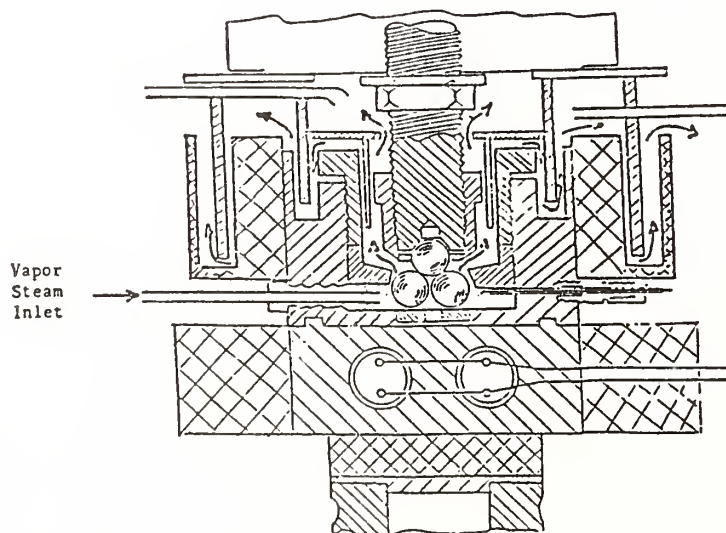used in the tests.

Figure 4. Four-ball wear tester modified for
           vapor delivered lubrication studies.

III. VAPOR DEPOSITION STUDIES

The vapor deposition apparatus described in previous sections was used to study the vapor deposition behavior of a wide variety of lubricants. The lubricating film deposition characteristics were found to be dependent on lubricant type, substrate material, substrate temperature, lubricant vapor concentration, and carrier gas composition. In this work, data were obtained for tricresyl phosphate (TCP), tributyl phosphate (TSP), diphenyl ditertiarybutylphenyl phosphate (GT), polyphenyl ether (PPE), trimethylolpropane triheptanoate (TMPTH), di-2-ethylhexyl sebacate (DEHS), and super-refined mineral oil.

The trends observed in the formation of the vapor deposited lubricating films are discussed in this section. The first discussion, on TCP vapor deposited films, is used to summarize the primary factors that influence vapor deposition.

A. Tricresyl Phosphate (TCP)

Effect of Substrate and Temperature: Deposition data were obtained for TCP on iron, stainless steel, copper, nickel, aluminum, and quartz at 500, 600, and 700°C in figures 5-7. The concentration of TCP in nitrogen carrier gas for this series of tests was 1.55 wt. percent. It has been shown by a number of investigators that phosphate esters exhibit a low energy decomposition path on certain transition metals such as iron. The data in figures 5-7 show that the initial deposition rates are high for copper, iron, and stainless steel. For iron and stainless steel these high rates decrease with test time and approach a constant rate. As the temperature increases, it takes less time to reach this constant deposition rate. At 700°C the same final deposition rates are achieved for iron and stainless steel. The lower catalytic effect of stainless steel compared to iron can be attributed to lower corrosion rates on stainless steel. The initial high deposition rates and the subsequent decrease of these rates with test time appear to be related to the availability of iron to react with TCP in forming the coating. As the thickness of the coating increases, this impedes the diffusion of iron molecules through the coating. Consequently, as the thickness of the coating increases, less iron is available for reaction and coating formation. Therefore, the rate of deposition decreases. It is anticipated that a similar loss in deposition rate will be observed for copper at longer times. Studies reported later in this report indicate that for long times or thick coatings, the rate of deposition becomes independent of the substrate and approaches the rate characteristic of a non-catalytic surface such as quartz.

Deposition data for TCP vapor on stainless steel for tests of 1 to 60 seconds duration is shown in figure 8. These tests were conducted using 0.049 to 1.23% TCP vapor in a nitrogen carrier gas at 700°C. These data clearly show the initial high deposition rate on stainless steel that decreases with test time to approach a constant rate.
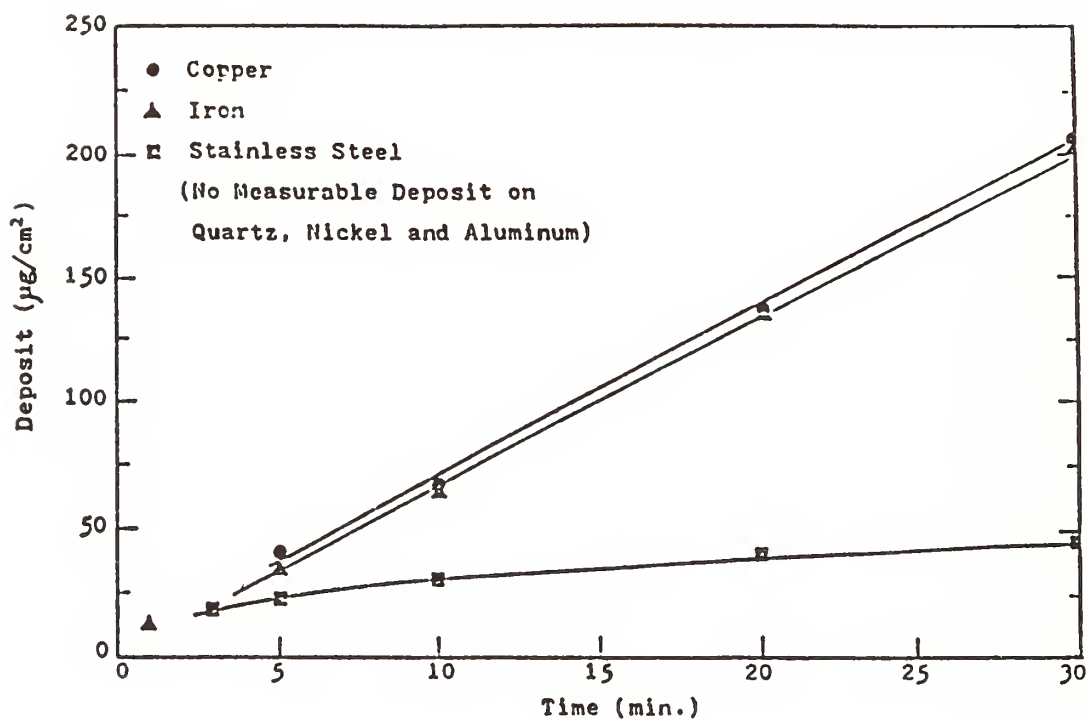
9

Figure 5.   Deposit thickness versus time for various substrates
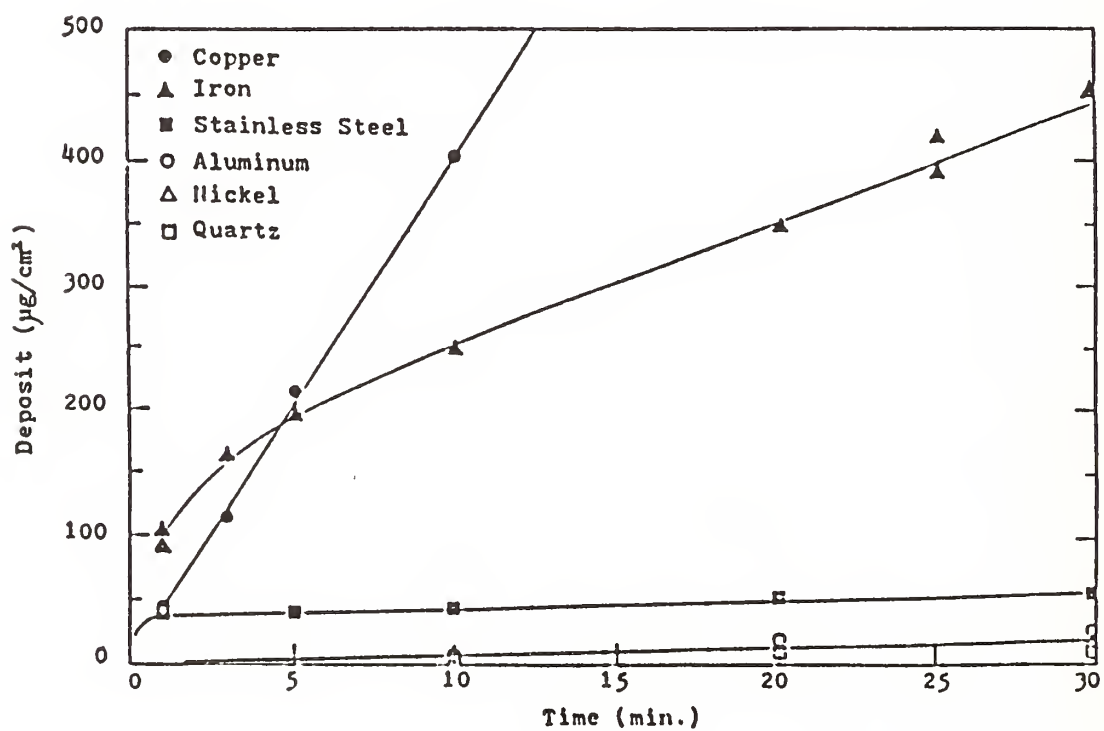exposed to a vapor of 1.55% TCP in nitrogen stream
at 500°C.

Figure 6.   Deposit thickness versus time for various substrates
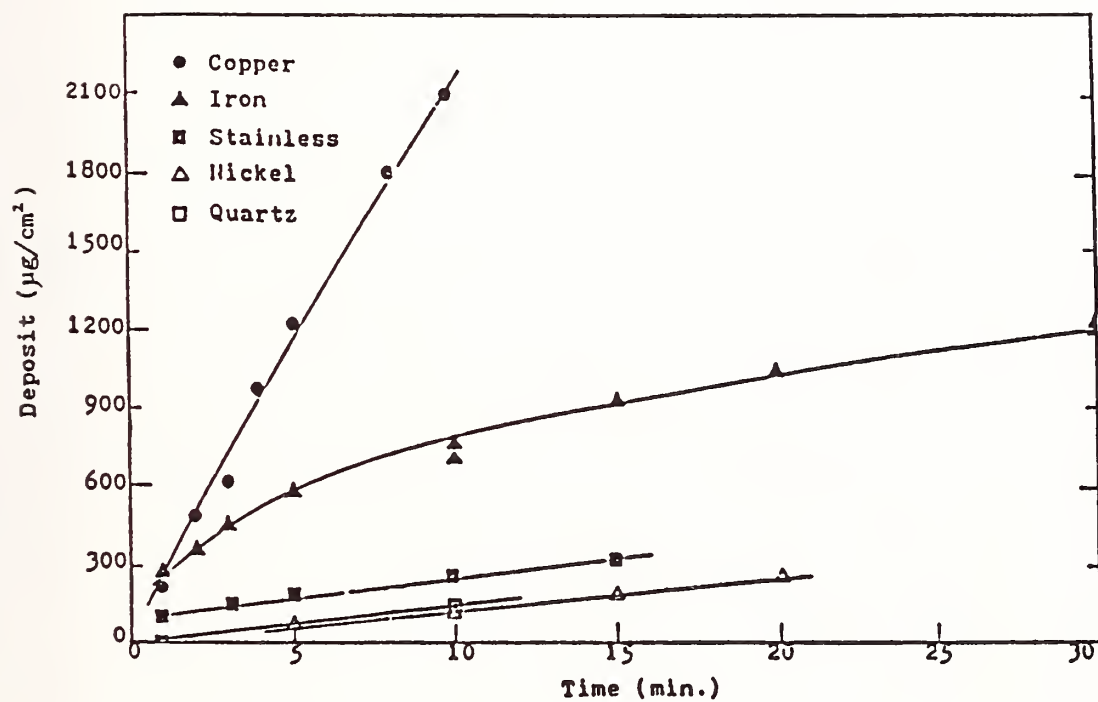exposed to a vapor of 1.55% TCP in nitrogen at 600°C.

10

Figure 7.   Deposit thickness versus time for various substrates
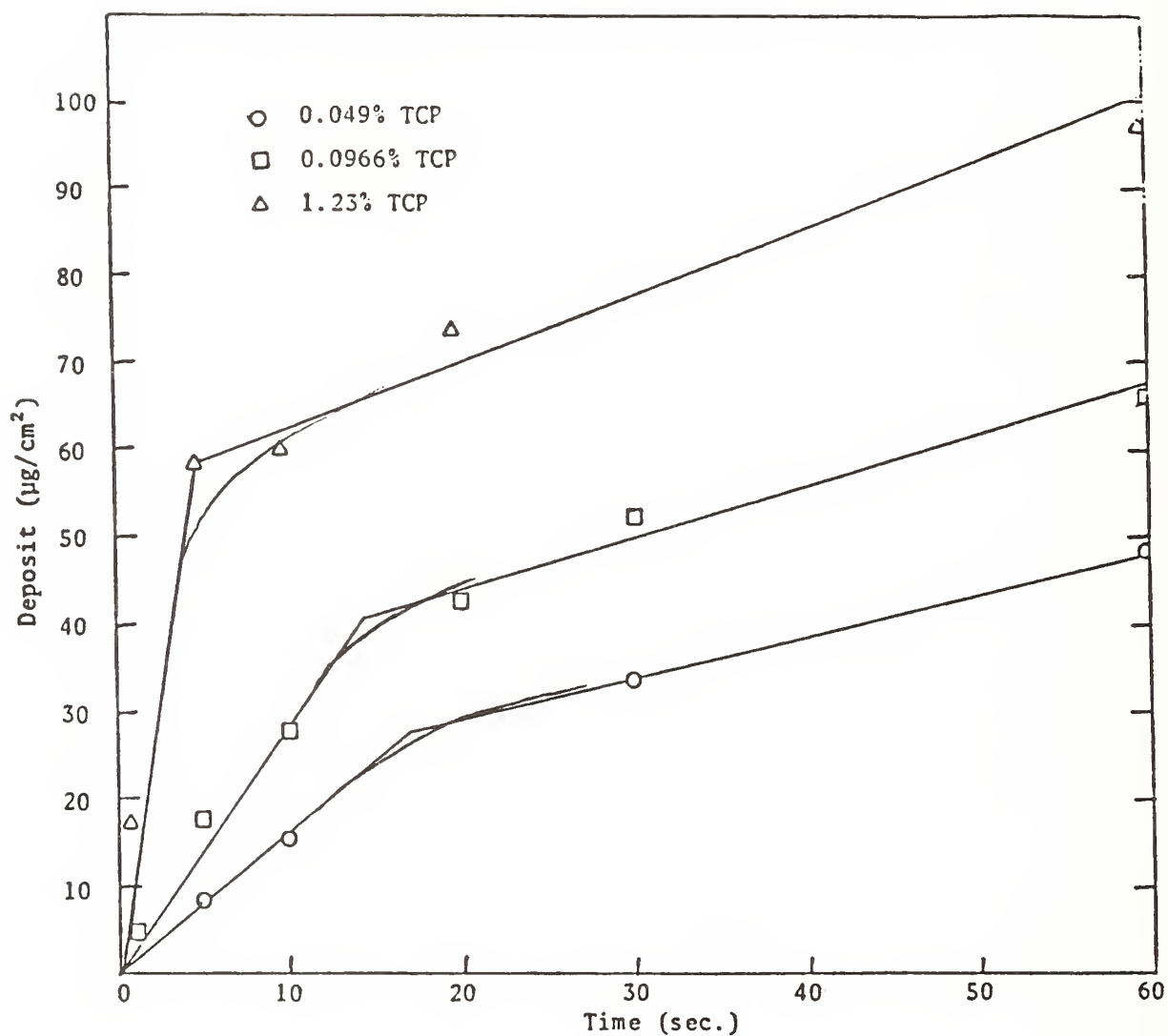exposed to a vapor of 1.55% TCP in nitrogen stream
at 700°C.

11

Figure 8. Deposit thickness versus time for stainless steel wire at
700°C exposed to vapor concentrations of TCP of 0.049% to
1.23% in a nitrogen carrier gas. [1 μg/cm² ≐ 10 monolayers].
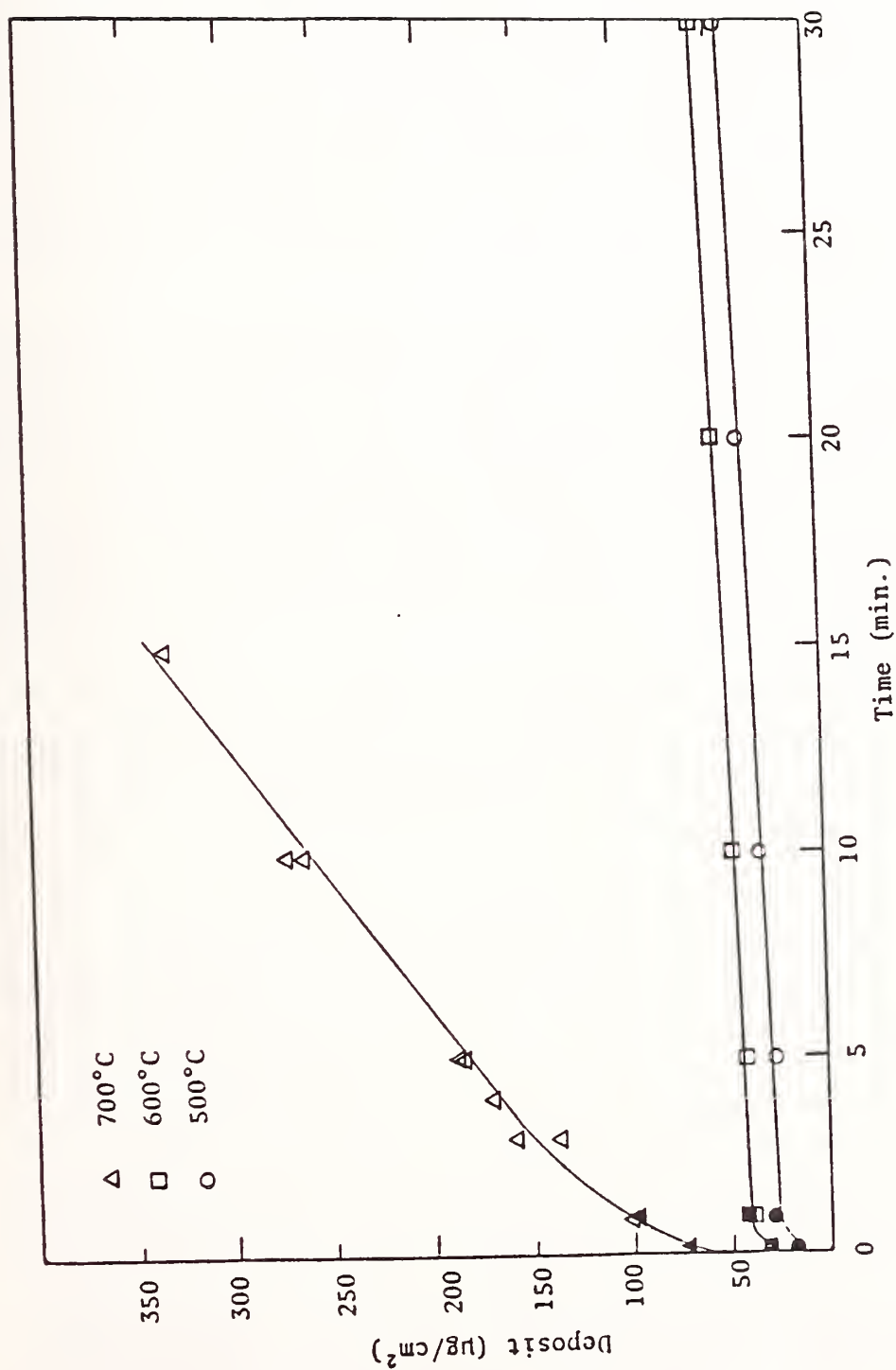
Figure 9. Long-time deposition of stainless steel wire exposed to a vapor of 1.55% TCP in a 200 cc/min nitrogen carrier gas.

13

Copper, nickel, aluminum, and quartz surfaces are compared at 500, 600, and 700°C with iron and stainless steel in figures 5-7. These data suggest that copper has a significant catalytic effect on TCP vapor deposition. The catalytic effect appears to persist at all three temperatures. Nickel, quartz, and aluminum all show little measurable TCP deposit after 30 minutes at 500°C. At 600°C these three materials show the same very low deposition rate over the 30-minute period. In all cases, the deposition rate appears to be linear from zero time and there appears to be no initial high rate. Aluminum melts between 600°C and 700°C and could not be tested at 700°C. Nickel and quartz again show the same low linear deposition rate at 700°C. Metal substrates that cause deposition rates higher than on quartz can be considered to have a catalytic effect on deposit formation. On this basis, these data demonstrate the significant catalytic effect of iron and copper and the lack of catalytic effect for aluminum and nickel for TCP vapor deposition.

The effect of temperature on TCP vapor deposition is also illustrated in figures 5-7. It is observed that increasing the temperature from 500 to 700°C significantly increases the deposition rates. A comparison of the increase in deposition rate with temperature is made on figure 9. Data are shown for TCP deposition on stainless steel using 1.55% TCP in nitrogen. These data indicate the expected increase in deposition rate with temperature. At 500 and 600°C, the catalytic effect is evident only at times of 5 minutes or less. The constant deposition rate above 5 minutes is indicative of the lack of a catalytic effect. At 700°C, the deposition rate is high and stainless steel shows significant catalytic activity for the duration of the test.

Effect of Lubricant Vapor Concentration: The effect of increasing the lubricant vapor concentration in the carrier gas on the deposition rate was examined. Figure 8 illustrates the effect of increasing TCP concentration in nitrogen carrier gas from 0.049 to 1.23% on the deposition rate on stainless steel at 700°C. The data shown in this figure are for short test times (less than 60 seconds).

During this short test period, stainless steel has a catalytic effect on TCP deposition. Figure 8 shows that increasing the TCP vapor concentration from 0.049 to 0.23% causes a significant increase in the TCP deposition rate. It should be noted, however, that the yield in deposit per mol of TCP vapor is highest for the lowest concentrations used. The effect of increasing the TCP vapor concentration on deposition on iron is illustrated in figures 10-13. Figures 10-12 show deposit data at 500, 600, and 700°C, varying the TCP concentration in nitrogen from 0.126 to 1.55%. These data show that at all three temperatures, the lowest TCP concentration, 0.126%, causes the highest deposition rate after 30 minutes. At 600 and 700°C, the 1.55% TCP vapor and the lower TCP vapor concentration curves cross within the 30-minute test period. These changes in rate with time and concentration appear to be associated with the coupling of the catalytic effect of the iron surface with the diffusion process related to the transport of iron through the coating. The catalytic effect of iron diminishes with the decrease in availability of iron with increasing film thickness. With higher TCP vapor concentrations, this diminishing
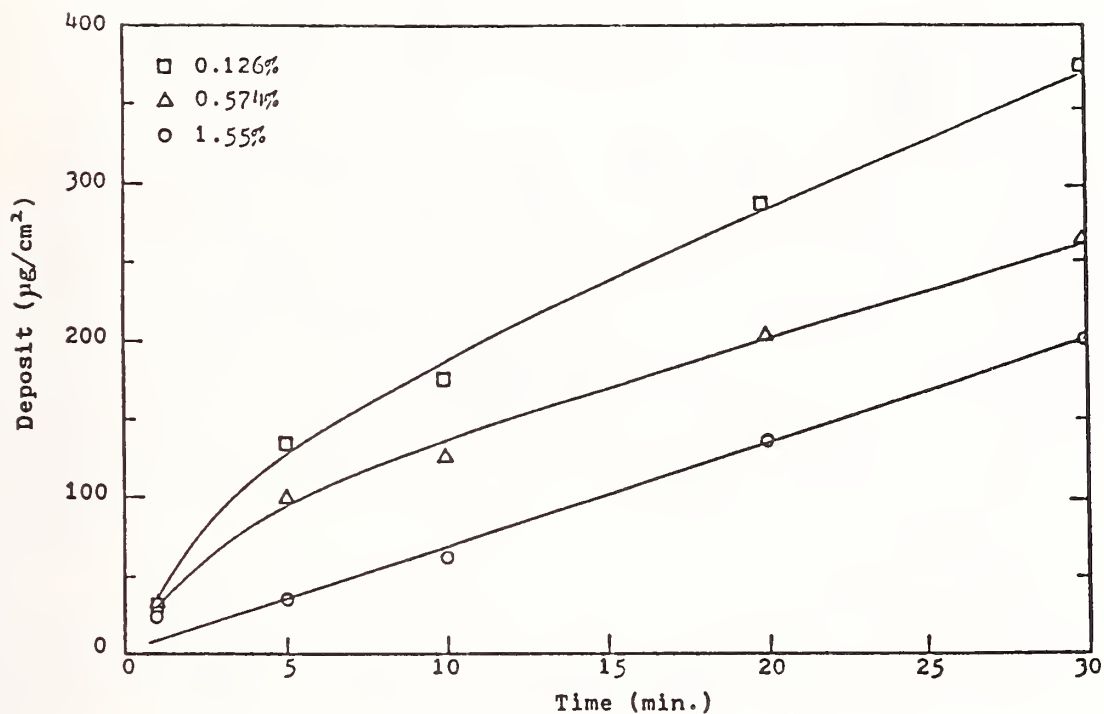
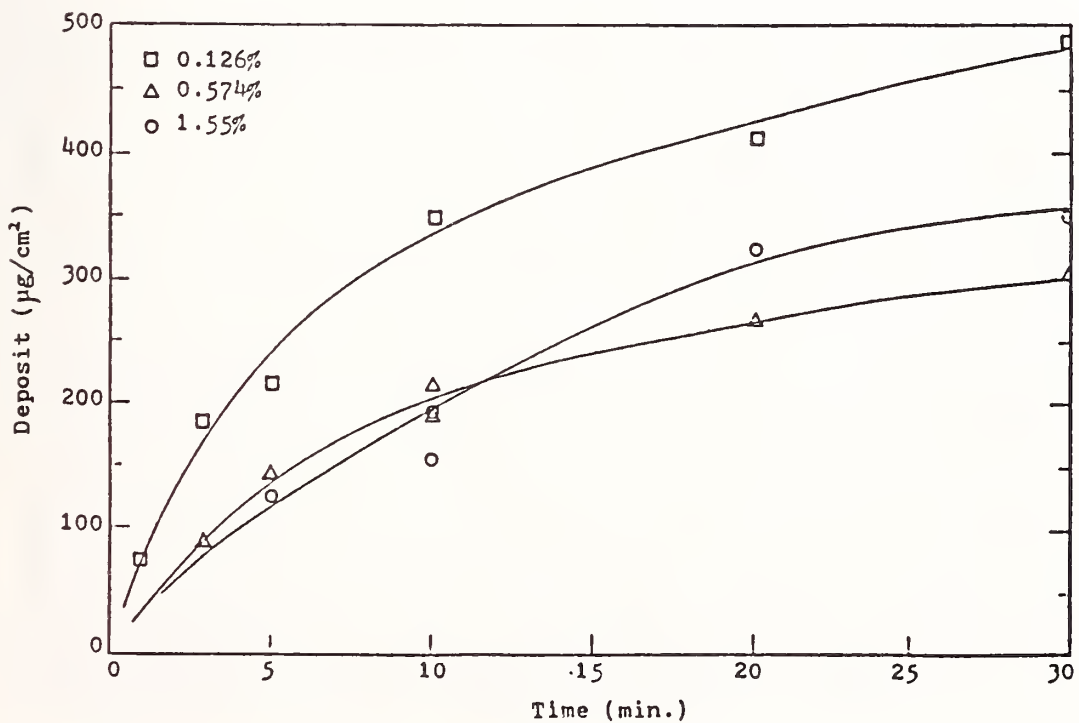Figure 10. Deposit thickness versus time for iron exposed to various TCP concentrations at 500°C.

Figure 11. Deposit thickness versus time for iron exposed to various TCP concentrations at 600°C.
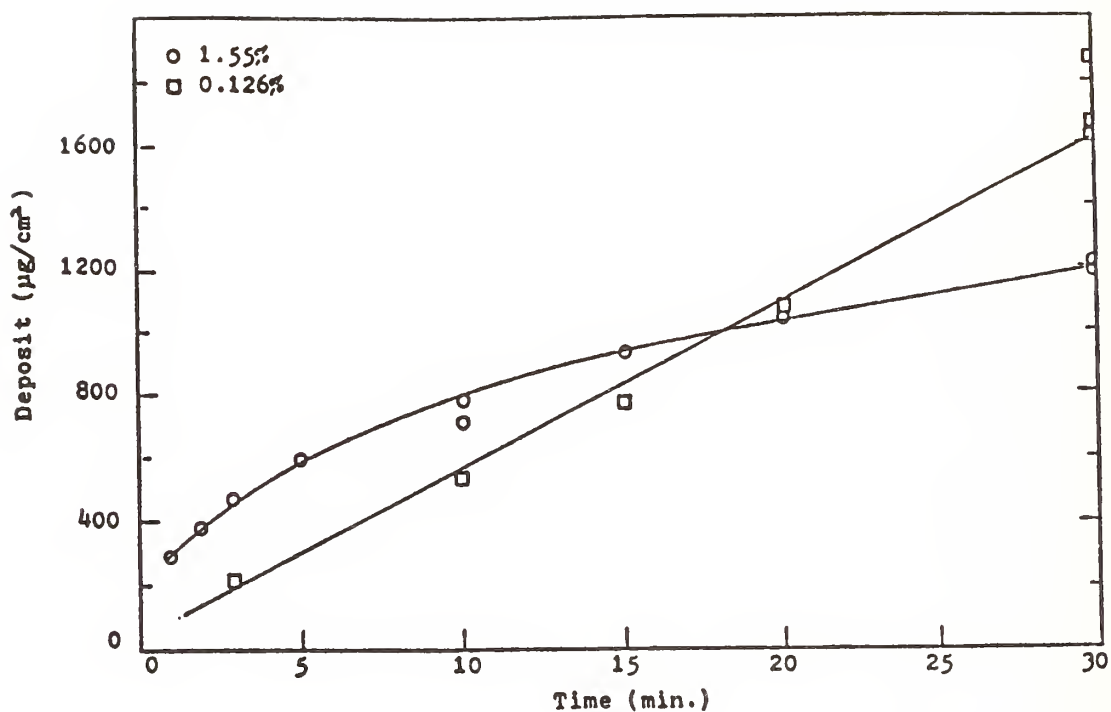
15

Figure 12.   Deposit thickness versus time for iron exposed to
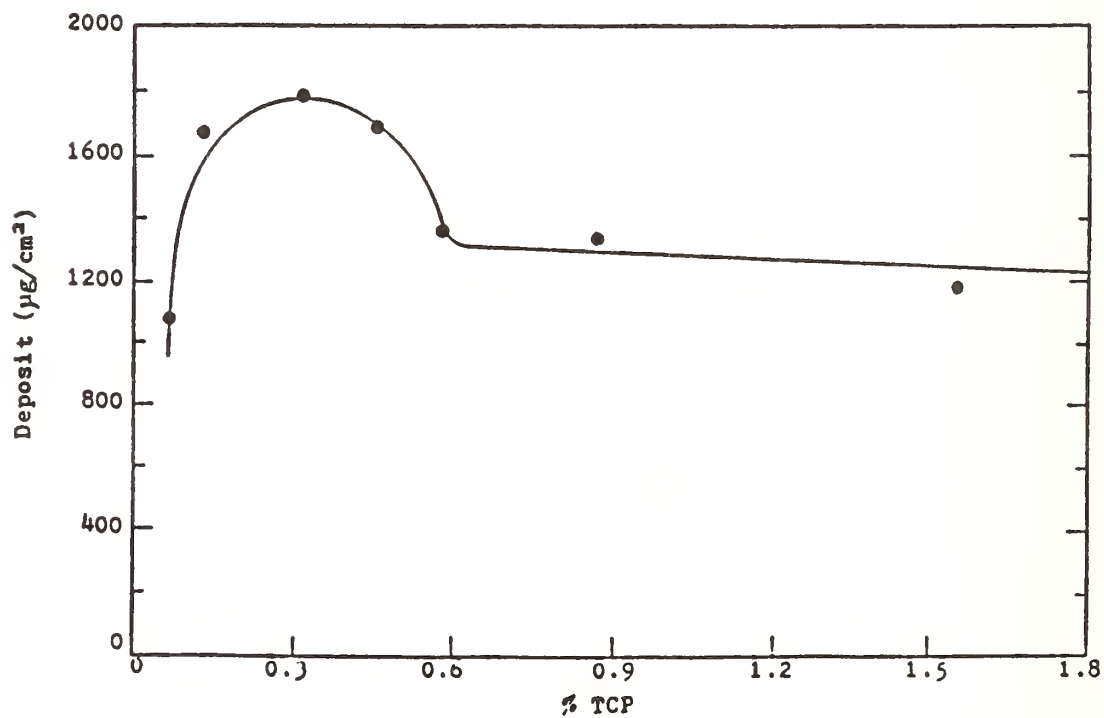two different TCP concentrations at 700°C.

Figure 13.   30 minute deposit versus TCP concentration for
iron at 700°C.

16

catalytic effect occurs in a shorter time period. This may be related to the influence of lubricant concentration on the coating morphology and subsequent diffusion rates. Figure 13 shows TCP deposit on iron as a function of TCP vapor concentration for tests of 30 minutes duration at 700°C. These data show that the maximum deposit occurs at a TCP vapor concentration of 0.3%. In the range 0.1 to 0.3% TCP vapor concentration, increasing the concentration increases the deposit. Using a TCP vapor concentration higher than 0.3% decreases the deposit. Conventional chemical kinetics would suggest that an increase in the TCP concentration would always increase the rate of coating formation. It is possible that changes in deposit morphology due to changes in concentrations of the vapor could influence the diffusion of iron or iron corrosive compounds to the surface.

The effect of increasing the TCP vapor concentration on deposition on copper is illustrated in figures 14-17. Figures 14-16 show deposit data at 500, 600, and 700°C, varying the TCP concentration in the nitrogen carrier gas from 0.126 to 1.55%. The effect of vapor concentration on deposition on copper differs substantially from that on iron. For copper all of the conditions studied show a linear deposition rate from time zero. In all cases the higher the TCP vapor concentration the higher the deposition rate. At 1.55% TCP vapor the deposit level after 30 minutes at 600 and 700°C is much higher on copper than on iron. At 1.55% TCP vapor concentration deposits at 500°C on iron and copper are about the same. At 0.126% TCP vapor concentration, the deposit levels on copper are higher than on iron at all three temperatures. The high levels of deposit formation on copper indicate the strong catalytic effect of the metal that persists through the 30-minute duration of the tests. Figure 17 illustrates TCP deposit on copper as a function of TCP vapor concentration for tests of 15 minutes duration at 700°C. The data show that increasing the TCP vapor concentration from 0.126 to 1.55% causes a linear increase in deposit level. In contrast to the results with an iron substrate, all the data obtained with copper are consistent with conventional chemical kinetics. It is the catalytic activity of copper has not been diminished even when the coating is equivalent to over 30,000 monolayers thick.

Effect of Carrier Gas Concentration: The effect of carrier gas on TCP deposition rates is illustrated in figures 18-21. Figures 18 and 19 show TCP deposit data on iron, copper, stainless steel, and nickel using 0.0155 and 0.126% TCP vapor in nitrogen. Figures 20 and 21 show data from tests conducted under conditions identical to those used in figures 18 and 19 except that air was used as the carrier gas instead of the inert nitrogen. It should be noted that deposit formation in the presence of air may involve a different mechanism than deposit formation in the presence of an inert gas such as nitrogen. This behavior has been observed in liquid phase TCP degradation where reaction in nitrogen gives rise to P-O-P bonding whereas, reaction in air causes aryl-to-aryl linkages with the formation of C-O-C bonds [15].

Comparison of figures 18 and 19 with figures 20 and 21 show that deposition rates in the presence of air are comparatively higher than in nitrogen. The influence of oxygen on the deposition rate is particularly
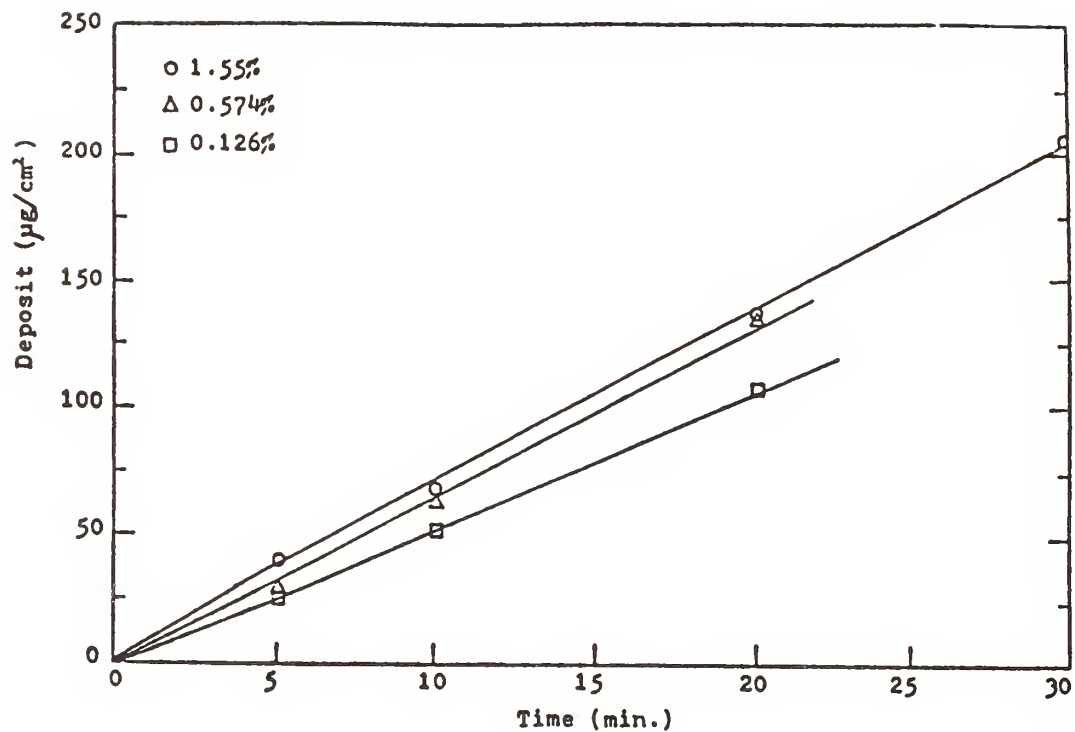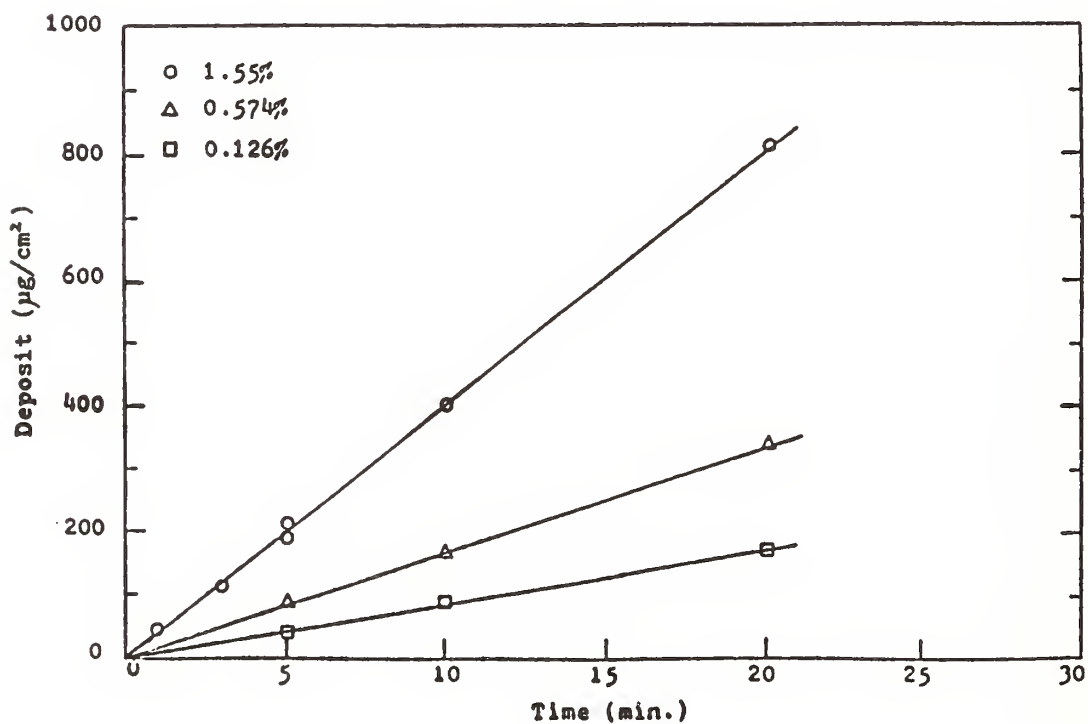
17

Figure 14. Deposit thickness versus time for copper exposed to various TCP concentrations at 500°C.

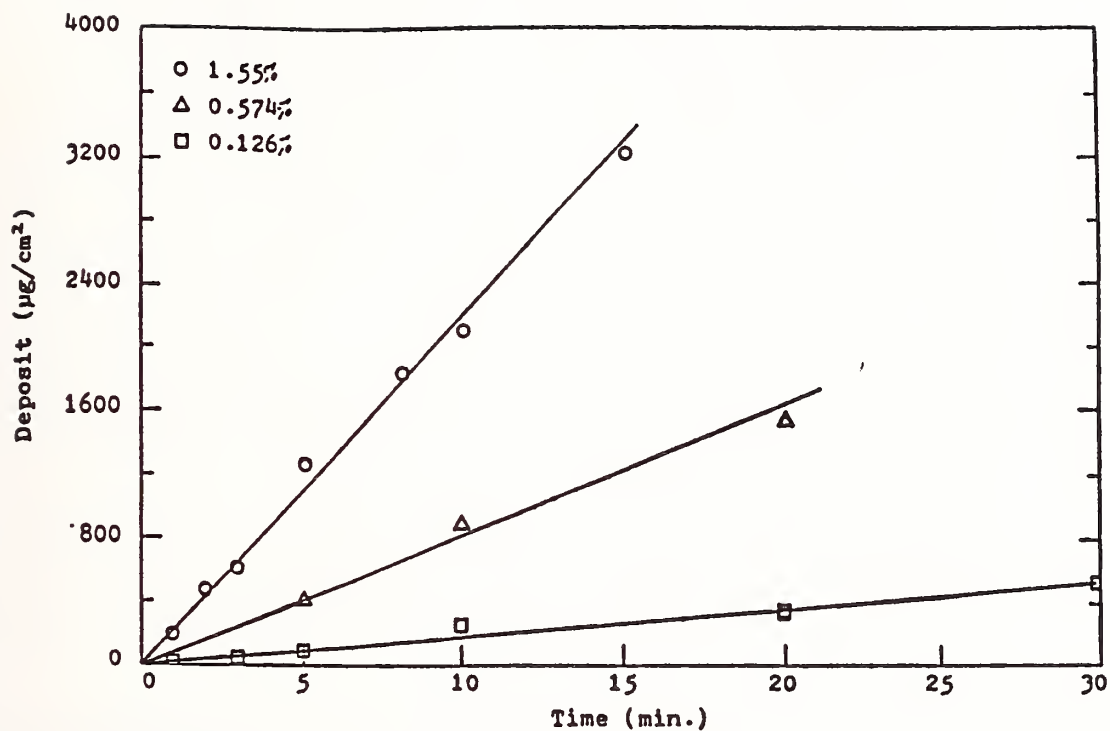Figure 15. Deposit thickness versus time for copper exposed to various TCP concentrations at 600°C.

18

Figure 16. Deposit thickness versus time for copper exposed
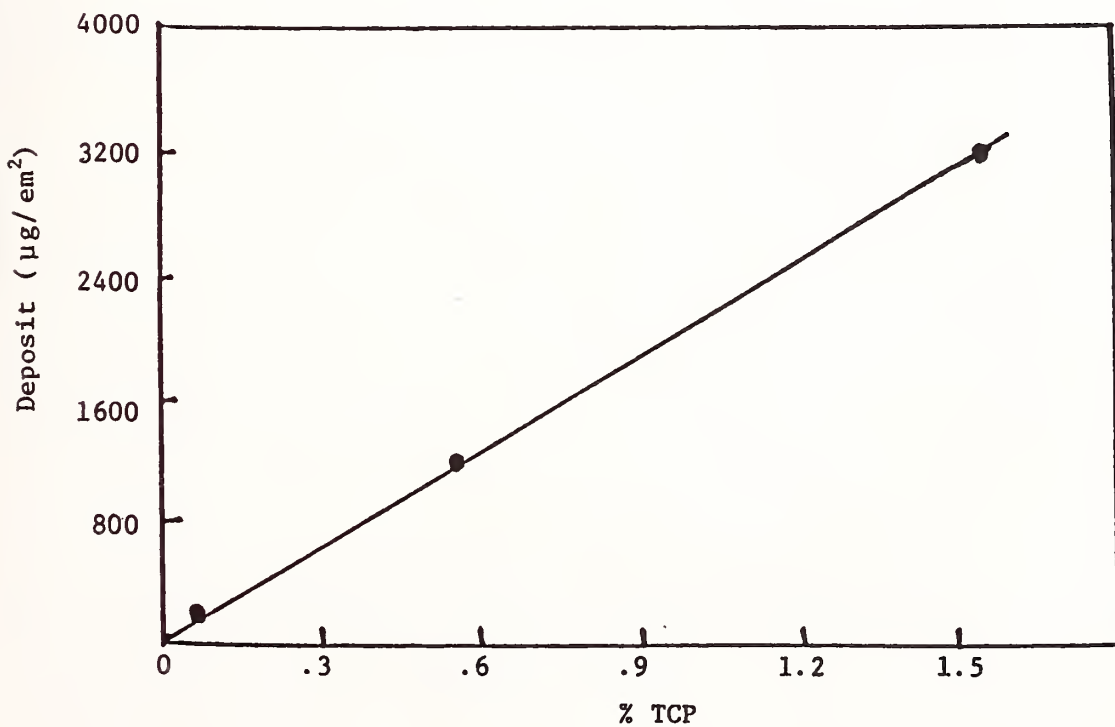to various TCP concentrations at 700°C.

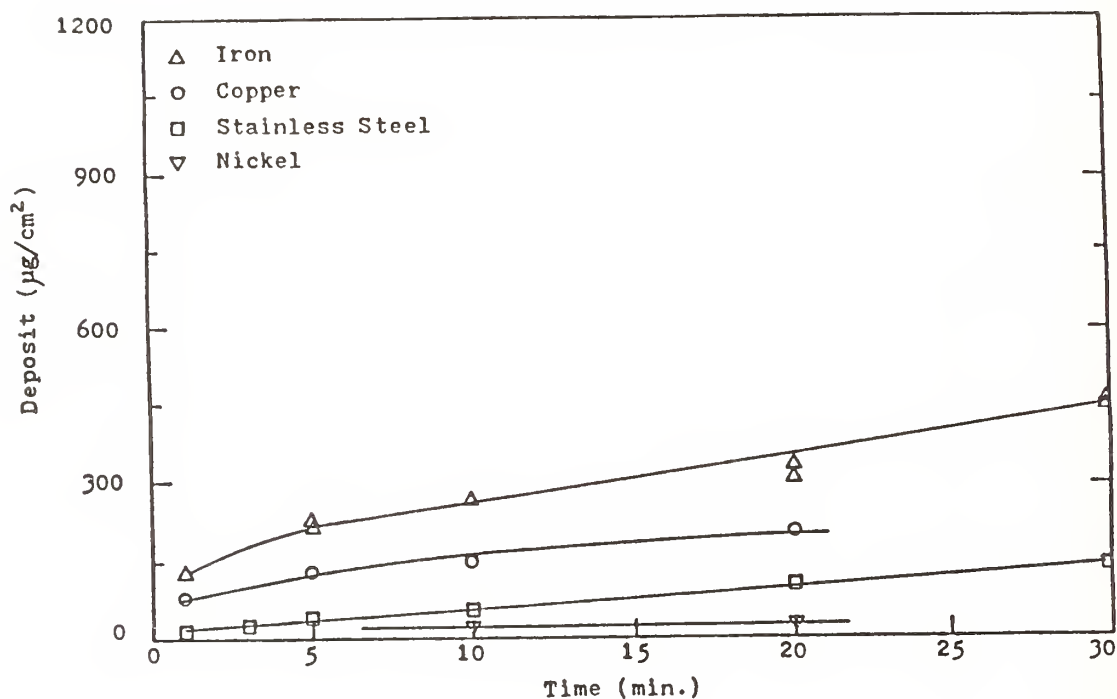Figure 17. 15-minute deposit versus TCP concentration for
copper at 700°C.

19

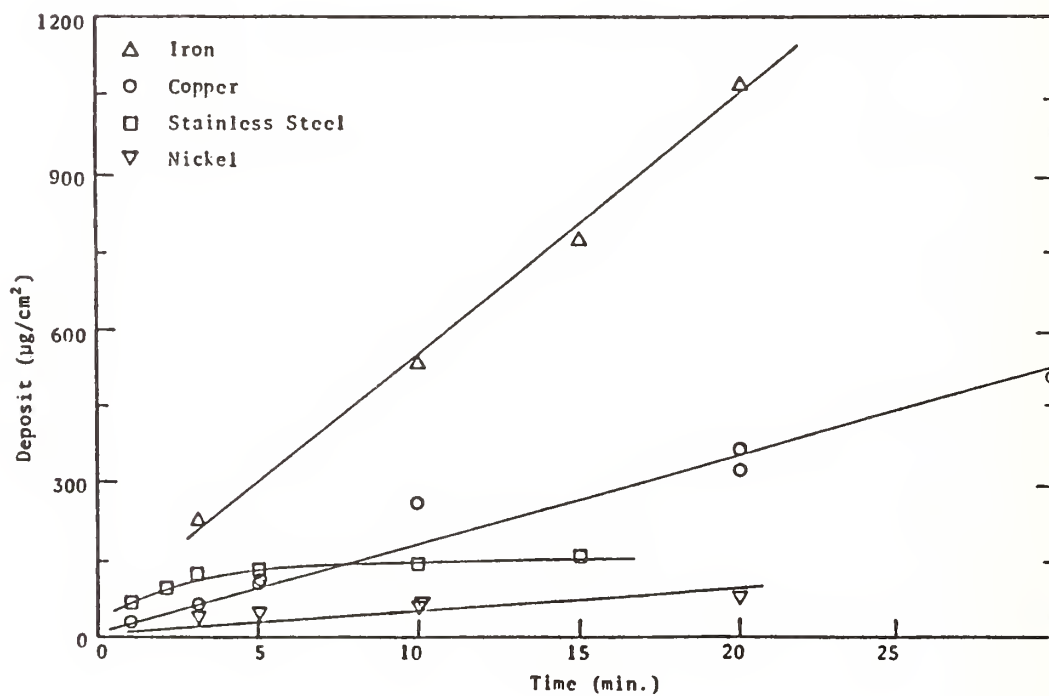Figure 18. Deposition curves for 0.0155% TCP in nitrogen stream on four metal substrates at 700°C.

Figure 19. Deposition curves for 0.126% TCP in nitrogen stream on four metal substrates at 700°C.
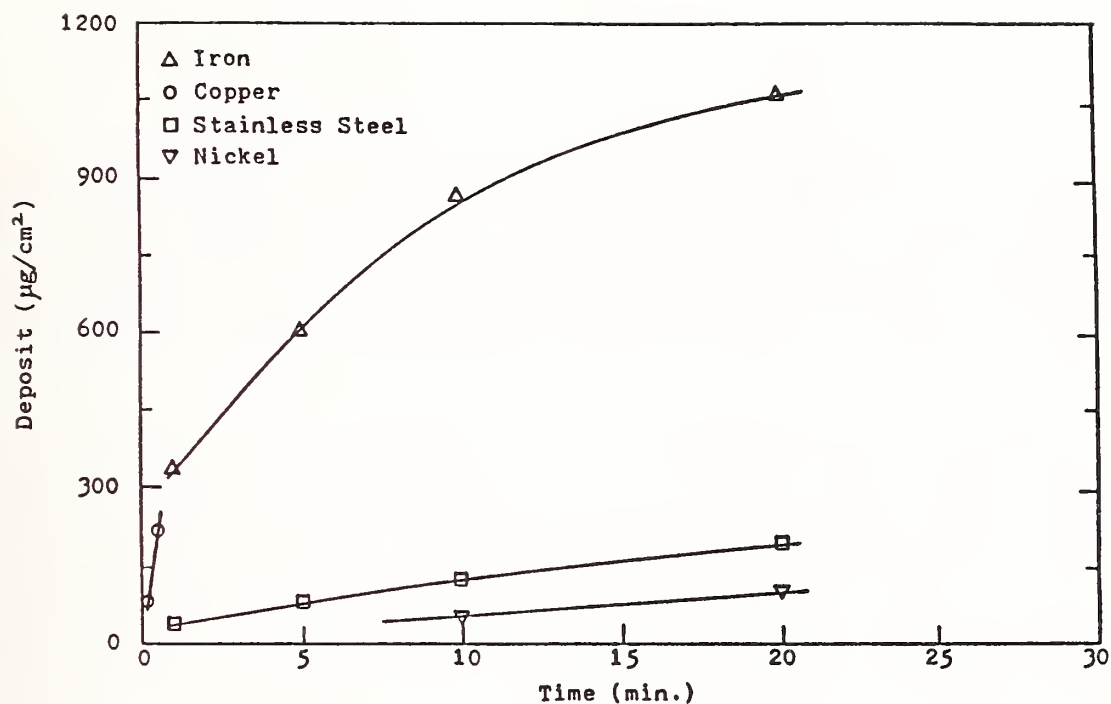
Figure 20. Deposition curves for 0.0155% TCP in air stream on four metal substrates at 700°C.
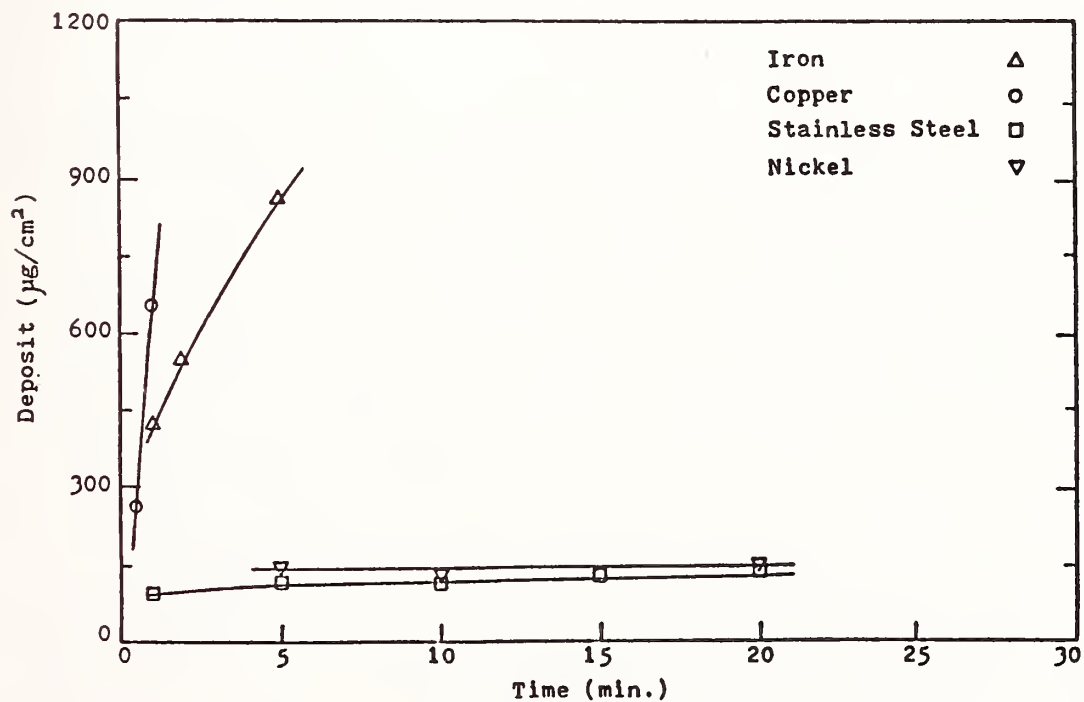

Figure 21. Deposition curves for 0.126% TCP in air stream on four metal substrates at 700°C.

21

significant when the metal substrate has a strong catalytic effect. Figures 18-21 show that the presence of air causes a significant increase in the deposition rate on the catalytic substrates iron and copper. The deposition rate on iron in the presence of air is initially high but gradually decreases with increasing coating thickness indicating that the catalytic effect of iron decreases with coating thickness. Tests on copper were limited to short time tests since the thick coatings would not adhere to the metal surface.

The catalytic effect of copper has not diminished even when relatively thick coatings have formed. These data clearly show that both iron and copper have significant catalytic effects in the presence of air. The deposition data on stainless steel shows that the effect of stainless steel is similar in both nitrogen and air. Stainless steel shows some catalytic activity at short exposure times, but this effect soon diminishes with coating thickness. The initial catalytic effect of stainless steel is more significant with higher TCP vapor concentrations. The initial deposition rate is higher in air than in nitrogen. Deposition data on nickel at low TCP vapor concentrations (figs. 18,20) show that in both air and nitrogen nickel is non-catalytic. At higher TCP vapor concentrations (figs. 19,21) it is observed that in nitrogen nickel remains non-catalytic, but in air a high deposition rate at short exposure times indicates some catalytic activity. This initial high rate is soon diminished to a non-catalytic constant rate. It is possible that the initial weight increase of nickel in air may be associated with oxidation of this substrate. These data clearly show that the carrier gas composition has a significant effect on the relative catalytic activity of metal substrates and the presence of air accelerates the rate of deposition.

SEM and EDAX Analysis: The morphology of the TCP deposits formed on stainless steel, iron, and copper were examined using scanning electron microscopy (SEM). Figure 22 shows the uncoated stainless steel surface. Figures 23-29 are SEM micrographs of TCP deposits on stainless steel ranging in thickness from 40 $\mu g/cm^2$ a relatively thin coating to 570 $\mu g/cm^2$, a relatively thick coating. All deposits were formed using 1.55% TCP in nitrogen at 700°C. These photographs show that the deposits have a granular structure. In relatively thin coatings, the granules appear smaller. As the coating thickness increases the granules appear to be larger. It is not clear whether the smaller granules grow to become larger or whether they are covered by another layer of larger granules. This increase in granular size with increase in coating thickness could be responsible for the reduction in the catalytic effect of stainless steel with coating thickness. These large granular structures could be acting as a diffusion barrier. There is less iron available for reaction and therefore, its catalytic effect on coating formation decreases. Figures 28 and 29 show the morphology of the deposit as a function of coating depth. The structure close to the metal surface appears to be porous. There is an apparent decrease in porosity with larger granular size as the coating depth increases. These photographs suggest that the overall coating may not be a liquid at the deposition temperature but rather an amorphous solid. Also, attempts to melt the resulting coating support the conclusion that the coating exhibits solid-like behavior at the deposition

temperature. SEM micrographs of TCP deposits on iron are shown in figures 30-35. SEM micrograph of uncoated iron surface is shown in figure 30. All deposits were formed using 1.55% TCP in nitrogen at 700°C. Figures 31-35 show deposits on iron ranging from 61 to 1200 μg/cm^2. The deposits on iron appear granular. The granules are smaller in thin coatings and larger in relatively thicker coatings. This increase in size of granules and corresponding decrease in availability of iron may be the cause of the diminishing catalytic effect of iron with increasing coating thickness.

Figure 35 shows a side view of the coating as a function of depth. This figure shows that the coating is relatively porous close to the surface, and relatively non-porous on top, away from the surface. Figures 37-40 show TCP deposits on copper: figure 36 is an SEM micrograph of uncoated copper surface. All deposits were formed using 1.55% TCP in nitrogen at 700°C. The coating thicknesses on copper range from 194 to 4000 μg/cm^2. TCP deposits on copper have a granular structure somewhat different from the deposits on iron. The granules appear to have a coarser texture. In figure 40, 4000 μg/cm^2 coating thickness, there appears to be some secondary growth on the granules. The granular size appears to be larger with increasing coating thickness. Figure 39 shows a side view of the coating. The deposit appears porous closer to the surface. Away from the surface the deposit appears to be more uniform.

The relative elemental composition of TCP deposits on iron and copper were examined using Energy Dispersive Analytical X-Ray Spectroscopy (EDAX). The deposits were formed using 1.55% TCP in nitrogen at 700°C for 30 minutes. The EDAX spectrum are shown in figures 41-42. The corresponding SEM micrographs are shown in figures 43-45. These data indicate that for deposits on iron, iron to phosphorous ratio is higher in coating material next to the surface compared to coating material away from the surface. The iron-to-phosphorous ratio next to the surface is approximately 1.5 to 1, while away from the surface the ratio is 0.75 to 1. The decrease in iron catalytic effect with increasing coating thickness is due to this decrease in availability of iron. For TCP deposits on copper, the ratio of elemental composition of copper to phosphorous on the top side of the chip away from the surface is 1.6 to 1. For both iron and copper a substantial concentration of metal is in the deposit. The strong catalytic effect of iron and copper in TCP vapor deposition is related to this increased availability of the substrate.

Figures 22 through 29 are SEM photos taken on stainless steel wire surfaces exposed to 1.55% TCP in nitrogen stream at 700°C. On figures 22 to 27, magnifications are 1,000X and 10,000X on the left frame and the right frame, respectively. The square window on the left frame is magnified 10 times and shown on the right frame.
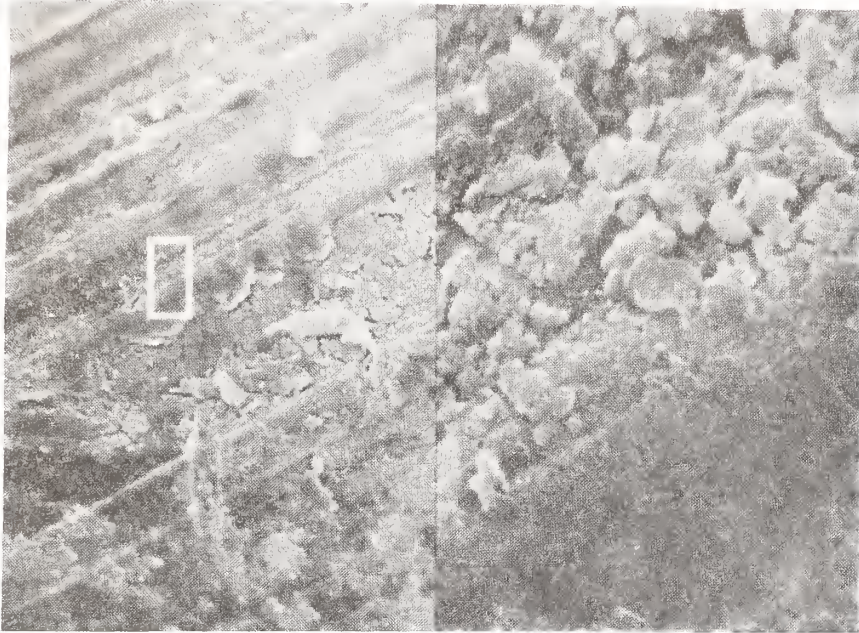

Figure 22.   Stainless steel wire surface (uncoated).

Figure 23.   2-second exposure forming a deposit of 40 µg/cm².

Figure 24. 5-second exposure forming a deposit of 55 µg/cm².
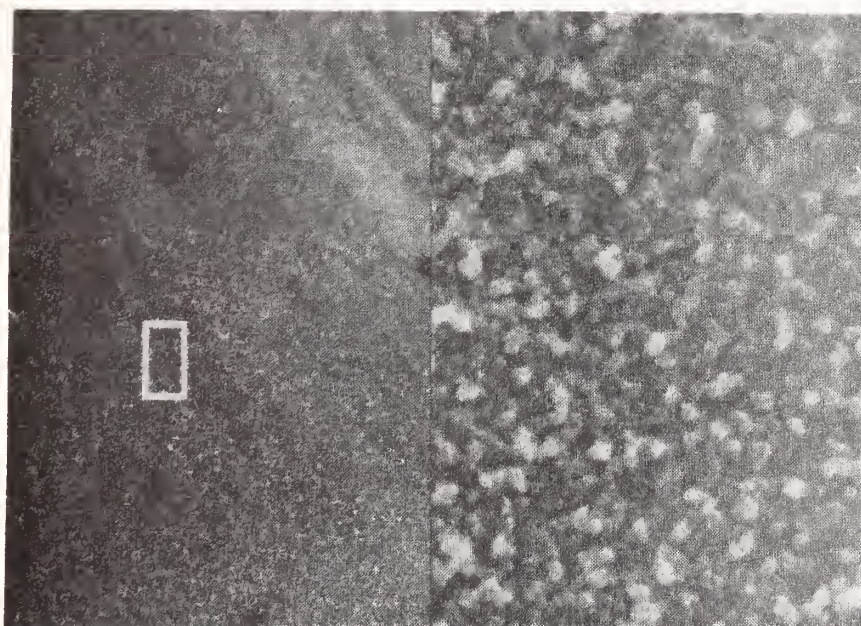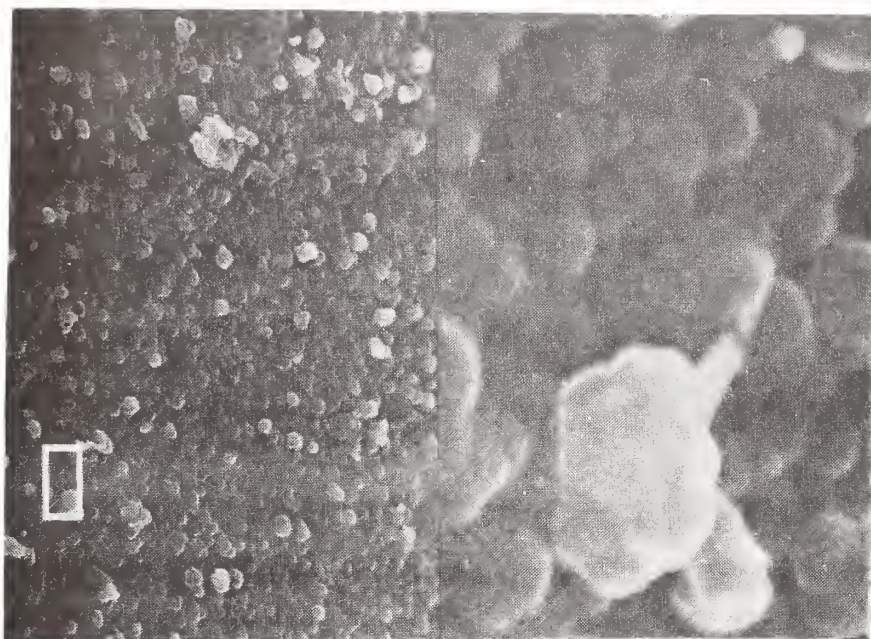

Figure 25. 1-minute exposure forming a deposit of 102 µg/cm².

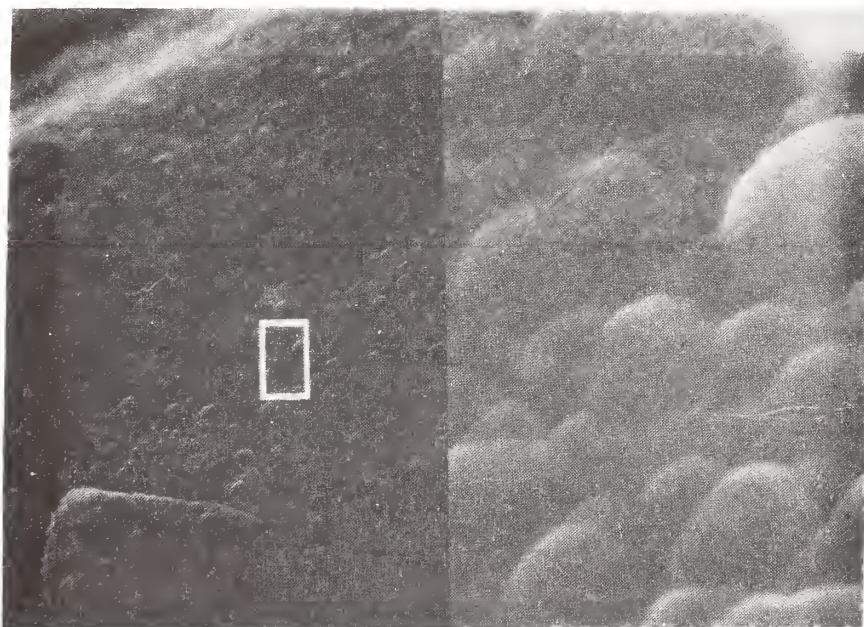Figure 26.   10-minute exposure forming a deposit of 273 µg/cm².

Figure 27.   30-minute exposure. The actual deposit could not be measured due to the coating cracking off after cooling down to room temperature. It is, however, estimated to be 570 µg/cm².
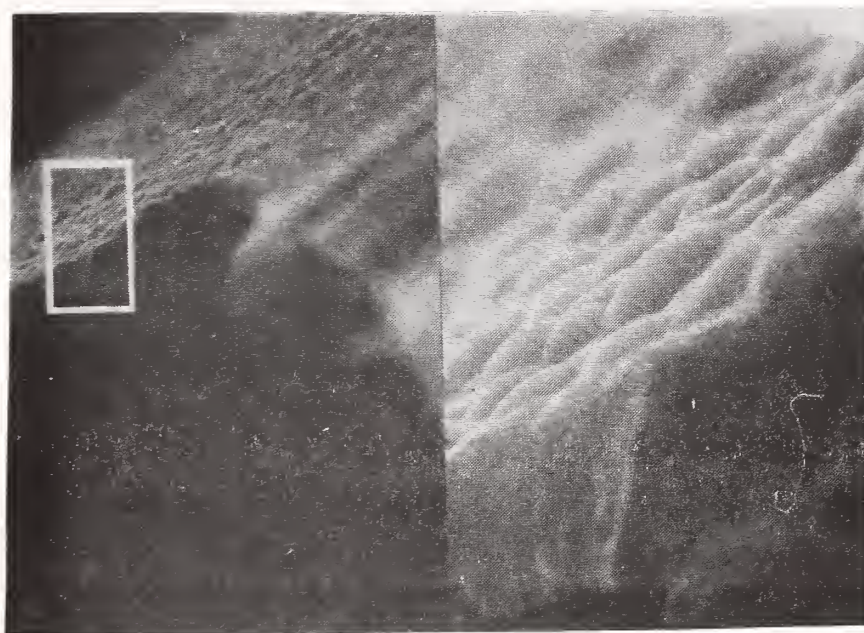
Figure 28. Sideview on the cracked coating of figure 27. Magnification is 2,000X on the left frame. The square window on the left frame is magnified 5 times and shown on the right frame.
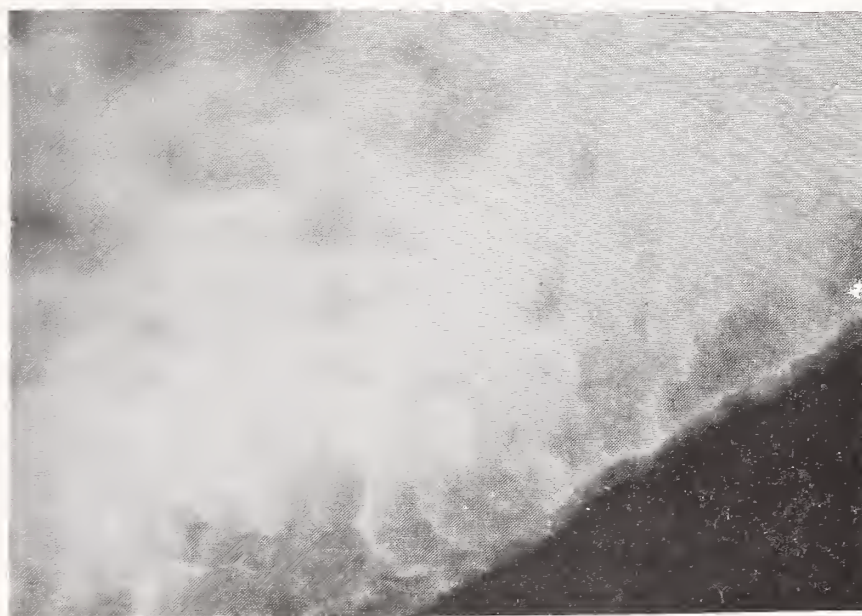

Figure 29. Sideview on the coating of figure 25 after making a scratch using a razor blade. Magnification is 50,000X.
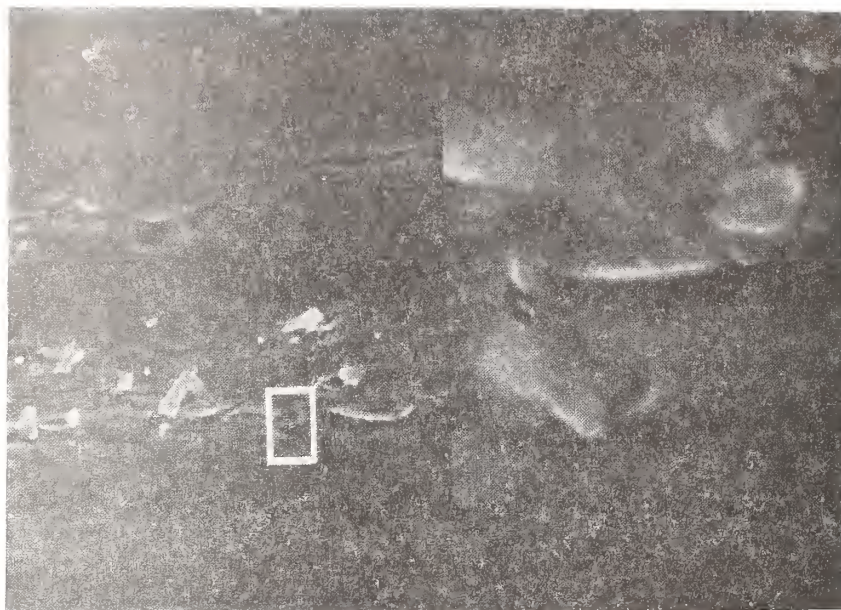
27

Figure 30.   SEM photograph of an iron wire surface. Magnification is 1000X
             on the left frame. The square window on the left frame is magnified
             10 times and shown on the right frame. Each marker represents the
             length on its frame.

Figure 31.   SEM photograph of a deposit 61 $\mu g/cm^2$ on an iron wire surface for
             2 seconds with 1.55% TCP at 700°C. Magnification is 1000X on the
             left frame. The square window on the left frame is magnified 10
             times and shown on the right frame. Each marker represents the
             length on its frame.

Figure 32. SEM photograph of a deposit 100 μg/cm² on an iron wire surface for 5 seconds with 1.55% TCP at 700°C. Magnification is 1000X on the left frame. The square window on the left frame is magnified 10 times and shown on the right frame. Each marker represents the length on its frame.
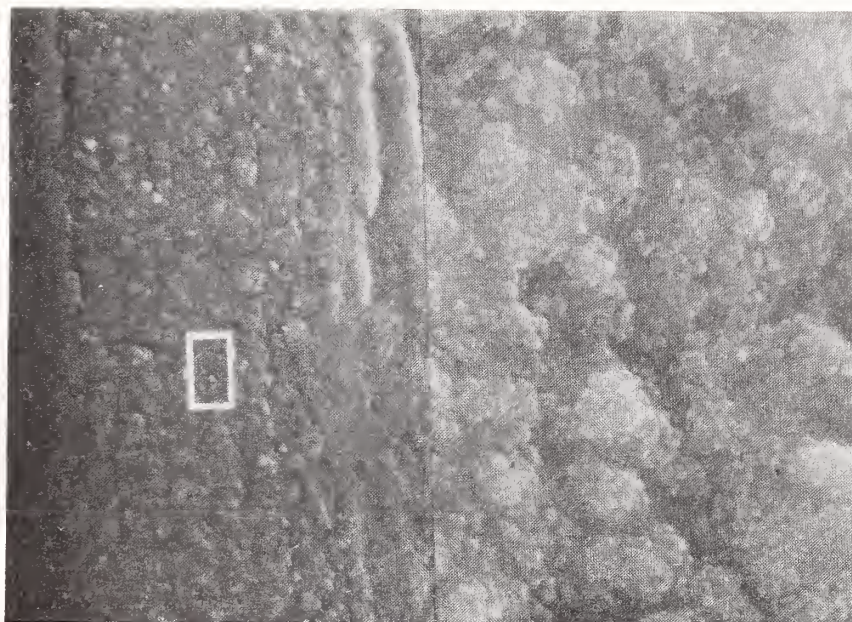

Figure 33. SEM photograph of a deposit 678 μg/cm² on an iron wire surface for 5 minutes with 1.55% TCP at 700°C. Magnification is 1000X on the left frame. The square window on the left frame is magnified 10 times and shown on the right frame. Each marker represents the length on its frame.
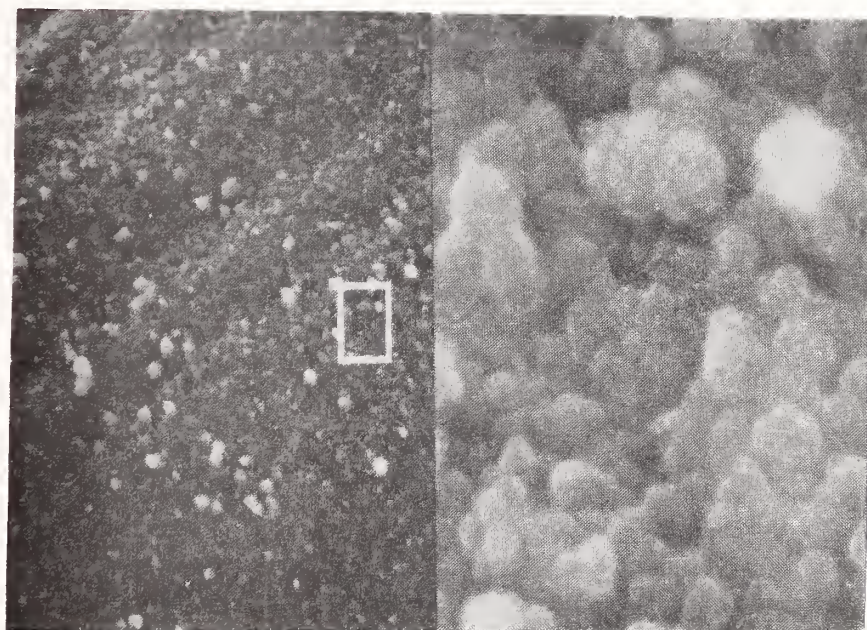
Figure 34. SEM photograph of a deposit 1200 µg/cm² on an iron wire surface for 30 minutes with 1.55% TCP at 700°C. Magnification is 2000X on the left frame. The square window on the left frame is magnified 5X and shown on the right frame. Each marker represents the length on its frame.

Figure 35. SEM photograph of a sideview of a deposit after fracturing the coating on the iron wire surface. (Same condition as fig. 34.) Magnification is 3000X. Marker represents the length.

Figure 36.   SEM photograph of a copper wire surface. Magnification is 1000X
on the left frame. The square window on the left frame is
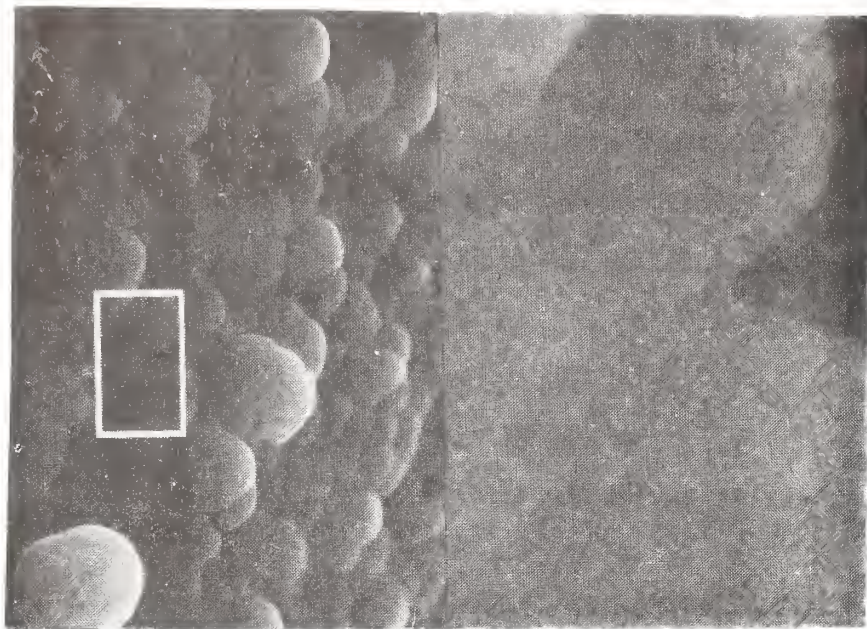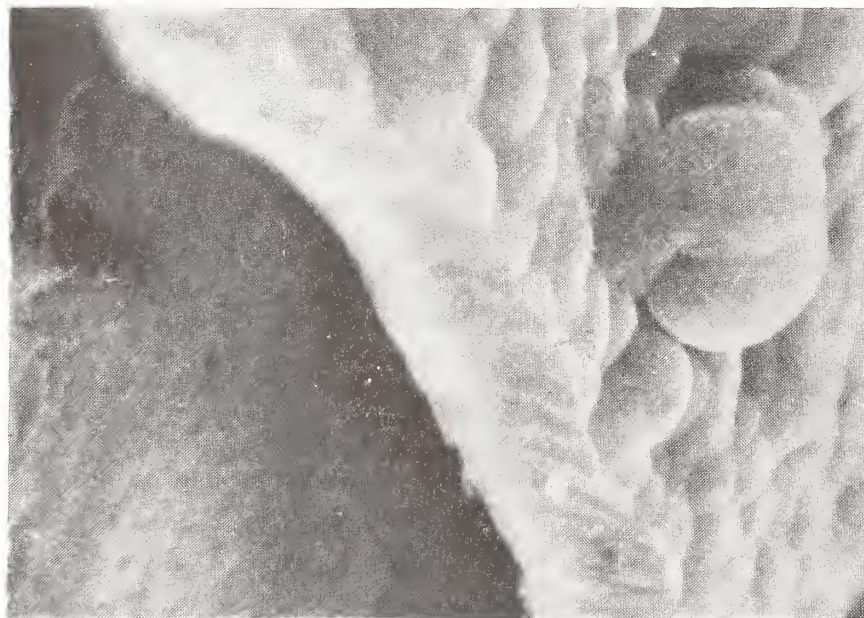magnified 10X and shown on the right frame. Each marker represents
the length on its frame.
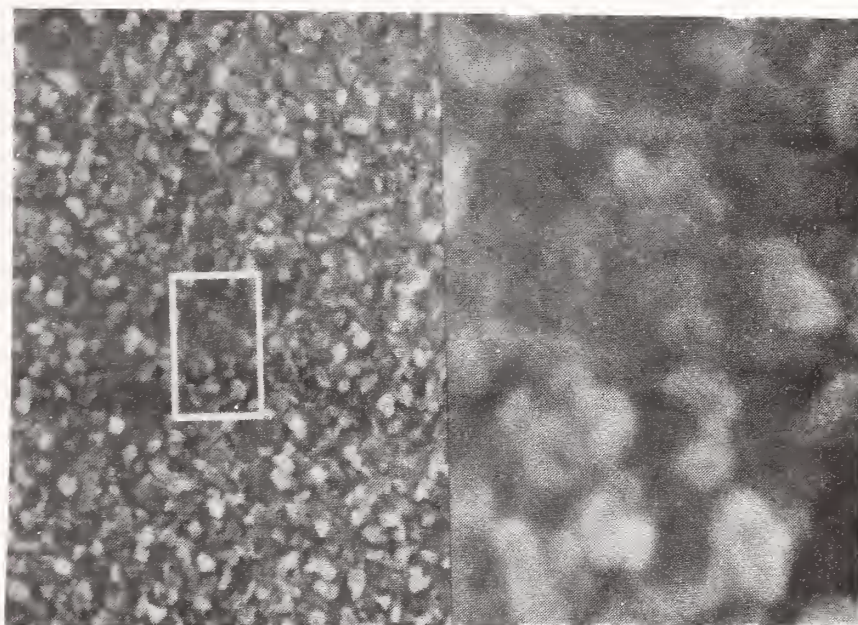
Figure 37.   SEM photograph of a deposit 194 µg/cm² on a copper wire surface
for 30 seconds with 1.55% TCP at 700°C. Magnification is 2000X
on the left frame. The square window on the left frame is
magnified 5X and shown on the right frame. Each marker represents
the length on its frame.

31

Figure 38.   SEM photograph of a deposit 1260 μg/cm² on a copper wire surface
for 5 minutes with 1.55% TCP at 700°C. Magnification is 1000X on
the left frame.   The square window on the left frame is magnified
10X and shown on the right frame. Each marker represents the
length on its frame.
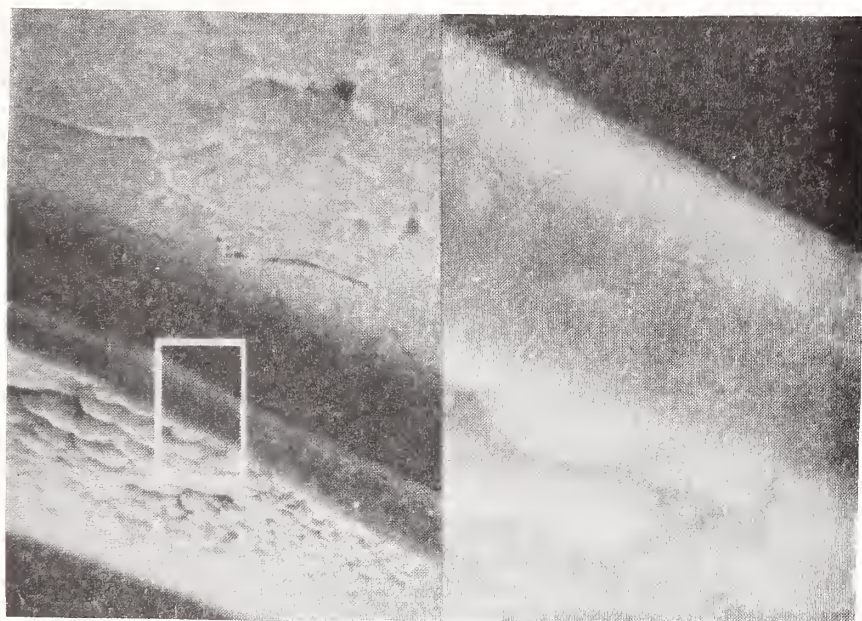
Figure 39.   SEM photograph of a heavily deposited copper wire surface for 20
minutes with 1.55% TCP at 700°C. The actual deposit could not be
obtained due to the coating cracking off when cooling down to room
temperature. However, it is estimated to be 4000 µg/cm². Note that
the upper right on the left frame is nearly the uncoated copper
surface after the deposit cracking off. Magnification is 573X on
the left frame. The square window on the left frame is magnified
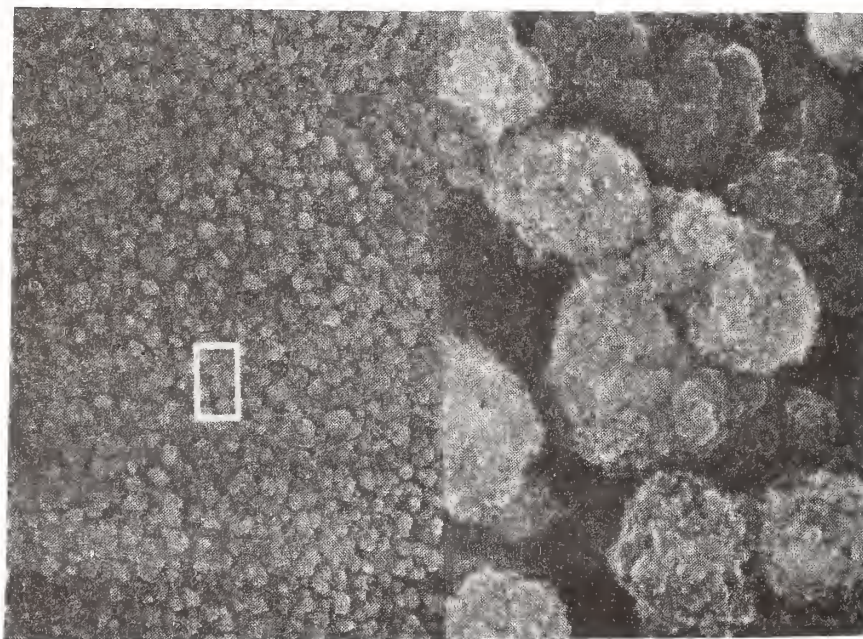5X and shown on the right frame. Each marker represents the length
on its frame.
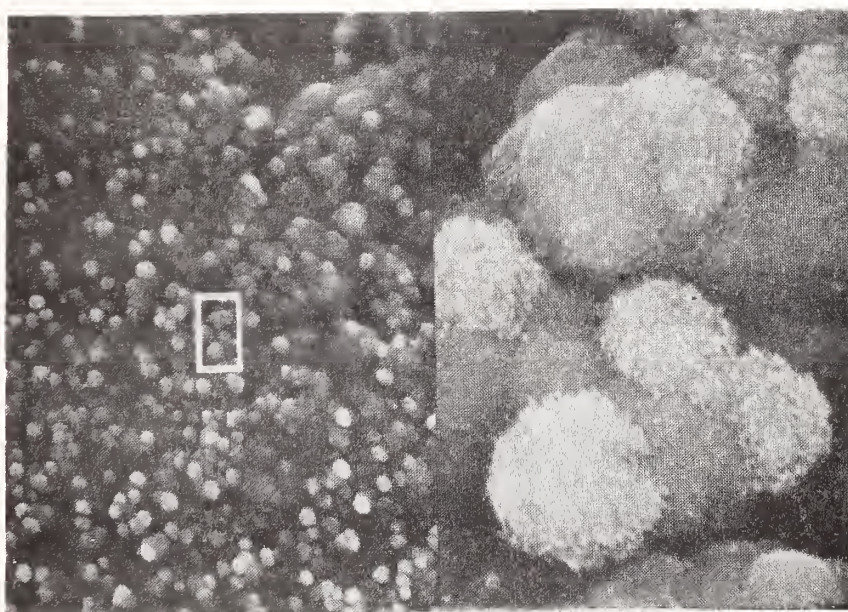
Figure 40.   Top view on the coating of figure 39. Magnification is 1000X on
the left frame. The square window on the left frame is magnified
10X and shown on the right frame. Each marker represents the
length on its frame.
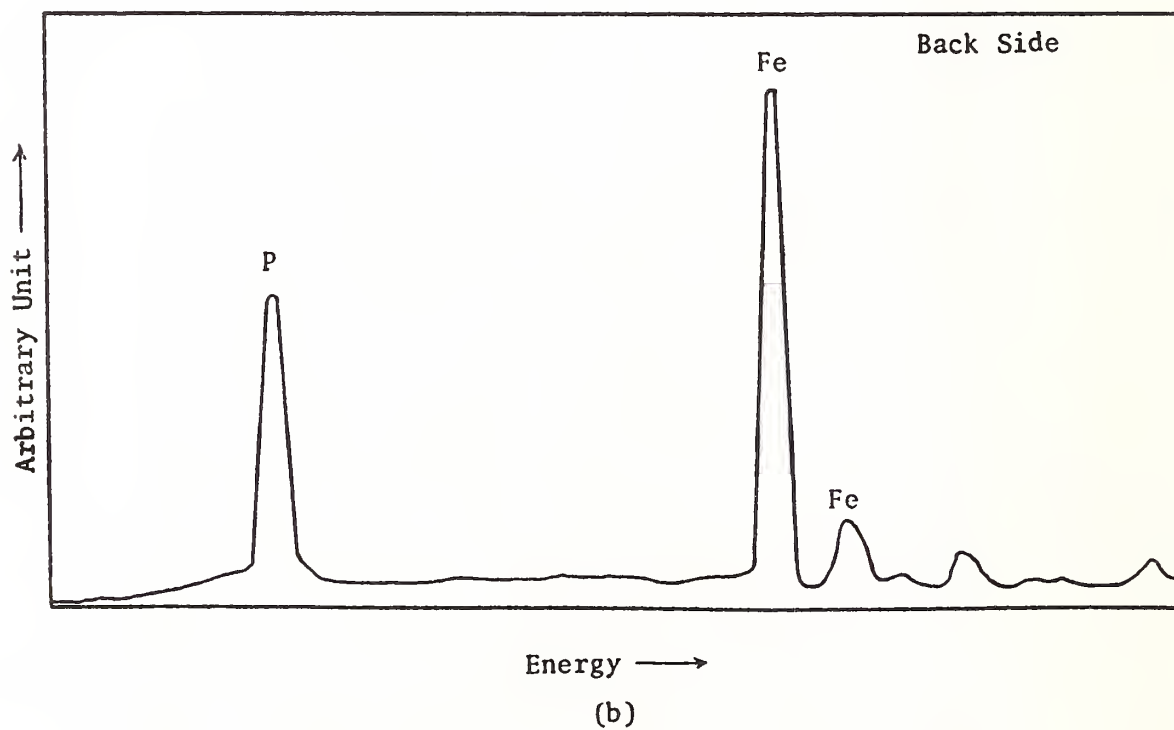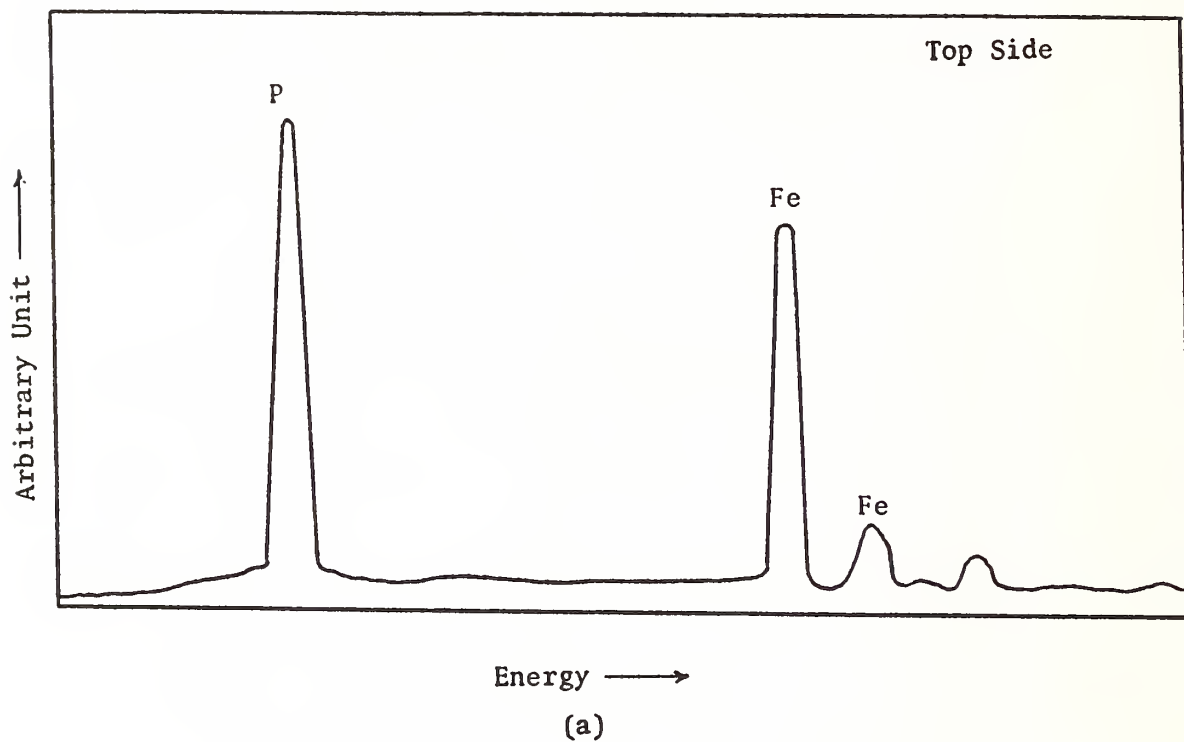
Figure 41. EDAX spectra with incident electrons illuminating the top side (a) and the back side (b) of cracked chips from TCP deposit on iron wire.
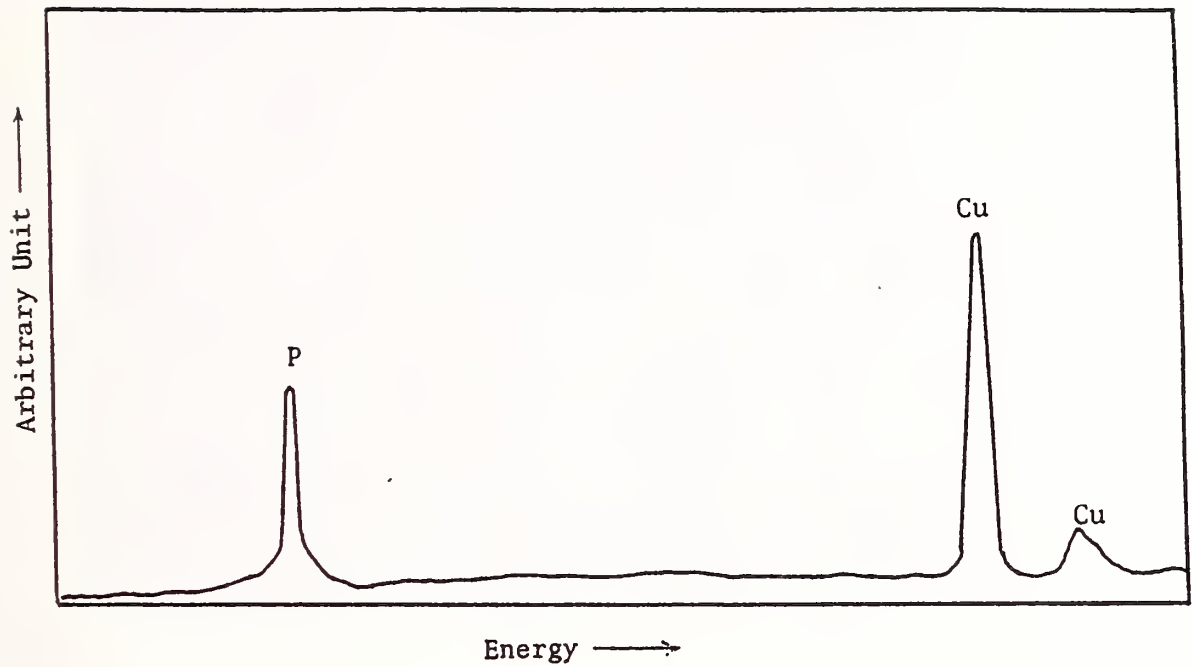
Figure 42.   EDAX spectrum with incident electrons illuminating the top side of
a cracked chip from TCP deposit on copper wire.
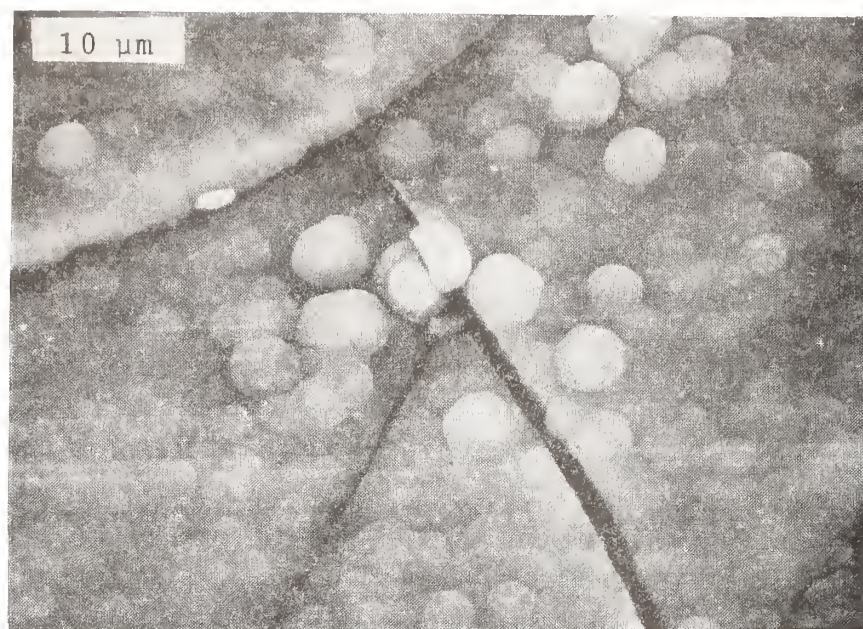
Figure 43.   EDAX illuminated area of a cracked chip (top side) from TCP
             deposit on iron wire.
             Magnification is 2000X.

Figure 44.   EDAX illuminated area of a cracked chip (backside) from TCP
             deposit on iron wire.
             Magnification is 5700X.

36
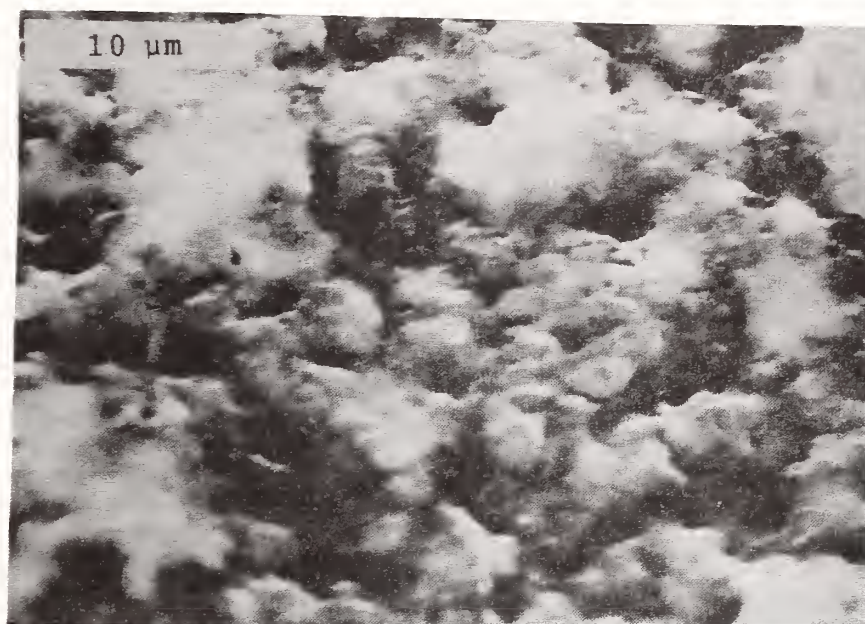
Figure 45. EDAX illuminated area of a cracked chip from TCP deposit
            on copper wire.
            Magnification is 3000X.

B. Diphenyl Ditertiarybutylphenyl Phosphate (GT)

Vapor deposition characteristics of GT on copper, iron, stainless steel, and nickel substrates were examined. Deposition tests were conducted in nitrogen and air. Figures 46-48 show deposit data for GT in nitrogen at 700°C. For this series of tests the GT vapor concentration in nitrogen was varied from 0.013 to 1.75%. These data clearly indicate that both the substrate material and lubricant vapor concentration have a significant effect on GT deposition rate. Deposition rates on iron and copper indicate that iron and copper have a strong catalytic effect at both low and high GT vapor concentrations. Copper maintains its strong catalytic effect for the duration of the test whereas iron shows a diminishing catalytic effect with increasing coating thickness. This decrease in iron catalytic effect with coating thickness is evident at all three GT vapor concentrations. The diminishing catalytic effect of iron is indicative of a decrease in the availability of iron with increasing coating thickness. Stainless steel and nickel in contrast to iron and copper have significantly less influence on GT vapor deposition. Stainless steel shows an initial deposition rate indicative of a catalytic effect at short exposure times; this rate soon diminishes to a non-catalytic constant rate. Nickel shows little or no catalytic effect under these conditions. Comparison of figures 46-48 clearly indicates that an increase in GT vapor concentration increases the rate of deposition but does not change the relative catalytic effects of the substrates. These trends on effect of GT vapor concentration and effect of metal substrate on deposition rate are consistent with the trends observed from the deposit data on TCP vapor deposition.

The effect of changing the carrier gas from nitrogen to air on GT vapor deposition was examined. The oxygen in air could have a significant effect on GT deposition. Figure 49 shows deposition rates on copper, iron, stainless steel, and nickel for tests conducted using 0.106% GT in air at 700°C. The influence of oxygen on the rate of GT deposition is demonstrated by a comparison of figures 47 and 49. The experimental conditions used to obtain the data presented in these two figures are identical except that nitrogen was used as the carrier gas for data presented in figure 47 while air was used as the carrier gas for the data presented in figure 49. The data show the presence of oxygen in the carrier gas does not cause any significant change in the deposition rate. The effect of oxygen on GT deposition rate essentially follows the same trends that were observed with TCP deposition. In figure 49, the arrows on the symbols for deposits on copper and iron signify that not all of the deposits were measurable because part of the coating cracked off of the substrate when the substrate was cooled from the test temperature of 700°C to room temperature. The thickness of the coatings gave some integrity to the deposit and upon cooling the differences in the coefficient of expansion of the coating and the metal substrate caused part of the coating to crack and flake off the metal substrate.

38

The morphology of GT vapor deposited films was examined using Scanning Electron Microscopy. Figure 50 is an SEM micrograph of GT deposit on stainless steel of 72 μg/cm^2 thickness. This relatively thin coating has a granular structure somewhat similar to TCP coatings of the same film thickness on stainless steel and iron. Since the deposition behavior for GT is similar to that for TCP, it would be expected that thicker GT coatings have a larger granular structure that is relatively non-porous similar to that for TCP. This would be consistent with the diminishing catalytic effect of iron with thick coatings. The larger granules could impede diffusion and migration of iron or iron compounds through the coating to contact the lubricant vapor. This decreased availability of iron can cause a diminishing catalytic effect for GT deposition.

Figure 46. Deposit thickness versus time for various substrates exposed to a vapor concentration of 0.013% GT in nitrogen stream at 700°C.

Figure 47. Deposit thickness versus time for various substrates exposed to a vapor concentration of 0.106% GT in nitrogen stream at 700°C.
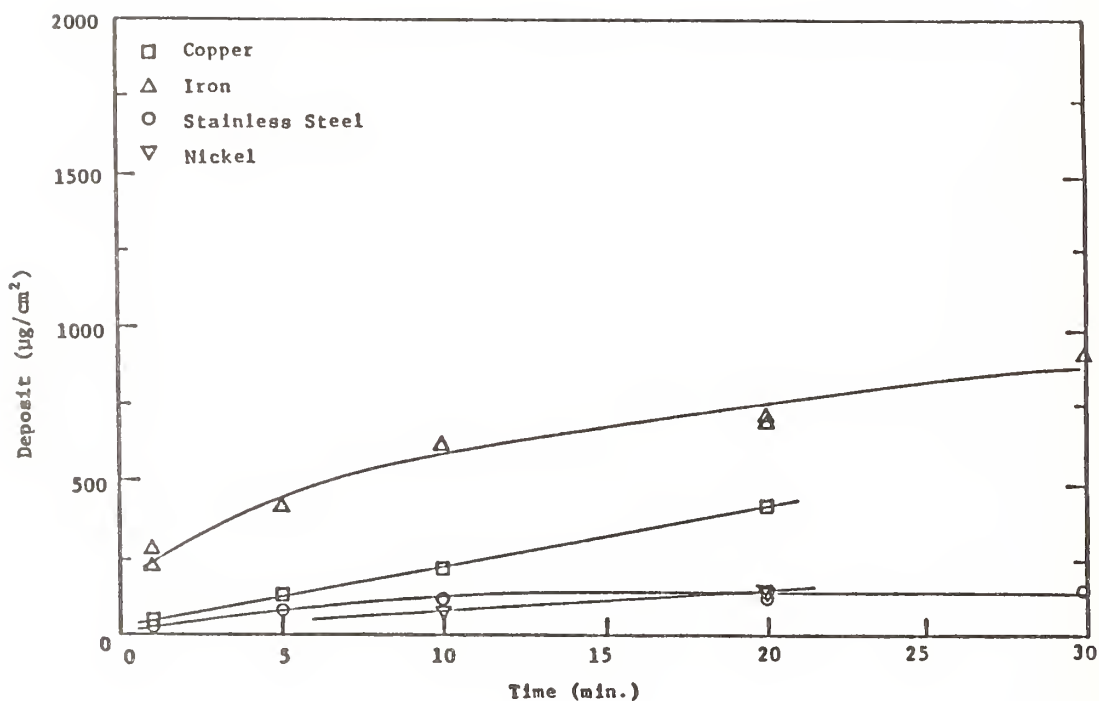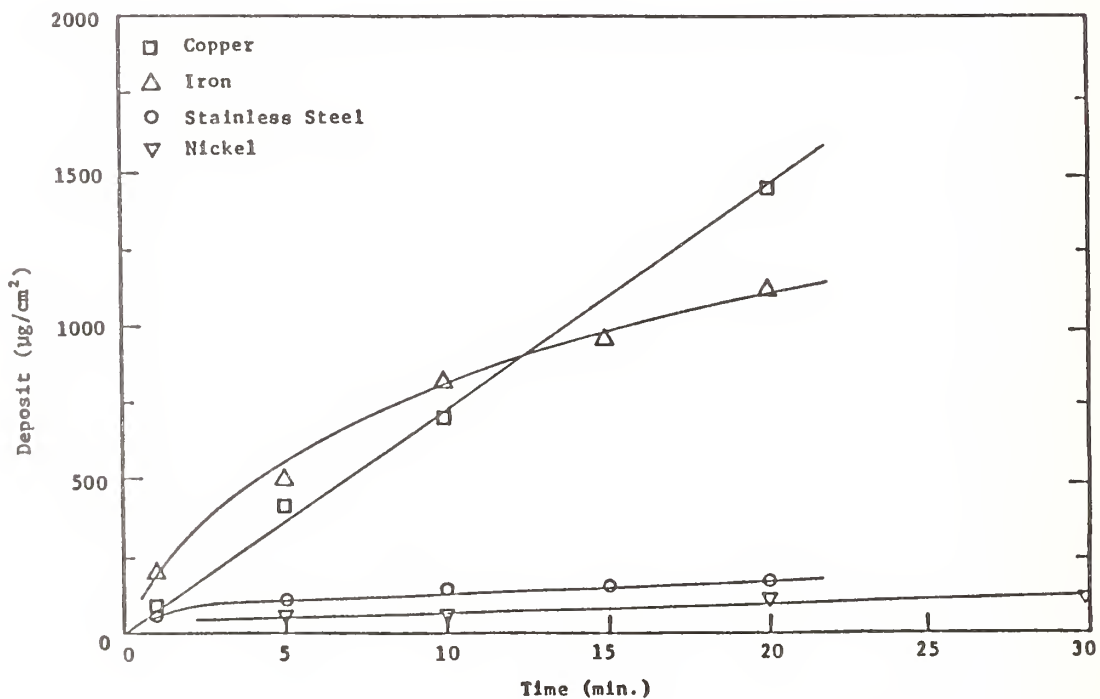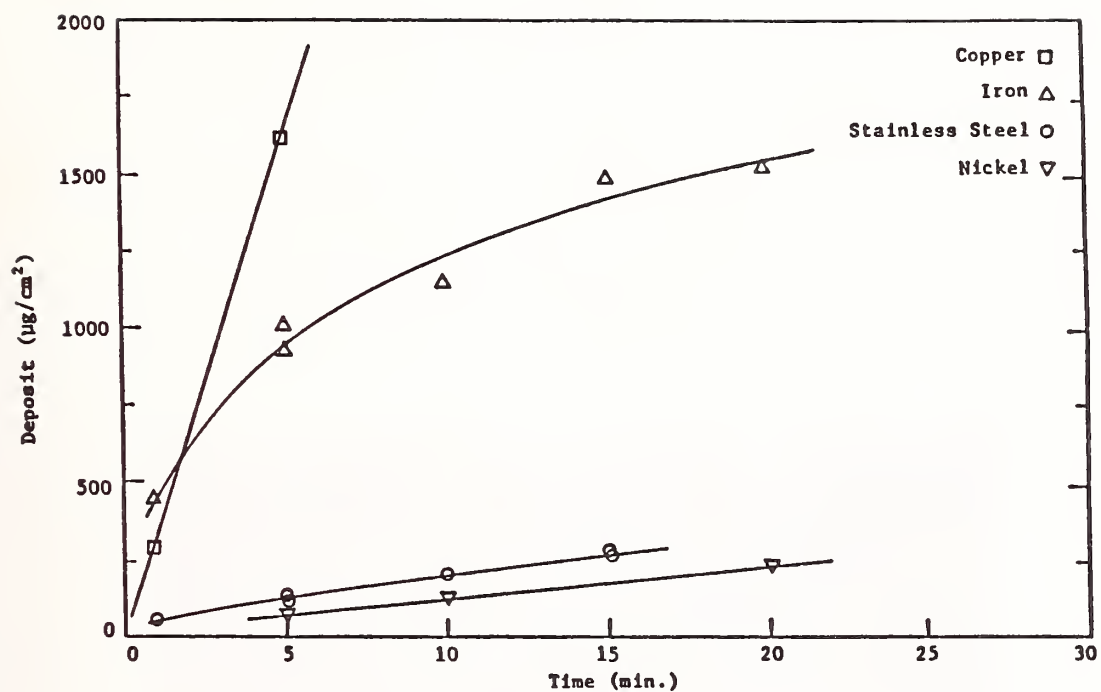
Figure 48.   Deposit thickness versus time for various substrates exposed to a
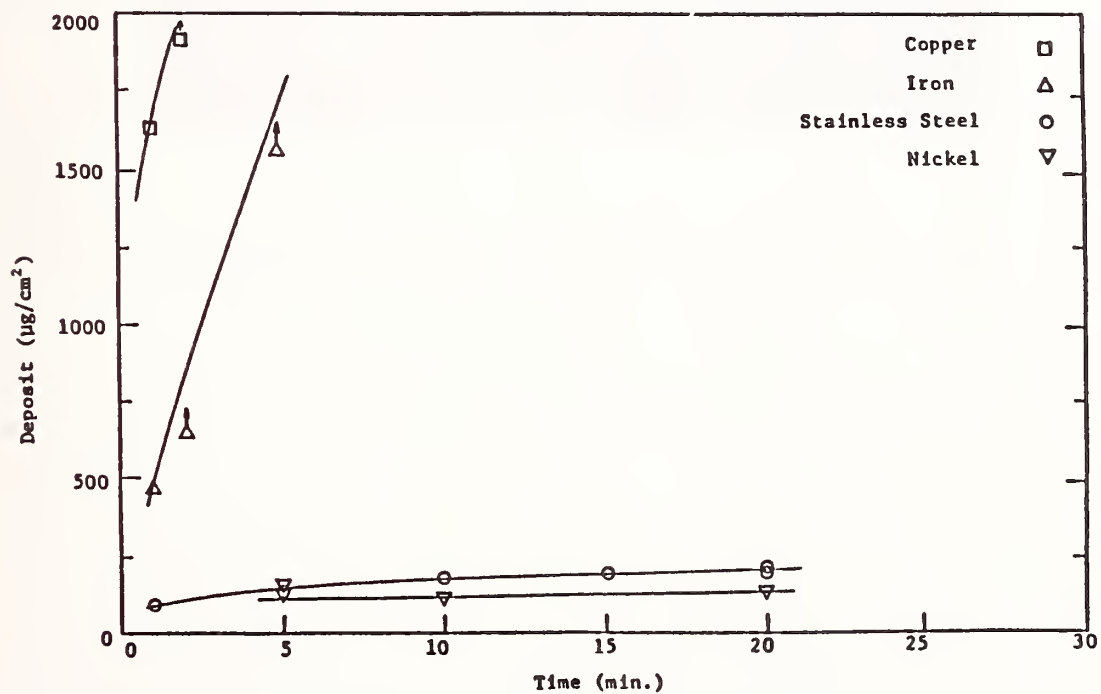vapor concentration of 1.75% GT in nitrogen stream at 700°C.

Figure 49.   Deposit thickness versus time for various substrates exposed to
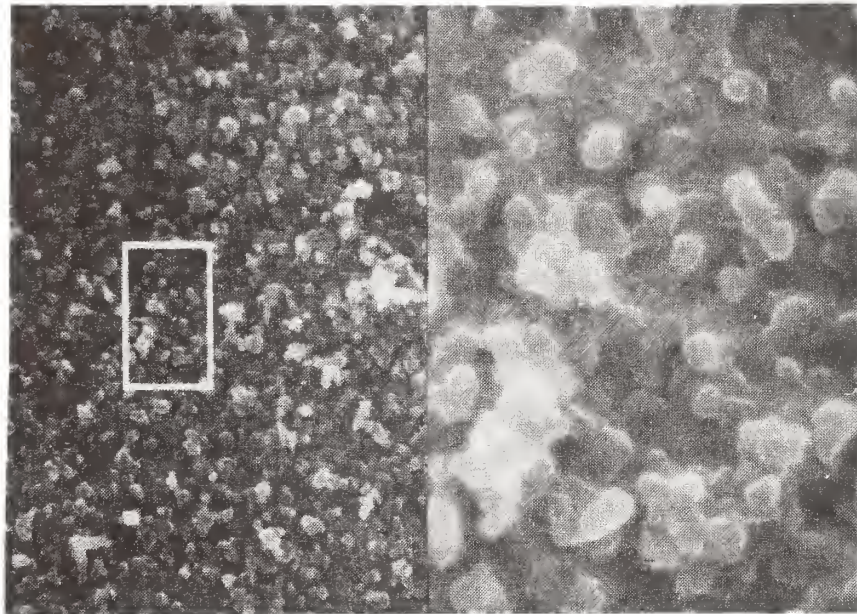a vapor concentration of 0.106% GT in air stream at 700°C.

Figure 50. SEM: 1000X. Stainless steel target at 700°C exposed 1 minute at 1.75% GT, 72 µg/cm².

C. Polyphenyl Ether (PPE)

The vapor deposition characteristics of PPE vapor were investigated.
The effect of metal substrate, operating temperature, and PPE vapor
concentration on deposition rate was examined. Tests were conducted using
copper, stainless steel, nickel, and iron substrates.

The effect of metal substrate on PPE deposition rate is shown in
figure 51. For this series of tests 1.0% PPE vapor concentration was used
in a nitrogen stream at 700°C. It is observed that for all four metals the
PPE deposition rate is linear from time zero for the duration of the test.
The deposition rates are different for each metal and can be considered
metal specific. This behavior can be attributed to a catalytic effect of
these metals. The linearity of the deposition rates suggests that the
coating thickness achieved in these PPE vapor deposition tests are not
sufficient to reduce the catalytic effect of the metal. It is expected,
as with the phosphate esters, that at longer test times or more severe
conditions, after a sufficient coating depth is achieved the metal will
lose its catalytic effect and the deposition rate will reach a constant
non-catalytic rate. The highest PPE deposition rates were on iron,
followed by nickel, stainless steel, and copper. The relatively strong
catalytic effect of nickel and weak catalytic effect of copper are in
contrast to the deposition behavior in phosphate esters, where copper had a
strong catalytic effect and nickel was essentially inert.

The effect of increasing temperature on PPE deposition rate is shown
in figure 52. Tests were conducted with 1.0% PPE in nitrogen using
stainless steel and iron substrates at 700, 800, and 850°C. The deposition
rate on both metals increases as the temperature increases. At all three
temperatures the deposition rates are linear from time zero for the
duration of the tests. The coating thicknesses achieved are not sufficient
to deter the catalytic effect of the metal. The deposition rates on iron
at all three temperatures are higher than the deposition rates on stainless
steel. The lower catalytic effect of stainless steel can be attributed to
lower iron corrosion rates with stainless steel. The effect of lubricant
vapor concentration on PPE deposition rate is shown in figure 53. Tests
were conducted with 0.6 and 1.0% PPE in nitrogen using stainless steel
substrates at 700, 800, and 850°C. At all three temperatures, the
deposition rates increase with increasing PPE vapor concentration. The
deposition rates are linear from time zero for the duration of the test.
The time and severity of the tests are not sufficient to deter the
catalytic effect of the metal substrate. Again as in the case
of the phosphate esters, the lowest concentration studied is the most
efficient in producing a unit of film thickness per mole of PPE vapor.
Scanning Electron Microscopy (SEM) was used to examine the morphology of
PPE deposits. Figures 54, 55, and 56 are SEM micrographs of PPE deposits
from tests conducted using stainless steel exposed to 1.0% PPE in nitrogen
at 700 and 800°C. Figure 54 is an SEM micrograph of a relatively thin PPE
coating (60 $\mu g/cm^2$). Figures 55 and 56 are SEM micrographs of relatively
thicker PPE coatings (278 and 315 $\mu g/cm^2$). The PPE deposits appear to have
granular structure somewhat different from phosphate ester deposits. As

43

the coating thickness increases from 60 to 278 $\mu g/cm^2$, the size of the granules appears larger.

SEM micrographs of PPE deposits on iron, nickel, copper, and stainless steel are contrasted in figures 56-59. The deposits were formed using 1.0% PPE in nitrogen at 700°C. The structure of the deposits on iron and nickel appear to be similar. It should be noted that both iron and nickel had strong catalytic effects on PPE deposition. The structure of deposits on copper and stainless steel appear to be similar to each other but different from the structure of deposits on iron and nickel. The deposits on copper and stainless steel appear more granular compared to deposits on iron and nickel. The lower catalytic effect of stainless steel and copper may be related to differences in deposit structure morphology.
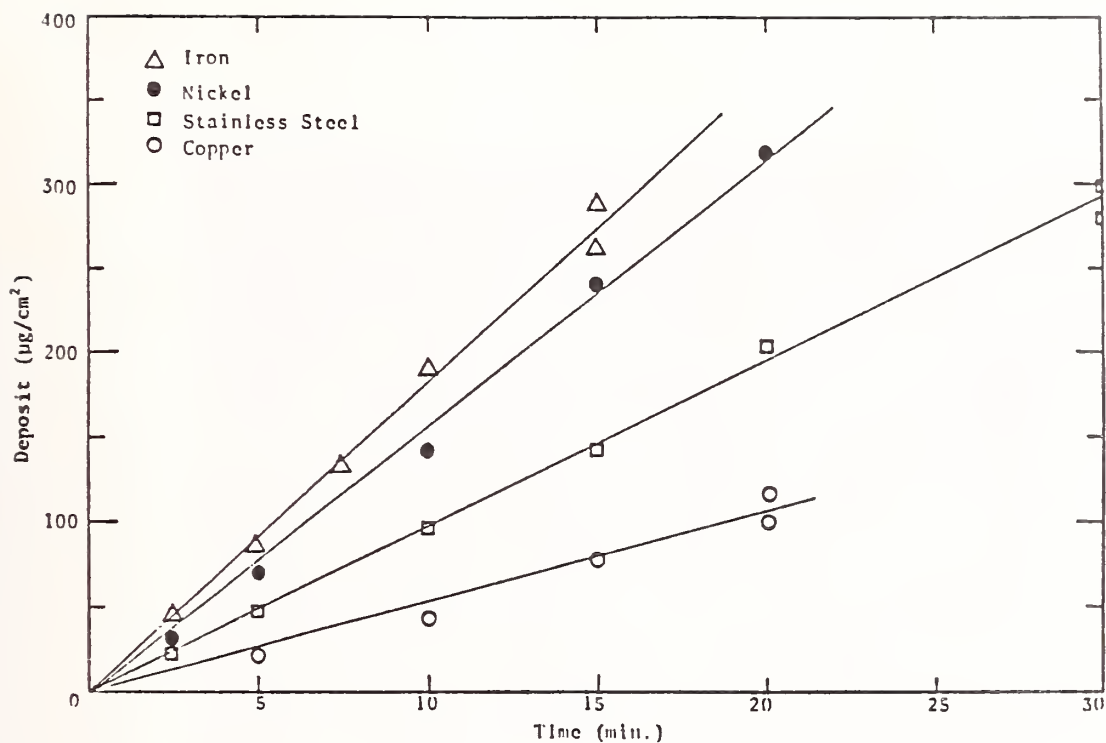
Figure 51. Deposit thickness versus time for different substrates exposed to 1.0% PPE concentration in nitrogen at 700°C.
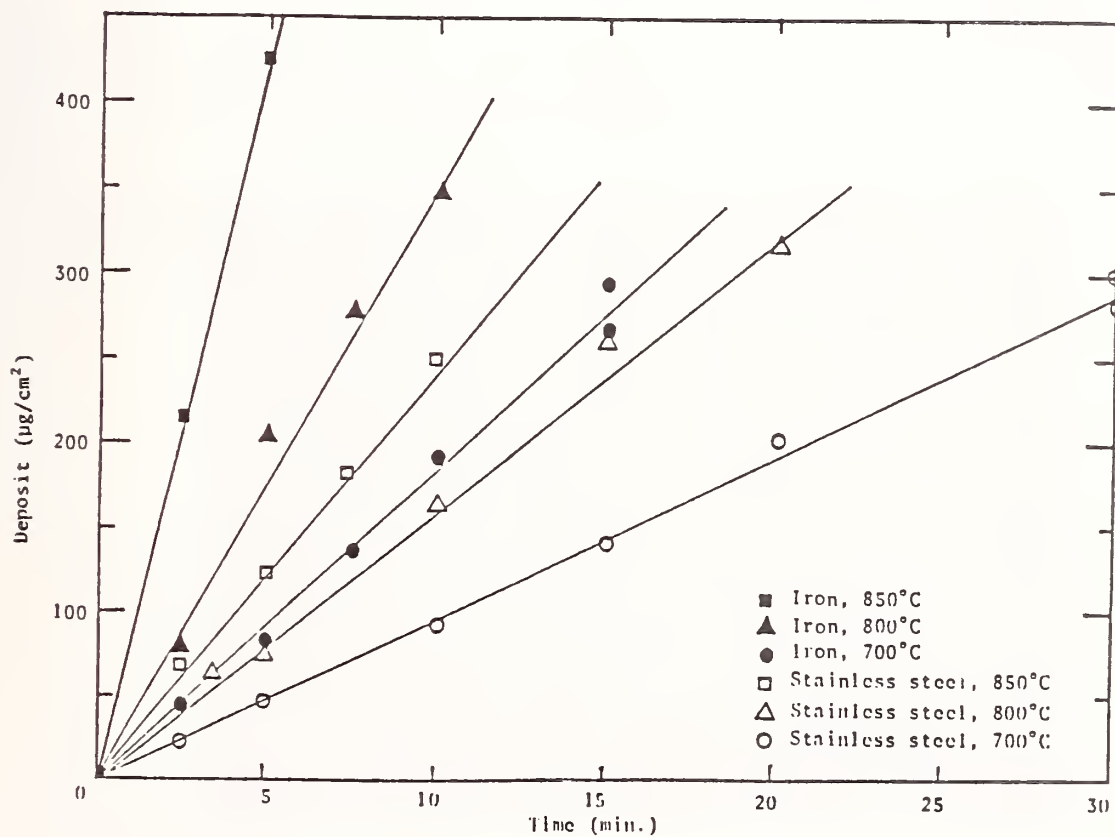
Figure 52. Deposit thickness versus time for stainless steel and iron substrates exposed to 1.0% PPE concentration in nitrogen at 700, 800, and 850°C.

45
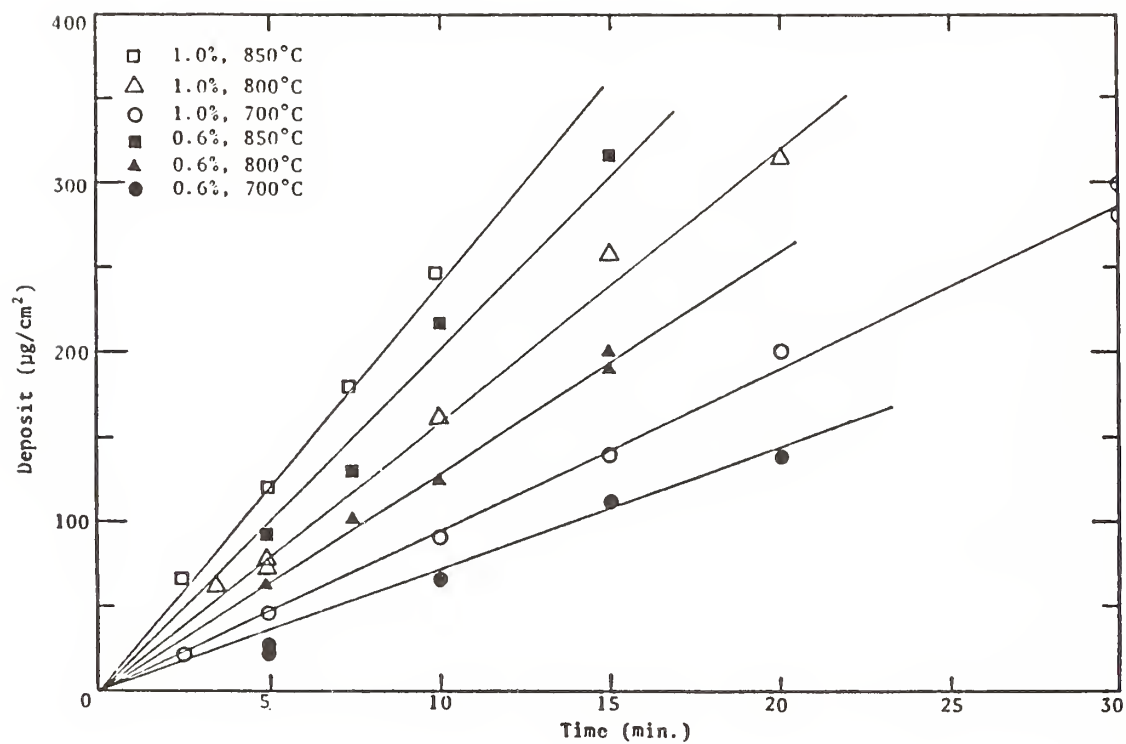
Figure 53. Deposit thickness versus time for stainless steel substrates exposed to two different PPE concentrations in nitrogen at 700, 800, and 850°C.
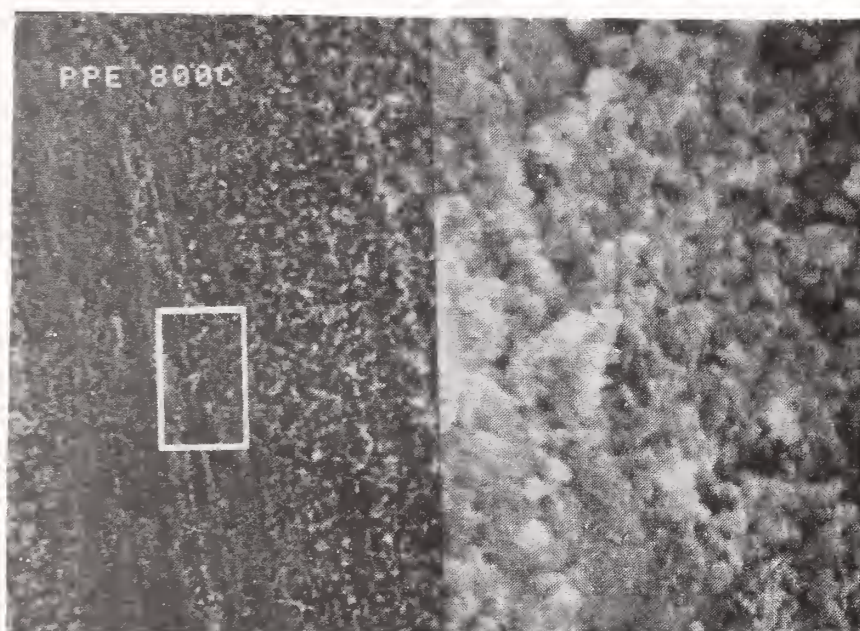
Figure 54. SEM photo of a deposit 60 μg/cm^2 on a stainless steel **wire** surface for 3.5 minutes with 1.0% PPE at 800°C. **Magnification** is 2000X on the left frame. The square window on the **left** frame is magnified 5X and shown on the **right frame.**
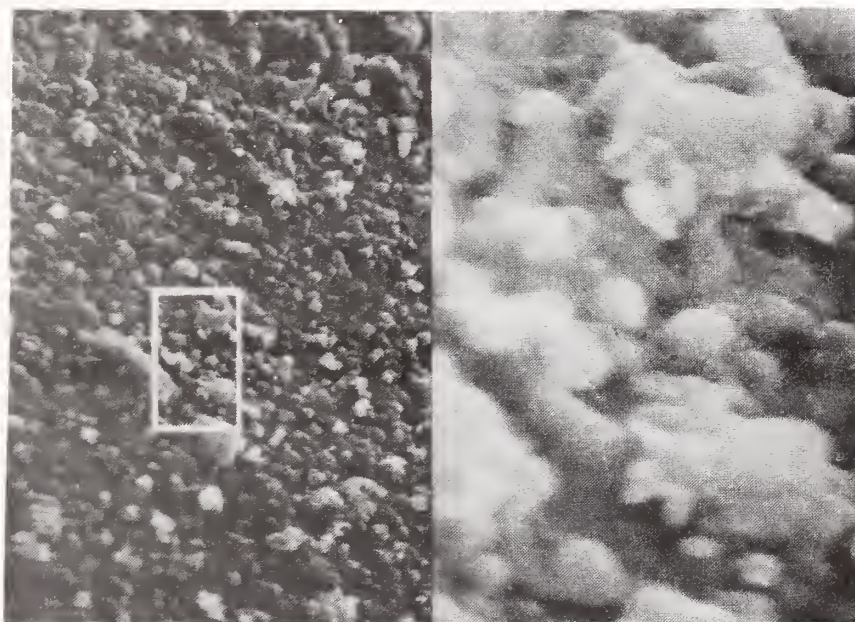
Figure 55. SEM photo of a deposit 315 μg/cm^2 on a stainless steel **wire** surface for 20 minutes with 1.0% PPE at 800°C. **Magnification** is 2000X on the left frame. The square window on the **left** frame is magnified 5X and shown on the right frame.
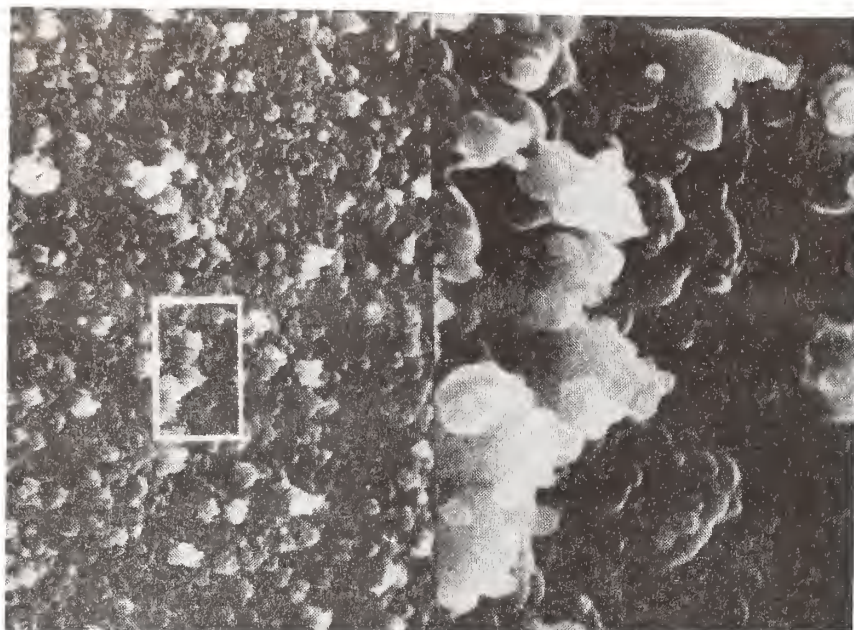
Figure 56. SEM photo of a deposit 278 $\mu g/cm^2$ on a stainless steel wire surface for 30 minutes with 1.0% PPE at 700°C. Magnification is 2000X on the left frame. The square window on the left frame is magnified 5X and shown on the right frame.
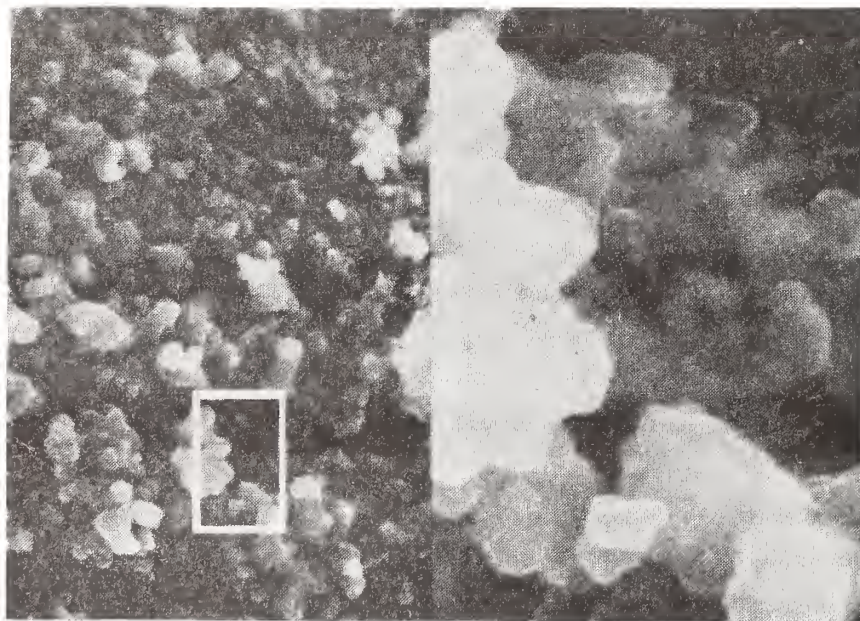
Figure 57. SEM photo of a deposit 133 $\mu g/cm^2$ on an iron wire surface for 7.5 minutes with 1.0% PPE at 700°C. Magnification is 2000X.
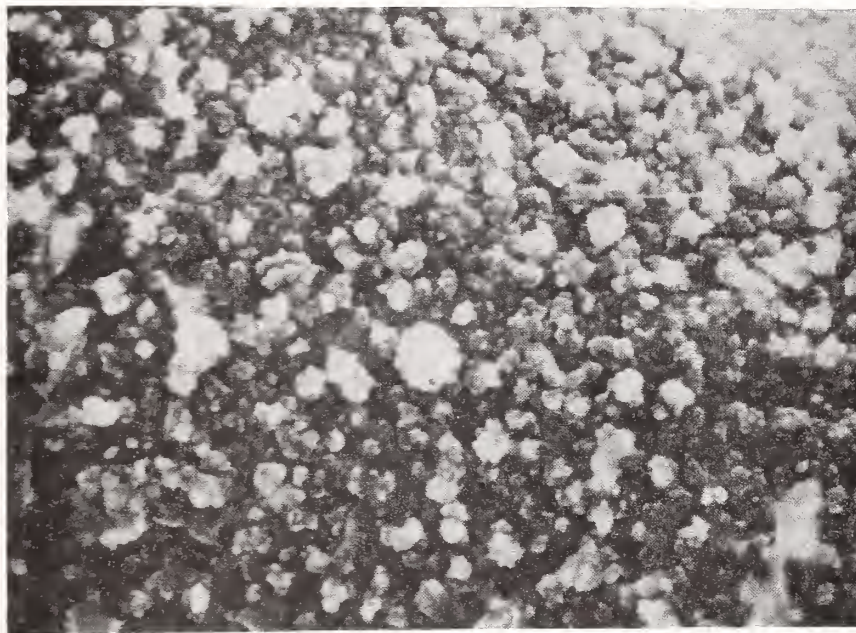
Figure 58. SEM photo of a deposit 243 $\mu g/cm^2$ on a nickel wire surface for 15 minutes with 1.0% PPE at 700°C. Magnification is 2000X.

Figure 59. SEM photo of a deposit 166 $\mu g/cm^2$ on a copper wire surface for 20 minutes with 1.0% PPE at 700°C. Magnification is 2000X.

D. Trimethylolpropane Triheptanoate (TMPTH)

The vapor deposition characteristics of TMPTH on copper, iron, stainless steel, quartz, and nickel were investigated. The effects of metal substrate, operating temperature, lubricant vapor concentration, and carrier gas composition on TMPTH deposition rate were examined.
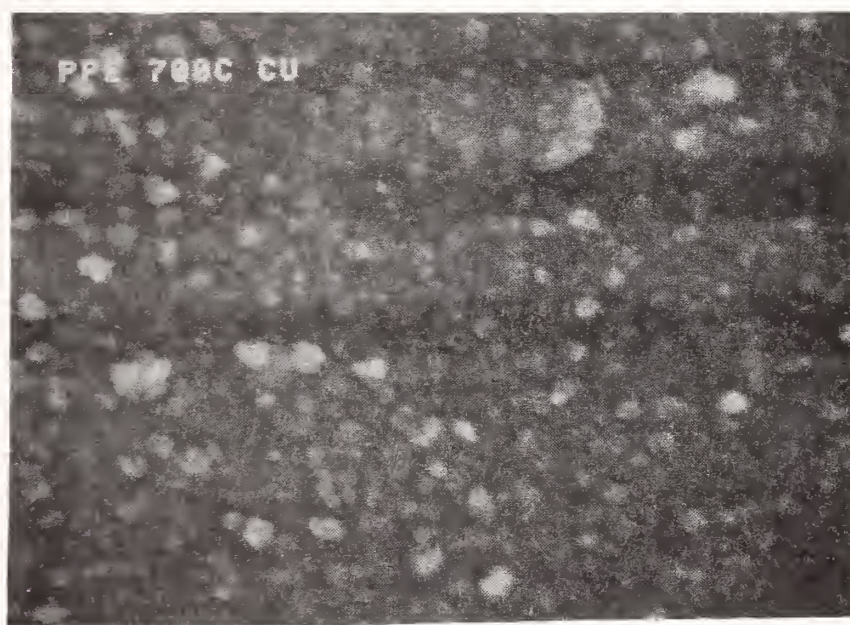
The effect of metal substrate on deposition rate is shown in figure 60. For this series of tests 1.0% TMPTH in nitrogen was used at 700°C. The data show that the deposition rates are metal specific. The deposition rates are unique for each substrate. The deposition rates on all substrates were linear from time zero for the duration of the tests. The highest rate was on iron followed by nickel, stainless steel, and copper and quartz which essentially have the same rate. The similarity of deposition rates on copper and on inert material, quartz, indicates that copper can be considered inert for TMPTH deposition. The relatively higher deposition rates on stainless steel, nickel, and iron indicate that these substrates have a catalytic effect on TMPTH deposition. The rate on iron is substantially higher than on the other substrates. The linearity of these rates indicates that for the duration and severity of these deposition tests catalytic metal substrates maintain their catalytic effect. It is expected that with thicker coatings under more severe conditions the catalytic effect of the metal substrates will diminish and the deposition rates will reach a constant non-catalytic rate similar to that on quartz. It should be noted that the effect of metal substrates on TMPTH deposition is similar to the effect of metal substrates on PPE deposition. In both cases iron had a strong catalytic effect followed by nickel and stainless steel. In both cases copper was essentially inert. In contrast to these trends, copper had a strong catalytic effect and nickel essentially no effect for deposition of phosphate esters. The order of catalytic activity observed for PPE and TMPTH deposition closely follows the order observed in hydrogenation-dehydrogenation and hydrogenolysis reactions of hydrocarbons [17].

The effect of increasing operating temperature on TMPTH deposition is shown in figure 61. Tests were conducted using 1.0% TMPTH in nitrogen using stainless steel substrates at 600, 700, and 800°C. The data show that increasing the operating temperature increases the deposition rates. At 600°C the rate appears linear from time zero. At 700 and 800°C the deposition rate decreases after 15 to 20 minutes test time. This decrease at the more severe conditions indicates a decrease in catalytic effect of the metal due to an increase in coating thickness and subsequent decrease in availability of metal. It should also be noted that at these higher temperatures the TMPTH deposit may not be stable and may be degrading [18]. Deposit degradation at these higher temperatures may be an additional factor causing an overall decrease in deposition rate.

The effect of carrier gas composition on TMPTH deposition rate is shown in figure 62. For this series of tests 1.0% TMPTH was used with stainless steel substrates at 700°C. The oxygen concentration in nitrogen carrier gas was varied from 0 to 21% by mixing nitrogen and air streams at different ratios. The data show that the highest deposition rates are in

air (21% oxygen) and the lowest in nitrogen. Increasing the oxygen concentration increases the deposition rate. 1.0% oxygen in nitrogen causes a deposition rate similar to that with just nitrogen. Increasing the oxygen concentration to 5% increases the deposition rate. Increasing the oxygen concentration to 21% increases the deposition rate further. For the conditions used in these tests the deposition rates are linear from time zero indicating that the metal catalytic effect is retained. For more severe conditions or longer test times it would be expected that the deposition rates would decrease due to diminishing catalytic effect of the metal with increasing coating thickness.

The effect of lubricant vapor concentration on TMPTH deposition rate is shown in figure 63. Tests were conducted using 0.4 and 1.0% TMPTH in nitrogen on stainless steel substrates at 700°C. The data show that increasing the TMPTH vapor concentration from 0.4 to 1.0% increases the deposition rate. The rates are linear from time zero indicating that for this severity of tests the stainless steel substrate retains its catalytic effect. Also, the rate is approximately linearly related to the lubricant concentration.

The surface morphology of TMPTH deposits was examined by Scanning Electron Microscopy (SEM). Figure 64 shows an uncoated stainless steel surface. Figures 65-67 show TMPTH deposits on stainless steel at a coating thickness of 78 and 113 $\mu g/cm^2$. These deposits were formed using 1.0% TMPTH in nitrogen. Figures 68-71 show thicker coating of TMPTH deposit on stainless steel using combinations of nitrogen and air as the carrier gas. Coating thicknesses range up to 413 $\mu g/cm^2$ (fig. 71). It is observed that TMPTH deposits are quite different from phosphate esters and PPE deposits. TMPTH deposits have a filamentous structure in contrast to the globular structure that was observed with phosphate esters and PPE deposits. The morphology of TMPTH deposits look very similar to that of coke deposits [19]. Several investigators have observed filamentous-tubular deposits in the formation of coke from hydrocarbons [20-22]. It has been reported that these deposits often contained highly dispersed metal particles [23]. Some researchers have observed metal particles concentrated at the tip of these filamentous deposit structures [22]. It was suggested that these metal particles are carried away from the substrate surface by the growth process. Figures 72-80 show SEM micrographs of TMPTH deposits on iron, nickel and copper. It is observed that for iron and nickel, the deposits appear similar to that on stainless steel. With thicker coatings the filamentous structure of the deposits become clearer. TMPTH deposits on copper appear to be different than that on iron, stainless steel, and nickel. Deposits on copper appear to have a more integral structure, while deposits on iron, stainless steel, and nickel appeared to be more dispersed. It should be noted that copper provided an essentially non-catalytic surface for TMPTH deposition. This lack of catalytic activity may be related to the different surface morphology observed on copper. It is interesting to note that SEM pictures of coke deposits on copper surfaces also show a different morphology than the filamentous deposit observed on nickel and iron surfaces [23]. The similarity in surface morphology between TMPTH deposits and coke deposits suggests similarities in mechanisms of deposit formation.
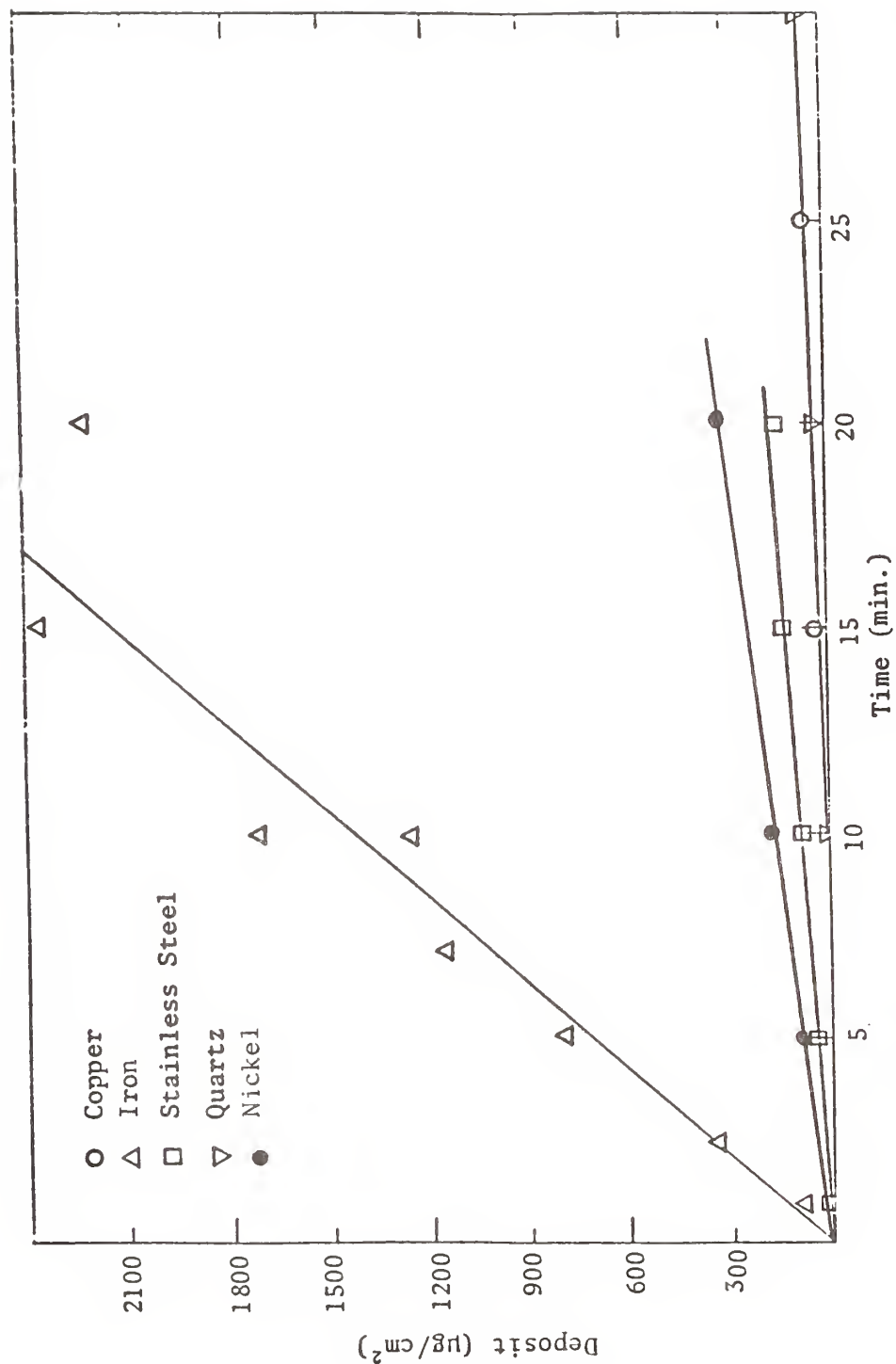
Figure 60. Deposit thickness versus time for different surfaces exposed to a vapor of 1% TMPTH in a nitrogen carrier gas at 700°C.

52
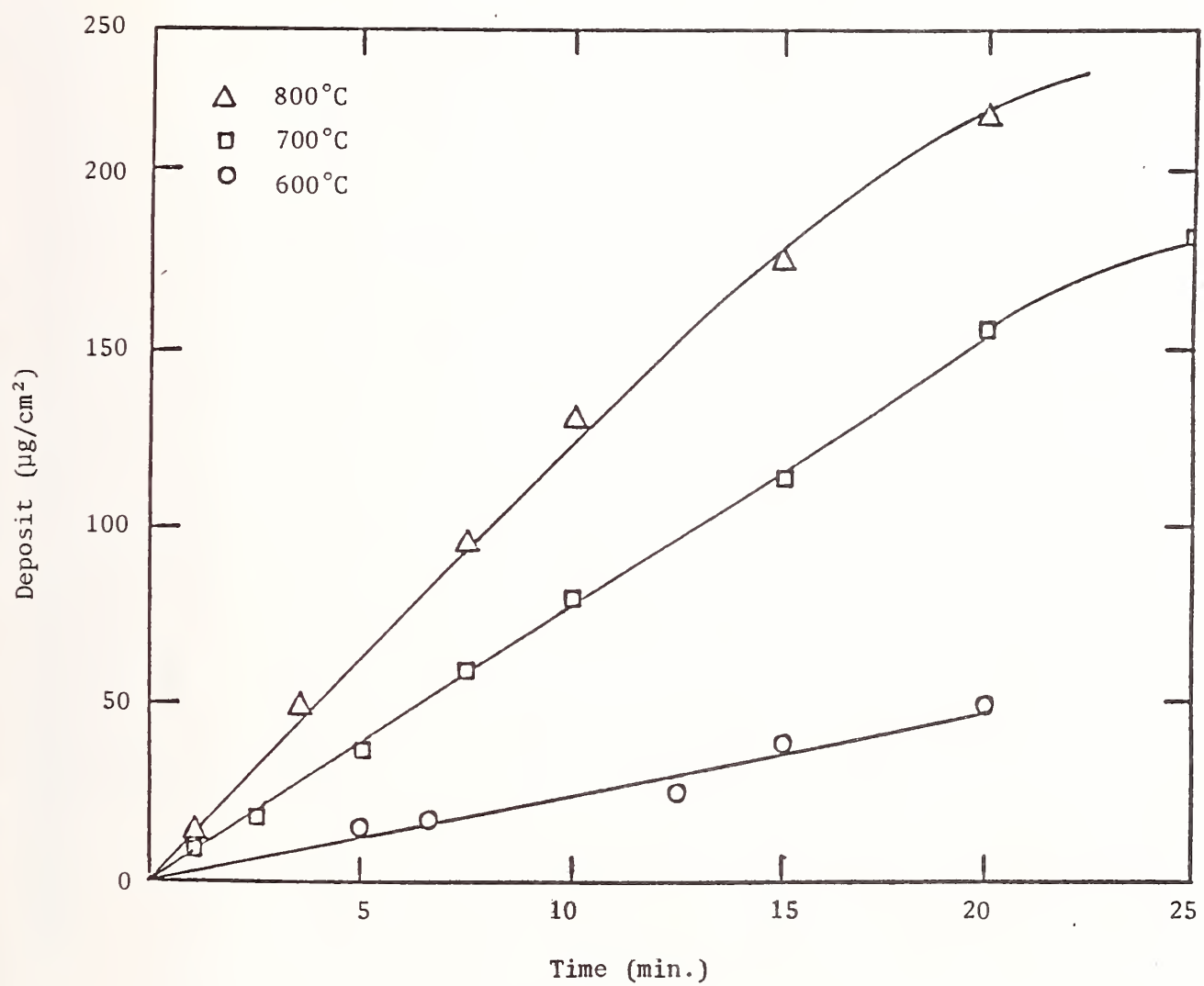
Figure 61.   Effect of temperature on TMPTH deposition on stainless steel. substrates.
         TMPTH concentration: 1.0% in nitrogen

53
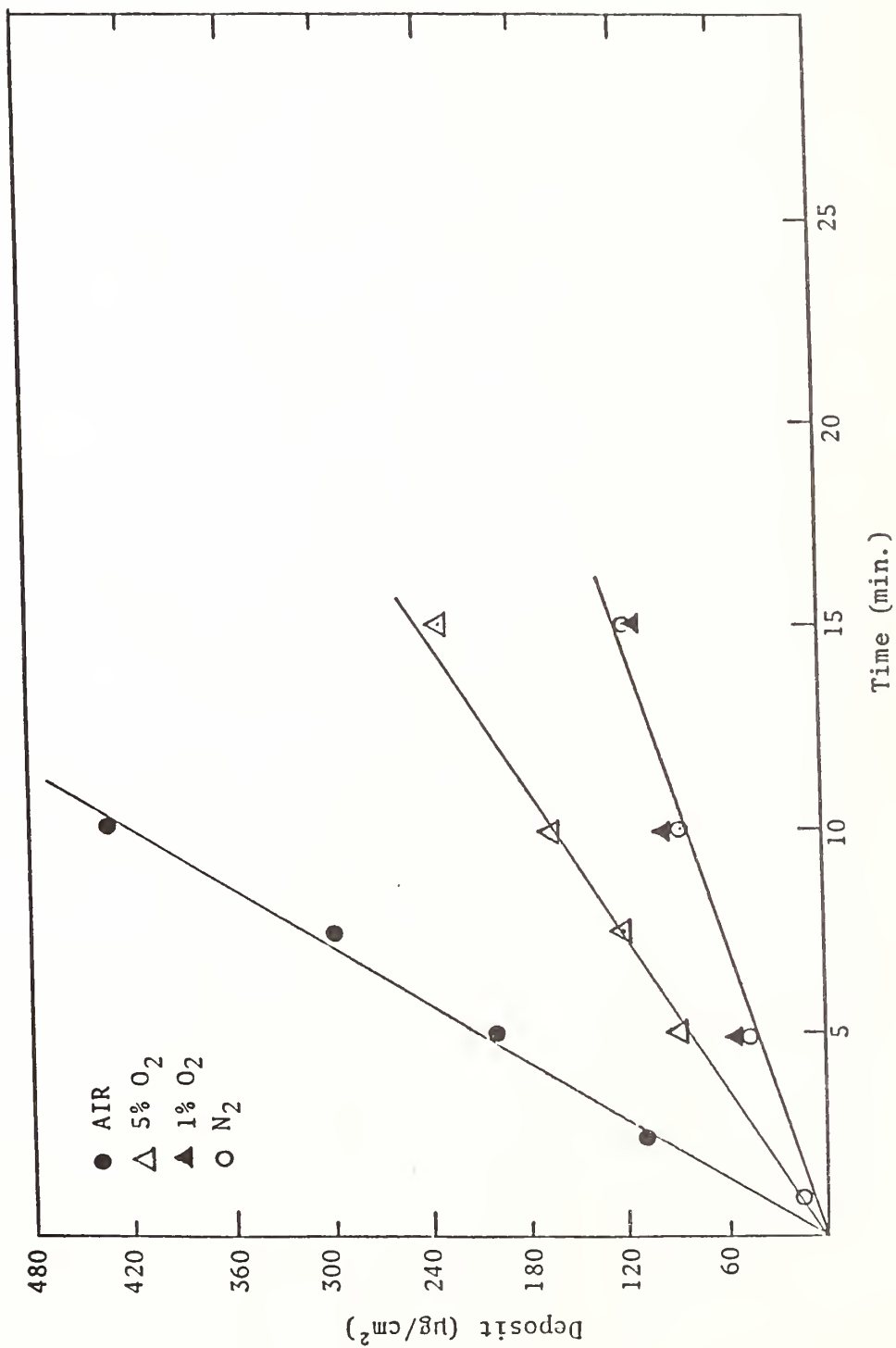
Figure 62. Deposit thickness versus time for stainless steel exposed to a vapor of 1% TMPTH with various oxygen concentrations from (0% to 21%) in nitrogen at 700°C.

54
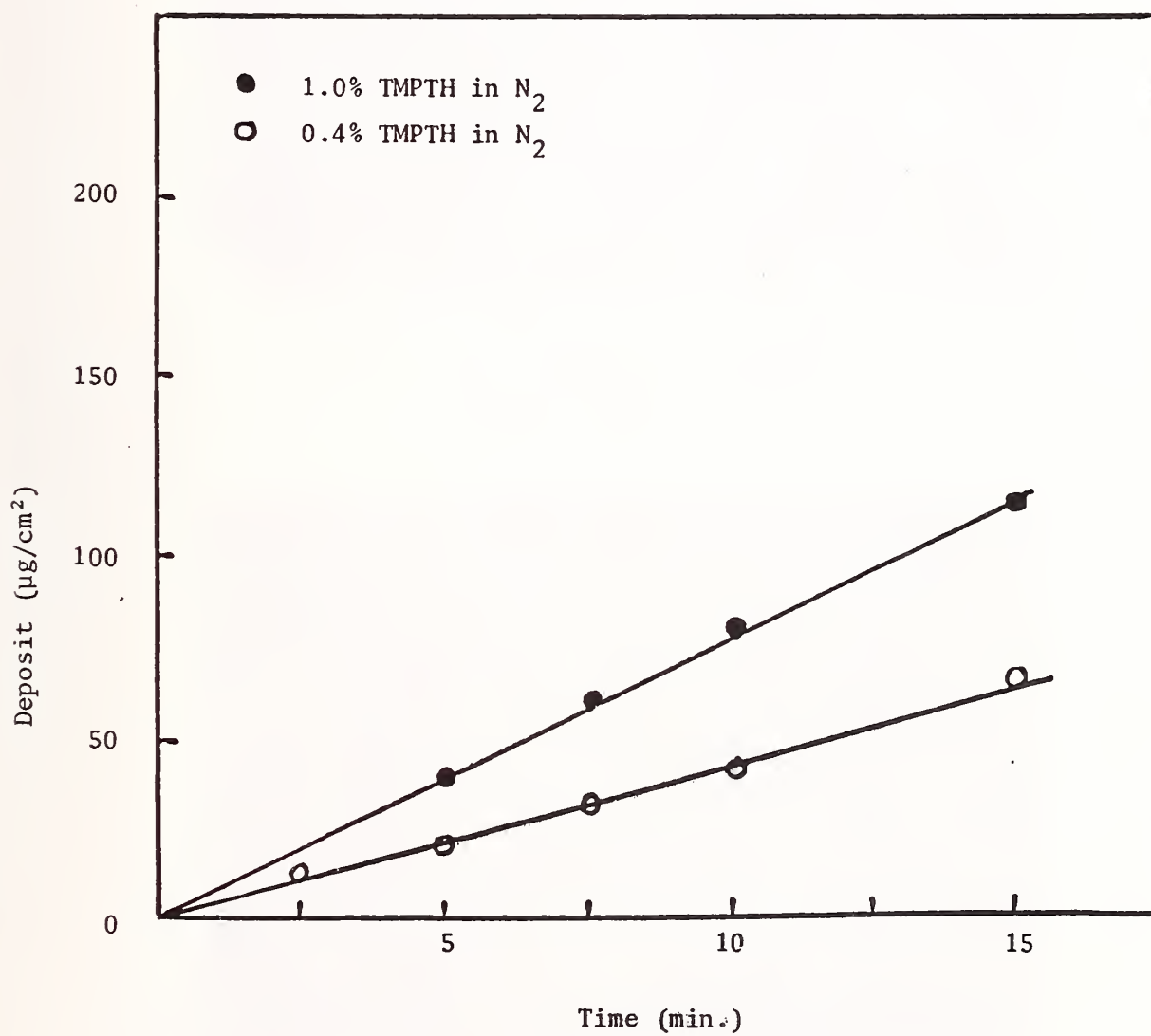
Figure 63. Effect of TMPTH vapor concentration on Deposition rate of TMPTH on stainless steel at 700°C.

Figure 64.   SEM picture of a stainless steel surface,
             preheated to 700°C.
             Magnification: 2000X
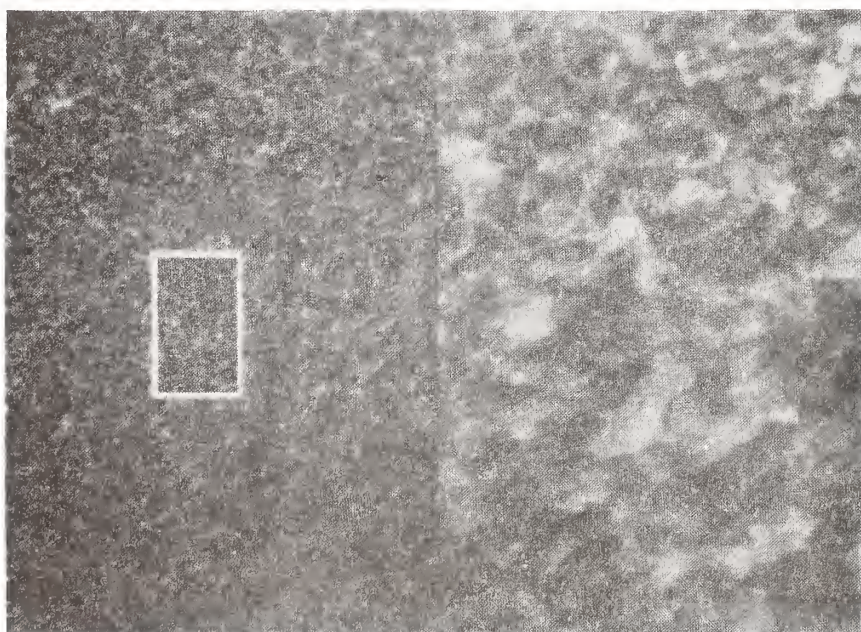
Figure 65.   SEM picture of a deposit 78.4 ug/cm^2 on a
             stainless steel surface.
             1.0% TMPTH in nitrogen, 700°C.
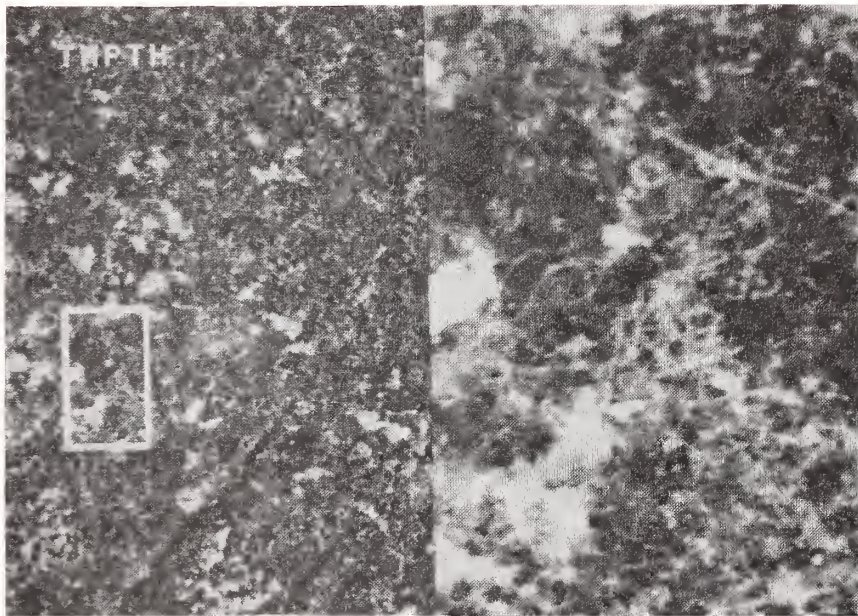
Figure 66.   SEM picture of a deposit 113 ug/cm on a
              stainless steel surface, 1.0% TMPTH in
              nitrogen, 700°C.
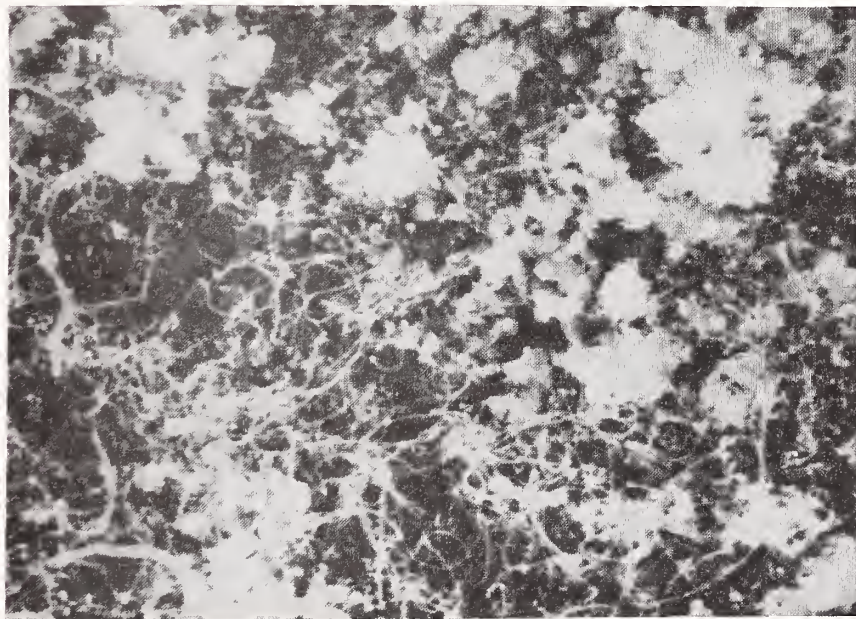
Figure 67.   Same deposit as in figure 66.
              Magnification: 10,000X.
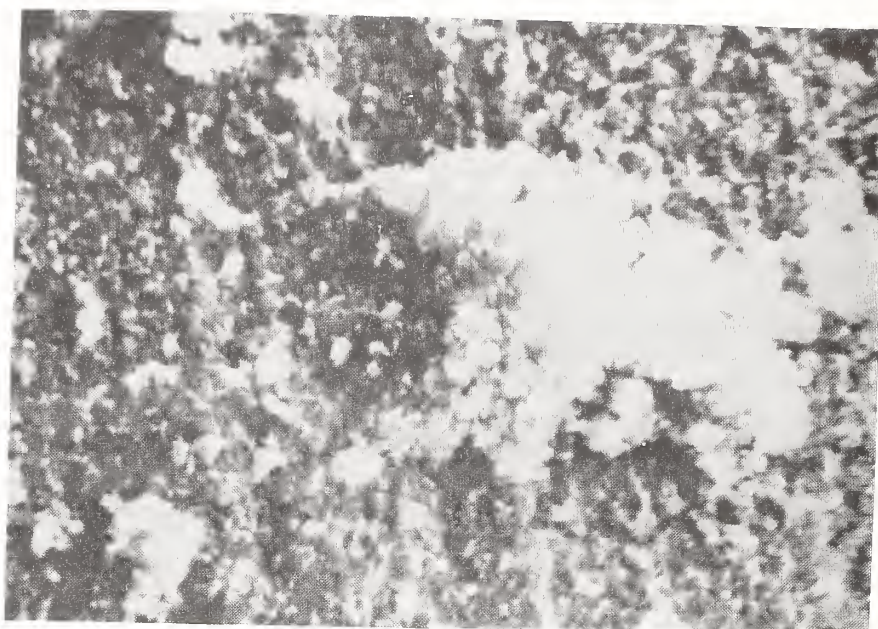
Figure 68.   SEM picture of a deposit 122 ug/cm^2 on a
             stainless steel surface 1.0% TMPTH in
             N_2 + 5% O_2, 700°C.
             Magnification: 2000X

Figure 69.   SEM picture of the same deposit shown in
             figure 68.
             Magnification: 10,000X
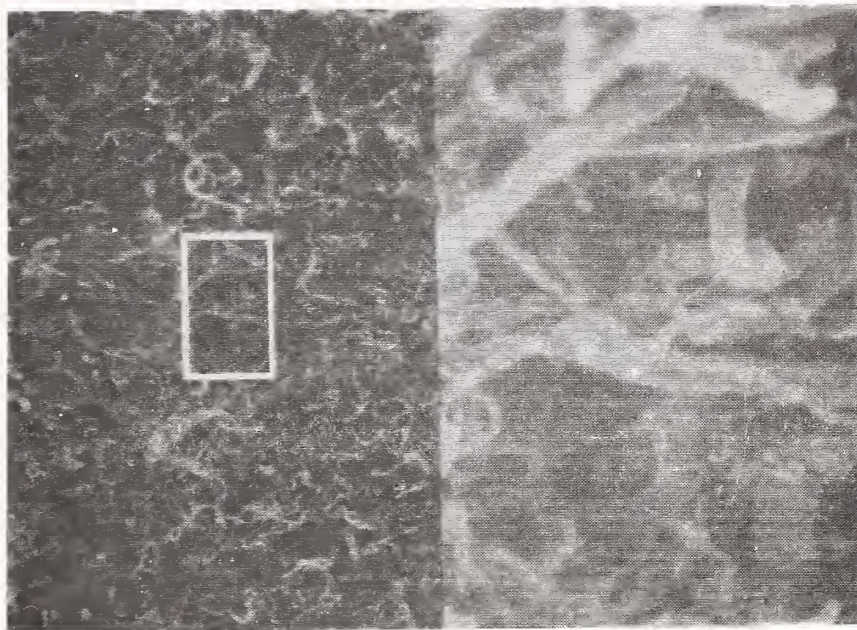
Figure 70. SEM picture of a deposit ($413 \ \mathrm{ug/cm}^2$) on
a stainless steel surface 1.0% TMPTH in air.
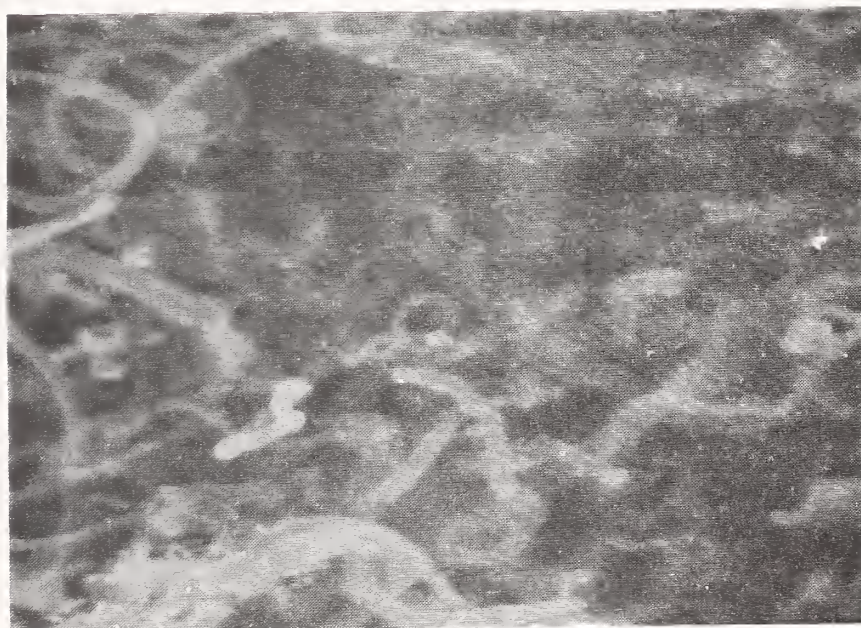
Figure 71. Same deposit as in figure 70.
Magnification 10,000X.

Figure 72.   SEM picture of an iron surface preheated
             to 700°C.
             Magnification: 2000X
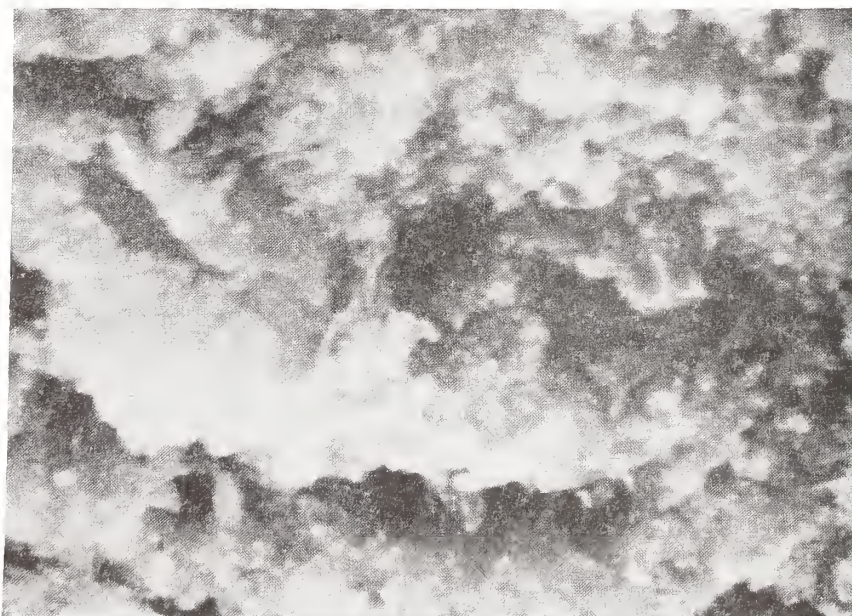
Figure 73.   SEM picture of a deposit (814 ug/cm) on an
             iron surface.
             1.0% TMPTH in nitrogen, 700°C.

Figure 74.   SEM picture of a deposit (2220 μg/cm) on
an iron surface.
1.0% TMPTH in nitrogen, 700°C.
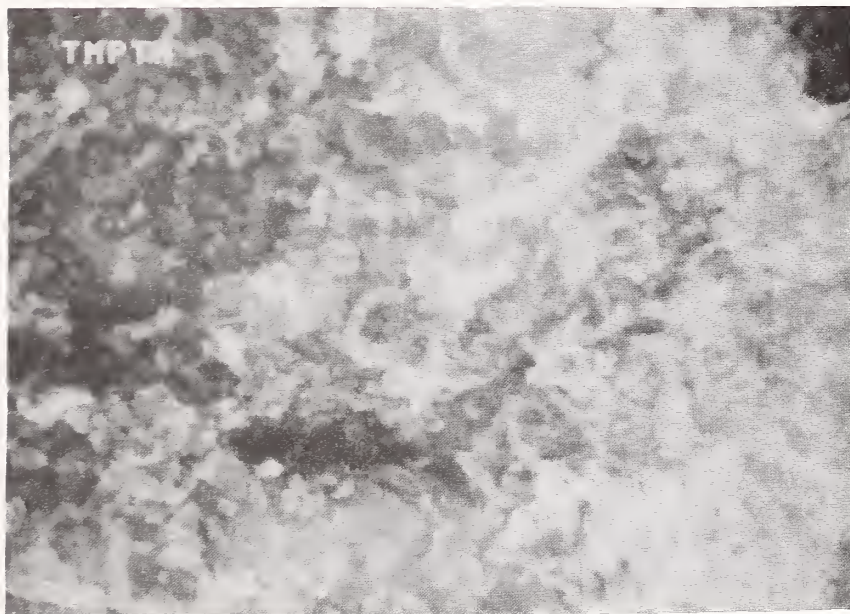
Figure 75.   Same deposit as in figure 74.
Magnification 10,000X.

Figure 76. SEM picture of a copper surface preheated to 700°C.
Magnification: 2000X

Figure 77. SEM picture of a deposit (173 ug/cm^2) on a copper surface.
1.0% TMPTH in air, 700°C.
Magnification: 2000X
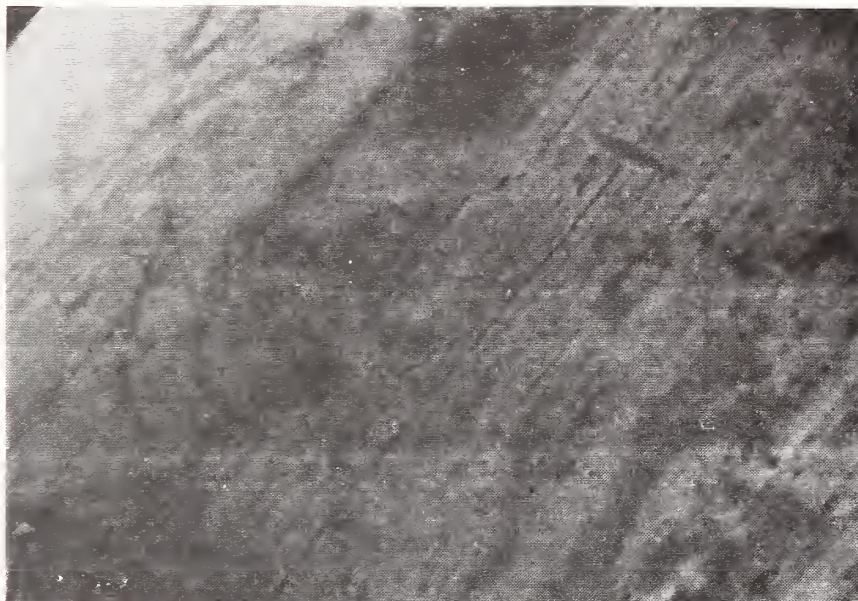
Figure 78. SEM picture of a nickel surface, preheated to 700°.
Magnification: 2000X
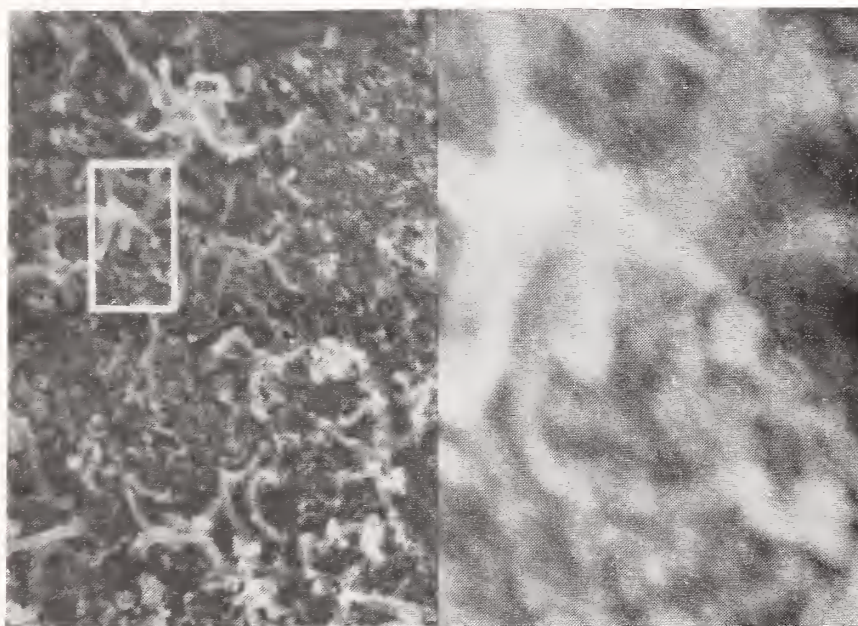
Figure 79. SEM picture of a deposit (220 ug/cm^2) on a nickel surface, 1.0% in nitrogen 700°C.
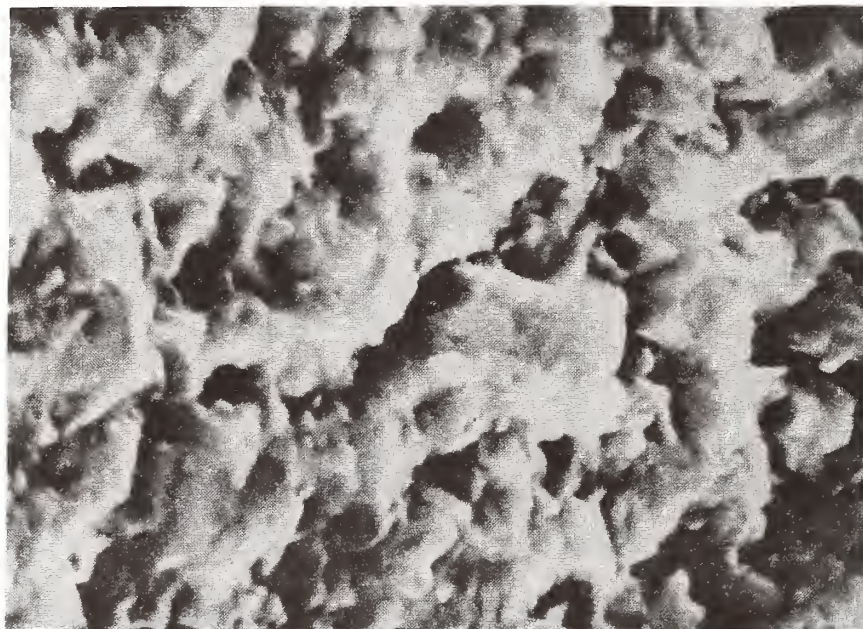
Figure 80.   SEM picture of a deposit (173 ug/cm^2) on
              a copper surface.
              1.0% TMPTH in air, 700°C.
              Magnification: 10,000X

E. Comparisons of Deposition Rates of Phosphate Esters and Non-Phosphate
   Hydrocarbons

    A comparison of the initial rates of deposit formation within the
first 1 minute of deposition of phosphate esters TCP and GT, and
non-phosphate hydrocarbons PPE and TMPTH is shown in table 1. Deposition
rates were compared on iron, copper, stainless steel, nickel, and quartz
with lubricant vapor in nitrogen stream at 700°C. These data clearly
indicate that deposition rates are metal specific. For the phosphate
esters TCP and GT the ranking of catalytic activity of metal substrates is
iron > copper > stainless steel > nickel. Nickel and quartz can be
considered to be inert substrates, while iron and copper are strong
catalysts for deposit formation even when relatively thick films are
present. Stainless steel falls between the two extremes.

    Although the relative catalytic activity of metals is the same for the
phosphate ester, the ranking of catalytic activity is different when
deposits are being formed from hydrocarbon lubricants which do not contain
phosphate. The main difference between deposit formation from phosphate
ester lubricants and non-phosphate ester lubricants and non-phosphate
hydrocarbons is the change in catalytic behavior of nickel. Nickel has the
characteristics of a strong catalyst for deposition from non-phosphate
hydrocarbons, while it behaves essentially as an inert substrate for
deposition of phosphate esters. It is also observed that under equivalent
conditions, deposition rates are higher for deposits formed from phosphate
esters than from non-phosphate hydrocarbons. The ranking of catalytic
activity of metals for deposition of non-phosphate hydrocarbons PPE and
TMPTH closely follows the order observed in hydrogenation-dehydrogenation
and hydrogenolysis reactions of hydrocarbons.

Table 1. Initial rates of deposit formation

Substrate	Lubricant Vapor in Nitrogen Stream at 700°C			
	1.55% TCP	1.75% GT	1% PPE	1% TMPTH
Iron	290	430	19	127
Copper	210	280	6	1
Stainless Steel	110	45	9	8
Nickel	15	10	16	24
Quartz	15	10	2	1

*All rates were based on initial 1 minute of deposition.

*All rates are in units of $\mu g/cm^2$ min. To convert this value to molecular
layers the multiplication factor is approximately 10.

F. Deposition Studies With Evaporating Liquid Delivery System

As mentioned in the experimental section, some of the early deposition data was obtained with a system in which liquid lubricants held in a crucible or boat at elevated temperatures evaporated into a flowing gas stream. The gas stream then passed over the metal specimen. This was a convenient technique to obtain data at low contact times since the direction of the gas flow could be changed quickly. However, the exact concentration of lubricant in the gas phase is not known, and it is possible that liquid-phase reactions in the crucible could modify the lubricant. Consequently, the syringe delivery system was developed and the preponderance of deposition data were obtained with that improved technique. However, some unique studies involving tributyl phosphate (TBP) and mineral oil were conducted with the evaporating liquid delivery system, and the results are reported in this section. These are the only deposition data available for these materials. The exact concentration of the lubricant in the vapor is not known for these studies, but the maximum concentrations which would be realized if the liquid in the crucibles saturated the gas phase are reported in the following tables. The actual lubricant concentration is approximately 5% of the saturation value.

Results presented in the wear test section of this report show that TBP is the most effective material studied for providing a lubricating film at low temperatures. A comparison of the deposition characteristics of TBP with other lubricants is presented in table 2. All of these results were obtained with the liquid evaporation delivery system so that they are comparable even though the exact lubricant concentrations in the vapor are not known. The TBP-produced deposits are nearly an order of magnitude thicker than the coatings produced by TCP under identical conditions. Similarly, the deposition effectiveness of TMPTH approaches TBP only when the deposition temperature is 250°C higher.

Further information concerning the deposition kinetics of coatings formed from TBP are presented in table 3. Measurable quantities of coating from TBP could be detected at low temperatures and very short contact times. These results are consistent with the wear results which indicated that TBP is the most effective lubricant studied for low-temperature applications. Deposition data for mineral oil are presented in table 2. Coatings can be formed from mineral oil vapors but the thickness of these coatings are low compared to the other materials considered in this study. As one might expect, the presence of oxygen might have a tendency to improve the coating characteristics of mineral oil. Liquid-phase oxidation studies indicate that low molecular weight oxidation products of mineral oil form high molecular weight materials and deposits by a polymer condensation process. It is possible that in the presence of oxygen, low molecular weight oxidation products that would form in the gas phase with these materials would then polymerize to form a coating on the metal surfaces. The influence of oxygen concentration on the deposition of three different lubricants is presented in table 4. The formation of coatings from mineral oil vapors shows a trend which is consistent with this

66

proposed mechanism. An increase in the concentration of oxygen in the carrier gas causes a corresponding increase in the amount of coating formed by mineral oil.

In contrast, the presence of oxygen does not appear to influence the formation of deposits formed from DEHS, while an increase in oxygen concentration reduces the formation of a deposit from vaporized TMPTH. It is possible that the reaction of oxygen with vaporized lubricants creates an oxidized product which is more susceptible to decomposition and the formation of deposits. In contrast, an alternative mechanism would involve the oxidative decomposition of a coating which would reduce the net amount of deposit present at any time. These data seem to indicate that this oxidative degradation may be occurring with TMPTH. However, studies concerned with the influence of oxygen on coatings formed from TMPTH using the syringe pump delivery systems show contradictory results. For example, figure 62 in the earlier section which discussed the deposition studies with TMPTH showed that oxygen increased the rate of deposit formation from this ester. The conflicting results obtained with these two deposition techniques may be due to one of the problems inherent with the evaporating liquid-delivery system. It is possible that oxidation of the liquid TMPTH occurs in the crucible at the elevated temperatures in the evaporation section of the apparatus. This oxidation process could lead to polymerization of the TMPTH in the liquid which would reduce the vapor pressure of the liquid and, consequently, reduce the amount of TMPTH in the gas stream when it impinges on the stainless steel substrate. Because of this and other possible complications associated with the evaporating liquid-delivery system, the syringe pump delivery system was the preferred technique in these studies. It should be noted, however, that the delivery system in an actual application may, in some cases, more closely simulate the evaporating liquid experimental technique. In conclusion, the concentration of oxygen in the gas stream can influence the kinetics of film formation. Oxygen can enhance or inhibit deposition rates depending upon the specific characteristics of the lubricant and the delivery system configuration.

Table 2.   Comparison of deposit formation of various lubricants

(°C)	Gas	Temperature Deposit ($\mu g/cm^2$)	Carrier	Lubricant
			10 sec. 6%	5 min. 1.2%
Tributyl Phosphate (TBP)	650	N_2	120	1350
Tricresyl Phosphate (TCP)	650	N_2	17	146
Mineral Oil	750	5% O_2 in N_2	22	132
Polyol Ester (TMPTH)	900	1% O_2 in N_2	170	1007

* Deposits were formed on stainless steel substrates

* 1 $\mu g/cm^2$ coating thickness corresponds to 10 monolayers

Table 3.   Effect of temperature on deposit formation of
                tributyl phosphate (TBP) on stainless steel

Time (sec.)	Deposit ($\mu g/cm^2$)		
	320°C	430°C	650°C
3	5	10	38
5	6	25	70
10	8	73	,120
15	10	85	175
20	12	113	190

* 6% TBP was used in nitrogen carrier gas

* 1 $\mu g/cm^2$ coating thickness corresponds to 10 monolayers

Table 4.   Effect of oxygen concentration on deposit
                formation of various lubricants

Lubricant	Temperature °C	Deposit ($\mu g/cm^2$) Oxygen Concentration (%)				
		1	2	3	4	5
Trimethylolpropane Triheptanoate (TMPTH)	800	390	353	315	231	189
Di-2-Ethyl hexyl Sebacate (DEHS)	800	105	103	104	107	106
Mineral Oil	750	93	107	107	118	132

* 1.2% of lubricant vapor was used in carrier gas

* Deposits were formed on stainless steel substrates

* Deposits shown are after 5 minutes test time

* 1 $\mu g/cm^2$ coating thickness corresponds to 10 monolayers

69

IV. WEAR STUDIES OF VAPOR-DEPOSITED LUBRICANT FILMS

The discussion in the preceding section on the kinetics of vapor
deposition clearly shows that at elevated temperatures, films of
substantial thickness are formed from lubricant vapors at relatively low
vapor concentrations. A modified four-ball wear tester was used to
investigate the wear characteristics of vapor-deposited lubricant films.
The wear tester and its operating procedure have been described in section
II of this report. All tests were conducted for 30 minutes using M-50
tool-steel balls and a rotational speed of 600 rpm. For most of the tests,
the operating temperature was maintained at 371°C (700°F). With TBP, some
tests were conducted at 270°C.

The wear scar diameter, measured using an optical microscope, was
taken to be a good indication of the wear resistance of the lubricant film.
The effect of load, lubricant vapor concentration, and carrier gas
composition on wear were examined.

A. Phosphate Esters (TCP, TBP, and GT)

The anti-wear effectiveness of vapor-deposited films from tricresyl
phosphate (TCP), tributyl phosphate (TBP), and diphenyl ditertiary butyl
phenyl phosphate (GT) were examined for films formed on M-50 tool-steel
balls. The selection phosphate esters exhibited substantially different
properties with respect to liquid phase thermal, oxidative, and
hydrolytic stabilities. The temperatures at which the wear tests were
conducted were always above the temperature at which water can exist in the
contact zone; therefore, hydrolytic stability was not considered an
important property.

TBP has relatively poor oxidation stability; TCP has good oxidation
stability; and GT has excellent oxidation stability. The thermal stability
of the alkyl phosphate (TBP) is generally not as good as that of triaryl
phosphates, TCP and GT [15]. The four-ball wear tests on vapor-deposited
lubricant films show no general correlation with either liquid-phase
thermal or oxidative stabilities.

The effect of load on wear scar is shown in figures 81 and 82 for
TBP, TCP, and GT vapor-deposited films. These tests were conducted at
371°C. For data in figure 81, 0.5% lubricant vapor concentration in
nitrogen was used. For data in figure 82, 0.75% lubricant vapor
concentration in nitrogen was used. In figures 81 and 82, the Hertz elastic
deformation line is shown to indicate zero wear.

The wear caused by the lubricated system can be considered to be the
difference between the wear scar and the Hertz elastic deformation value.
A good lubricant will show wear parallel to the Hertz deformation line
until seizure occurs. Seizure or scuffing produces wear that can be
several times that noted during pre-seizure conditions.

The data in figures 81 and 82 show that at both 0.5 and 0.75% lubricant vapor, TCP provided excellent wear protection over the range of loads studied, with no seizure even at 50 kg load. A comparison of figures 81 and 82 shows that increasing the TCP vapor concentration from 0.5 to 0.75% caused no significant change in wear values for TCP. The data for TBP indicate that while using 0.5% TBP in nitrogen (fig. 81), seizure occurred at 30 kg load. During pre-seizure at lower loads, wear values using TBP were similar to that using TCP. Increasing TBP vapor concentration from 0.5 to 0.75% (fig. 82) increased the wear scar at equivalent loads, but the seizure load was raised to 40 kg. The increase in wear values maybe attributable to an increase in coating rate and a subsequent increase in three-body wear caused by trapping of wear particles in the coating.

The data for GT indicate that while using 0.5% lubricant vapor concentration (fig. 81), wear values were somewhat higher than for the other phosphate esters under equivalent conditions. Seizure occurred at a load of 30 kg. Increasing the GT vapor concentration from 0.5 to 0.75% (fig. 82), the wear values improved slightly but there was no improvement in seizure load. Seizure still occurred at 30 kg load.

It should be noted that in wear tests conducted with a typical liquid mineral oil lubricant at 75°C, wear values are about the same or somewhat higher than that observed with the vapor-deposited films from phosphate esters. With liquid mineral oil lubricants, seizure occurs at 30 to 50 kg load depending on the type and grade of mineral oil. Also, the best correlation between four-ball wear tests and hydraulic pump lubrication is in the range of 5 to 10 kg load. On this basis, it may be concluded that the vapor-deposited films from the phosphate esters studied, TCP, TBP, and GT, provide good lubrication.

The effect of lubricant vapor concentration on wear is shown in figure 83. A series of tests were conducted using TBP, TCP, and GT in nitrogen at 371°C. The wear data were compared at a constant 10 kg load. The actual wear caused by the lubricated system is the difference between the measured wear scar and wear scar caused by elastic deformation (Hertz line). These data show that TCP has a minimum wear value at about 0.5% TCP vapor. This behavior has been attributed to deposit formation. At low vapor concentrations, the deposition rate may be adequate in providing an easily sheared film that is being continuously replenished. At higher lubricant vapor concentrations and, hence, higher deposition rates, excess deposit may trap or collect wear debris which could cause abrasive three-body wear. The data in figure 83 show that with GT vapor, there is a decrease in wear over the concentration range of 0.2 to 0.8%. If there is an optimum GT concentration for minimum wear, it would be expected to be in the concentration range above 0.8%. For TBP, the data in figure 83 show that over the concentration range 0.2 to 1.0%, the wear scar observed is about the same. At concentrations less than 0.1%, there is a significant increase in wear scar due to seizure.

71

Figure 81.   Four-ball wear scar diameter versus load for 0.50 lubricant
            vapor concentration in nitrogen stream. Tests were conducted
            using M-50 tool steel balls at 371°C, 600 rpm.

Figure 82.   Four-ball wear scar diameter versus load for 0.75 lubricant
            vapor concentration in nitrogen stream. Tests were conducted
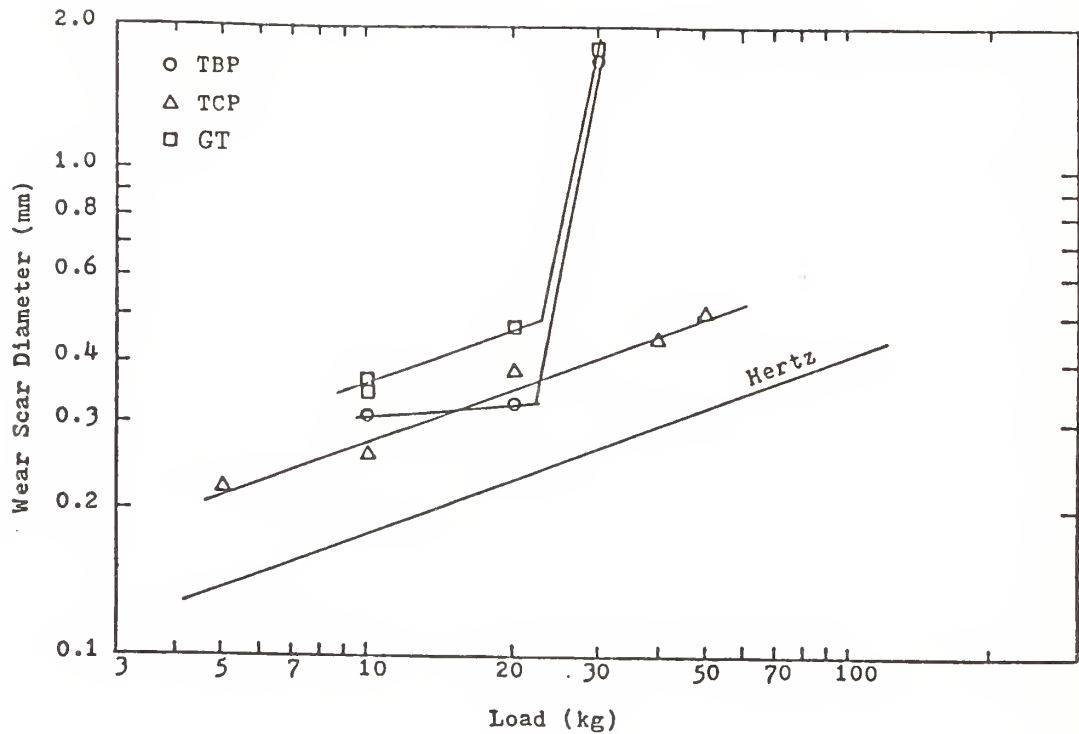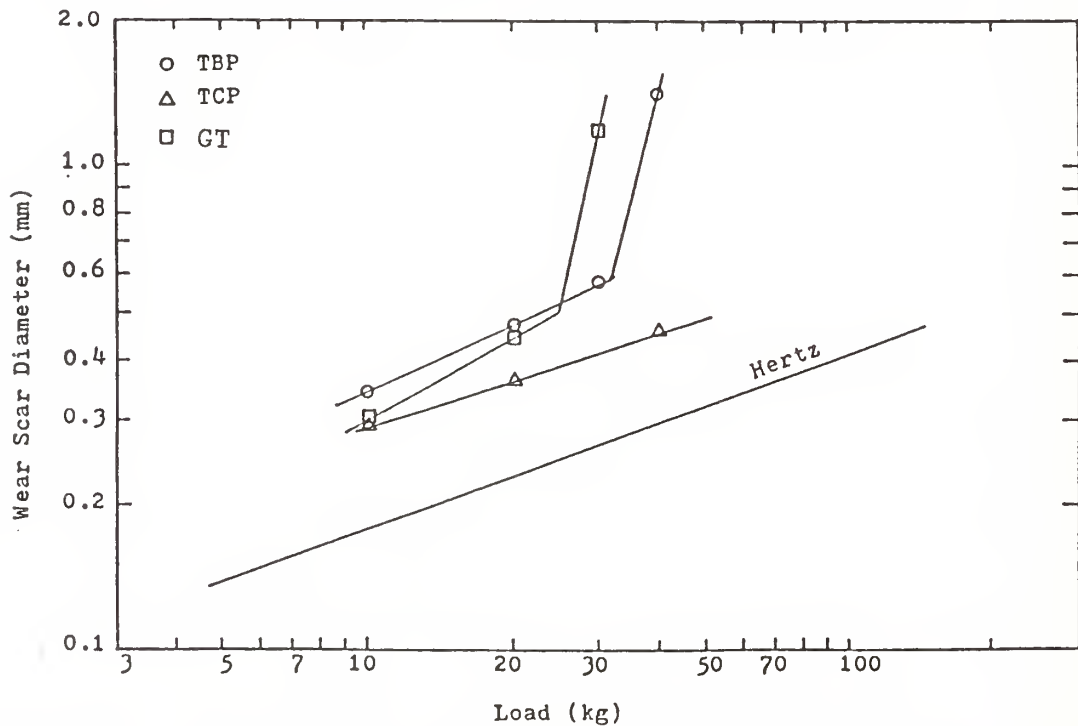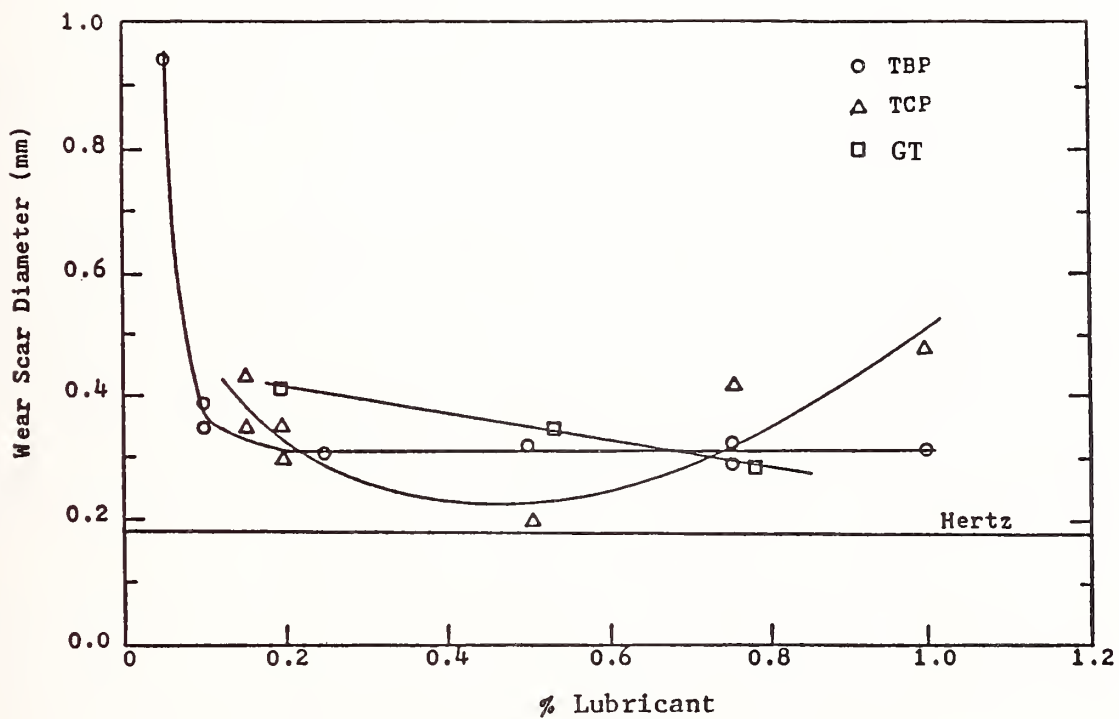   using M-50 tool steel balls at 371°C, rpm.

Figure 83. Four-ball wear scar diameter versus lubricant vapor
concentration in nitrogen stream. Tests were conducted using
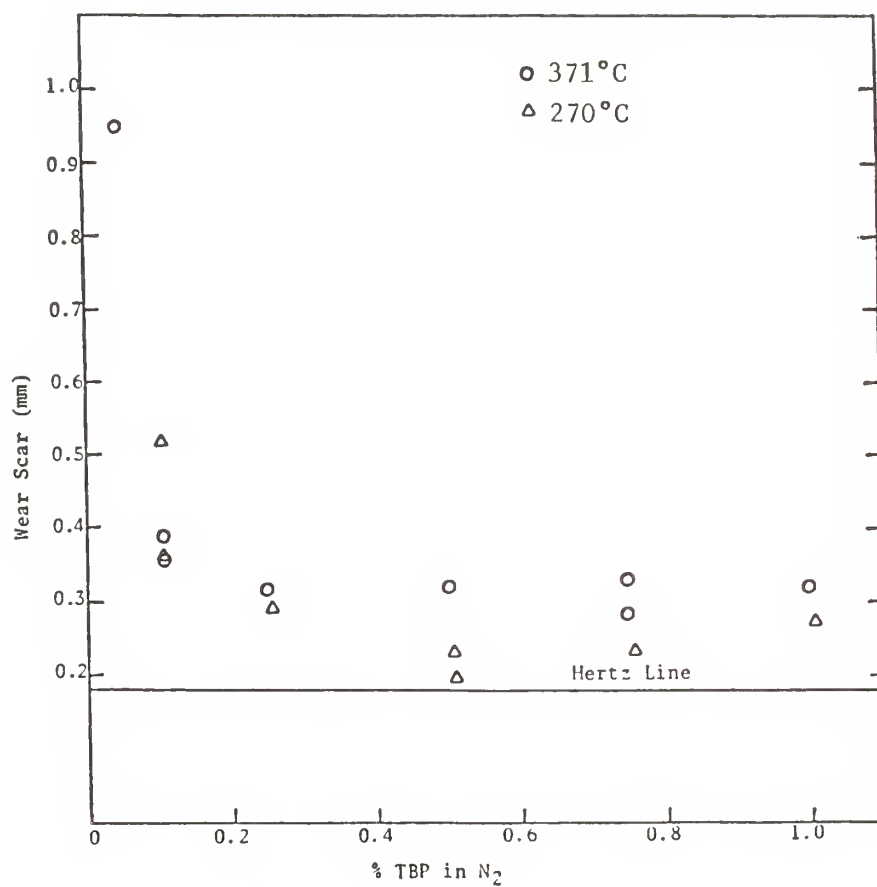M-50 tool steel balls at 371°C with 10 kg load, 600 rpm.

Figure 84. Four-ball wear scar diameter versus concentration of tributyl phosphate at 270°C and 371°C, M-50 steel balls, 600 rpm, 10 kg load.

Figure 84 compares the effect of TBP vapor concentration on wear at two different temperatures (371 and 270°C). The data show that at 270°C minimum wear occurs at an optimum TBP vapor concentration of 0.5%. Lower vapor concentrations cause higher wear. Lower deposition rates at lower concentrations may not be adequate in replenishing the lubricant film at a sufficient rate. Increase in wear at higher vapor concentrations is caused by abrasive wear due to wear particles trapped in excess deposit. Comparison of wear data at 371 and 270°C indicate that at all vapor concentrations wear values at 270°C are lower than wear values at 371°C. With a decrease in temperature, there is an apparent decrease in wear.

The effect of carrier gas composition on wear was examined using GT vapor in nitrogen and air at three different concentrations. Wear data from tests conducted using 0.03, 0.20, and 0.46% GT vapor in nitrogen and air are shown in figures 85 and 86. These figures also include the Hertz elastic deformation line to indicate zero wear. These data clearly demonstrate that even at low vapor concentrations in both nitrogen and oxygen, effective lubricant films are formed that have good anti-wear characteristics at elevated temperatures. Comparison of figures 85 and 86 indicates that the influence of oxygen in air on the lubricating characteristics of the vapor-deposited films is not nearly as significant as the influence of oxygen in air on the rates of film deposition. Also, wear appears to be a significant function of lubricant vapor concentration when nitrogen rather than air is the carrier gas. Figure 85 shows that the influence of the lubricant concentration on wear reverses as one traverses across a range of loads. At low loads, the minimum wear is realized at low concentration while the optimum concentration is higher at high loads.

The basis of good wear characteristics is a balance of the rates of competing processes. The lubricant coating is formed from the gas phase at a rate that is usually enhanced by increases in temperature and lubricant concentration in the vapor. The coating is dissipated or removed by wear at a rate that is enhanced by variables such as load and velocity. If the rate of coating formation is too small compared to the rate of removal, the resulting coating will be too thin to give sufficient lubrication, and extensive wear of the metal surface will occur. If the rate of formation overwhelms the rate of removal, excess coating will gather on the surface and trap debris particles thereby causing undesirable three-body wear.

Figure 85 indicates that at the low loads, the lowest lubricant concentration is adequate to maintain an optimum lubricating coating. In contrast, at the high loads, higher vapor concentrations are required to maintain adequate coating thickness.

The data in figure 86 show that in air with a lubricant vapor concentration of 0.03%, seizure occurs at a 20 kg load. With higher lubricant vapor concentrations, seizure has not yet occurred at a 20 kg load, but conditions may be close to seizure. The relative insensitivity of lubricant vapor concentration to wear in the presence of oxygen may be due to higher deposition rates in the presence of air even with low lubricant vapor concentrations.

These studies on wear characteristics of phosphate ester vapor-deposited lubricant films have shown that films formed from TCP, TBP and GT are effective and have excellent anti-wear characteristics at elevated temperatures.

Figure 85. Four-ball wear scar diameter versus load for various GT vapor concentrations in nitrogen stream at 371°C. Tests were conducted using M-50 tool steel balls at 600 rpm for 30 minutes.

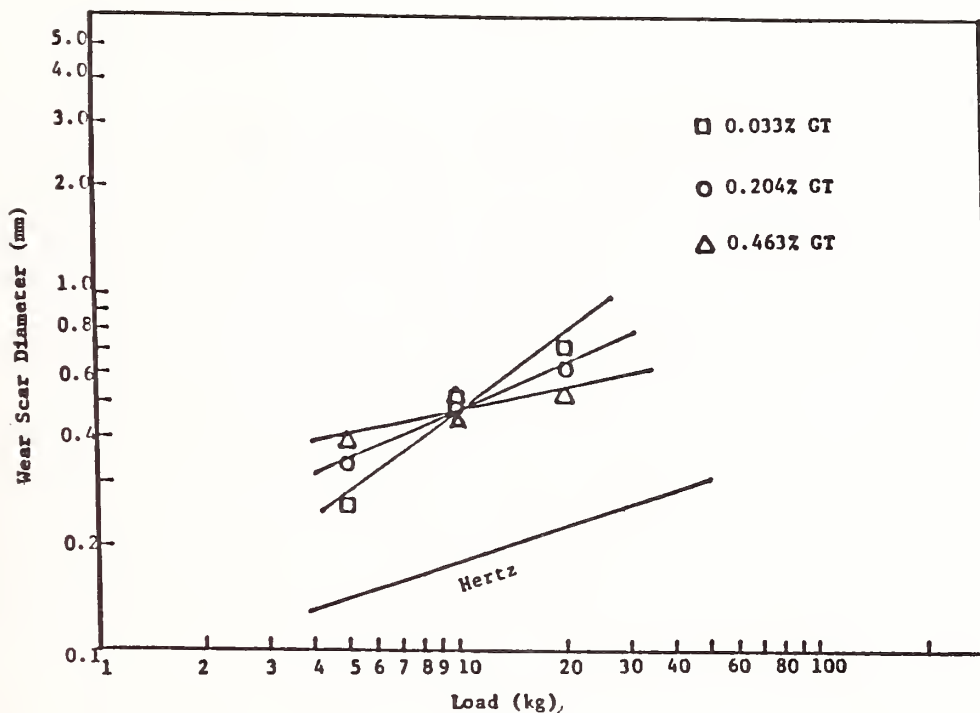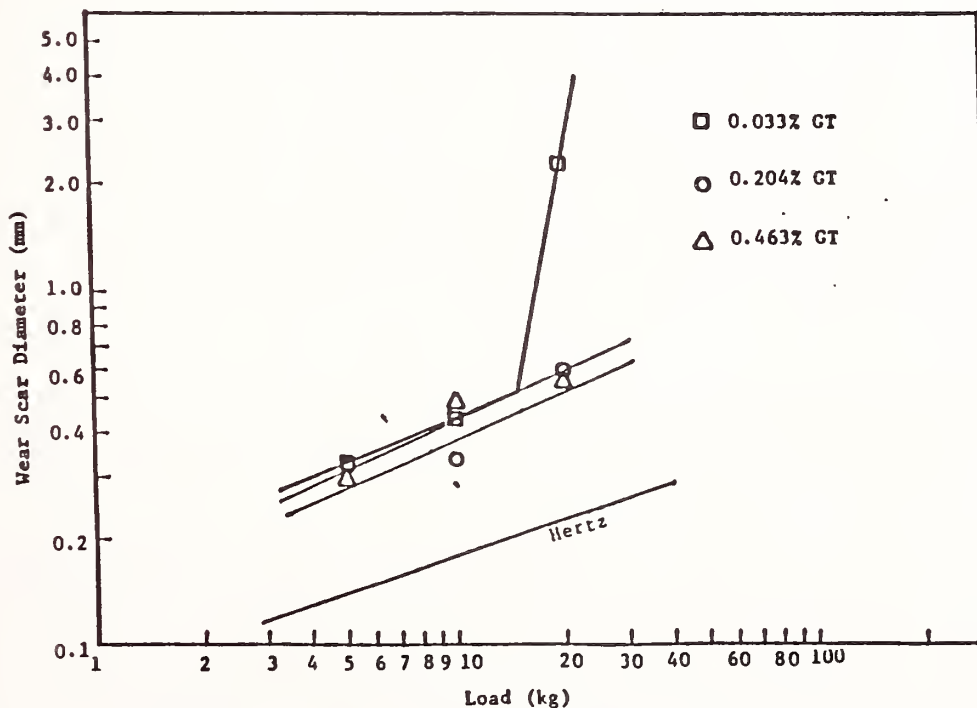Figure 86. Four-ball wear scar diameter versus load for various GT vapor concentrations in air stream at 371°C. Tests were conducted using M-50 tool steel balls at 600 rpm for 30 minutes.

B. Non-Phosphate Hydrocarbons (PPE and TMPTH)

The modified four-ball wear tester was used to examine the anti-wear characteristics of vapor-deposited films formed from PPE and TMPTH. The effect of load, carrier gas composition and lubricant vapor concentration was investigated. Figures 87-89 show wear data for PPE vapor-deposited films. The effect of load on wear scar diameter is shown in figure 87. For these tests, 0.11% PPE vapor was used in an air stream at 371°C. The Hertz elastic deformation line is shown to indicate zero wear. These data show that the PPE vapor-deposited film acts as a good lubricant at 5 and 10 kg loads. Seizure with recovery occurs at a 20 kg load. Based on the criteria that the best correlation between four-ball wear tests and hydraulic pump lubrication is in the range of 1 to 10 kg load, the PPE vapor-deposited film can be considered a good lubricant at these load conditions. Figure 87 also shows a comparison of the anti-wear behavior of PPE vapor-deposited lubricant and PPE liquid lubricant. The liquid lubricant tests were conducted at standard four-ball wear test conditions (10 ml liquid lubricant at 75°C). At a 10 kg load, the wear scar diameter using vapor-deposited lubricant at 371°C is less than the wear scar diameter using the liquid lubricant at 75°C. These data indicate that at the relevant load conditions, the vapor-deposited lubricant provides better wear protection than the liquid lubricant.

The effect of oxygen concentration in the carrier gas on wear is shown in figure 88. 0.11% PPE was used in a carrier gas that was a mixture of nitrogen and air where the oxygen concentration was varied from 0 to 21%. These data show that in this concentration range there is no significant change in wear scar diameter with oxygen concentration. The effect of PPE vapor concentration on wear is shown in figure 89. Tests were conducted in air at 371°C at a 10 kg load. The PPE vapor concentration was varied from 0.045 to 0.5%. The data show that an increase in PPE vapor concentration causes an increase in wear. This increase is more significant at low PPE vapor concentrations. Increase in wear with increasing lubricant vapor concentration can be due to abrasive three-body wear caused by wear particles trapped in excess deposit.

Figures 90-91 show wear data for TMPTH. Figure 90 shows the effect of load on wear scar for tests conducted using 0.5% TMPTH in air. A range of loads from 5 to 60 kg was used. The Hertz elastic deformation line is shown to indicate zero wear. These data show that even up to a load of 50 kg, the TMPTH vapor-deposited film is acting as a good lubricant and seizure has not occurred. It is apparent from the somewhat greater increase in wear scar at a 60 kg load that seizure conditions are being approached. These data indicate that at the relevant load conditions of 1 to 10 kg where there is good correlation between four-ball test data and hydraulic pump lubrication, the TMPTH vapor-deposited film acts as an excellent lubricant. Even with more severe conditions up to a load of 50 kg, the TMPTH vapor-deposited film is a good lubricant.

The effect of oxygen concentration in the carrier gas on wear for TMPTH vapor-deposited films is shown in figure 92. For this series of tests, 0.5% TMPTH was used in a carrier gas that was a mixture of nitrogen and oxygen. The oxygen concentration was varied from 0 to 20% The data are shown for a range of loads from 5 to 50 kg. The Hertz deformation line is shown to indicate zero wear. The data show that at low oxygen concentrations, increasing the oxygen concentration decreases wear. At higher oxygen concentrations, increasing the oxygen concentration has little effect on wear. In more severe conditions at high loads and high oxygen concentrations, there may be a slight increase in wear with increasing oxygen concentration. This behavior indicates that at low oxygen concentrations, increasing oxygen concentration leads to a corresponding increase in deposition rate that is beneficial in decreasing wear, but, at high oxygen concentrations under more severe conditions, increasing oxygen concentration leads to a corresponding increase in deposition rate to levels that can cause additional wear due to wear particles being trapped in excess deposit and causing abrasive three-body wear.

The effect of TMPTH vapor concentration on deposition rate is shown in figure 92. For this series of test, a lubricant vapor concentration of 0.2 to 1.45 % was used in air at 371°C. The tests were conducted at a constant load of 10 kg. The Hertz deformation line is shown to indicate zero wear. These data show that there is an optimum TMPTH vapor concentration for minimum wear. This optimum occurs at about 0.8% TMPTH vapor concentration. This optimum compares with an optimum of 0.5% obtained for TCP and TBP. An optimum was not observable in the concentration ranges studied for GT and PPE. At low lubricant vapor concentrations, increase in TMPTH concentration causes an increase in deposition rate. An increase in coating thickness under these conditions decreases the wear scar. At higher lubricant vapor concentrations, increase in TMPTH vapor concentration and corresponding increase in deposition rate causes additional wear due to wear particles being trapped in excess deposit and causing three-body wear. At the optimum TMPTH vapor concentration, the deposition rate is such that a sufficient coating thickness is maintained without an excess deposit and the corresponding abrasive wear.

These studies on wear characteristics of PPE and TMPTH vapor-deposited films have shown that at elevated temperatures lubricant films formed from PPE and TMPTH vapor are effective and act as good lubricants in reducing wear.

It should be noted that the limitations of the modified four-ball wear test limited the temperature levels at which measurements could be conducted. The temperatures considered are relatively low when the kinetics of deposition formation are presented in the previous section are considered. The deposition studies would indicate that only very thin films would be formed under the temperature and lubricant concentration conditions of these wear studies. The anticipated film thickness would be reduced even further by the short exposure time of the wear test. Consequently, the most significant result of these wear studies is that

effective lubrication can be realized with a very thin vapor-deposited coating. The vapor-deposition kinetic measurements indicate that higher temperatures would be more conducive for the formation of coatings, and effective lubrication can probably be realized with a very low lubricant concentrations at elevated temperatures.
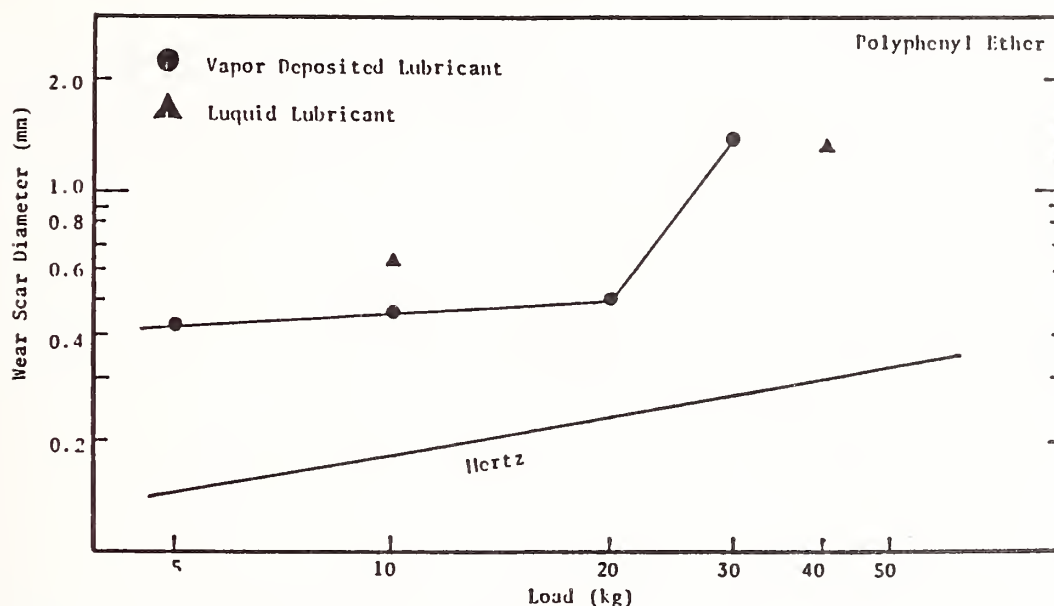
Figure 87. Four-ball wear scar diameter versus load for vapor
deposited lubricant (0.11% lubricant vapor concentrtion
in air stream at 371°C) and liquid lubricant (10 ml liquid
lubricant at 75°C). Tests were conducted using M-50 tool
steel balls at 600 rpm for 30 minutes.
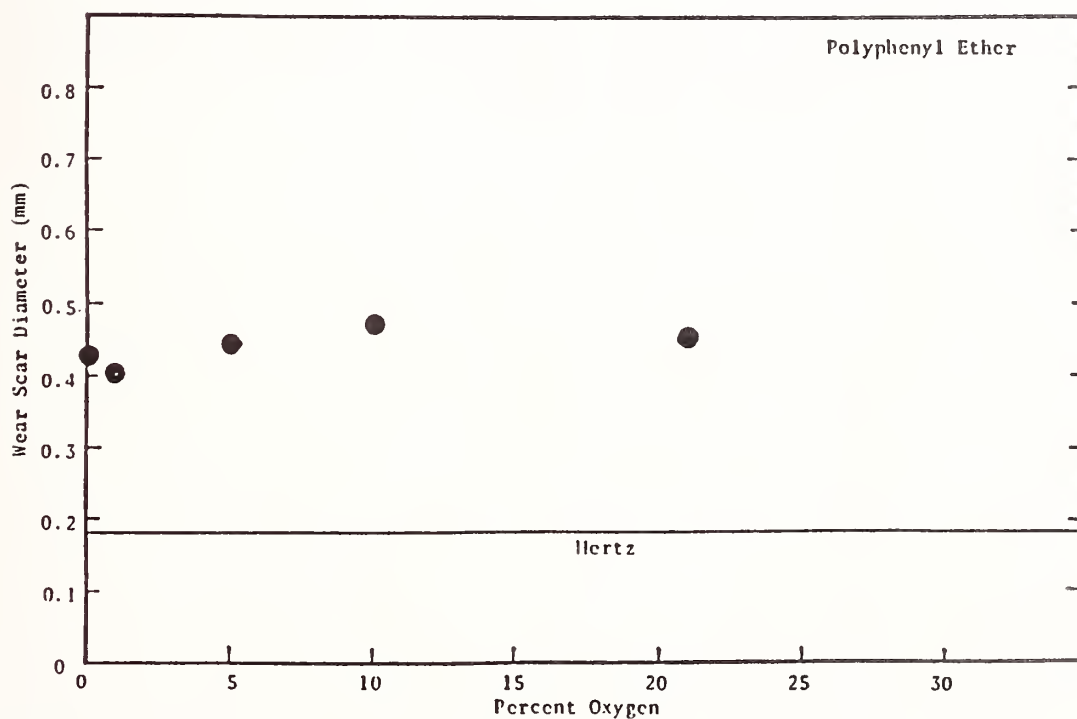
Figure 88. Four-ball wear scar diameter versus oxygen concentration
in vapor stream. Tests were conducted using M-50 tool steel
balls at 371°C with 10 kg load, 600 rpm, for 30 minutes.

81
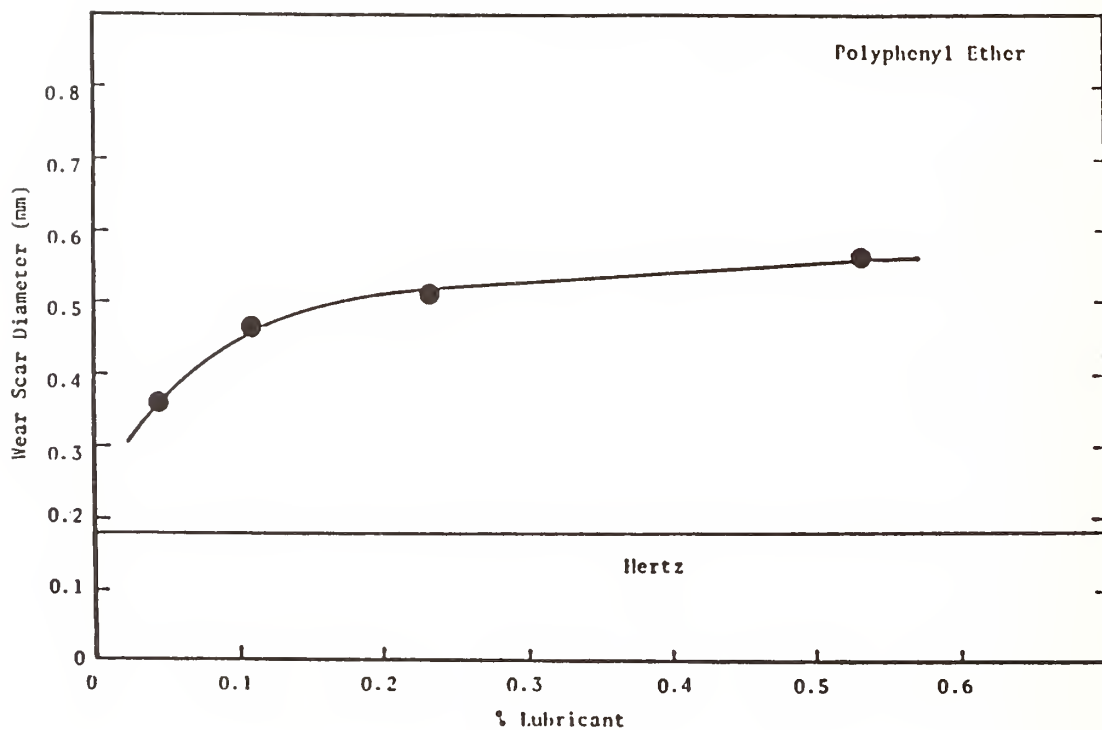
Figure 89. Four-ball wear scar diameter versus lubricant vapor concentration in air stream. Tests were conducted using M–50 tool steel balls at 371°C with 10 kg load, 600 rpm, for 30 minutes.
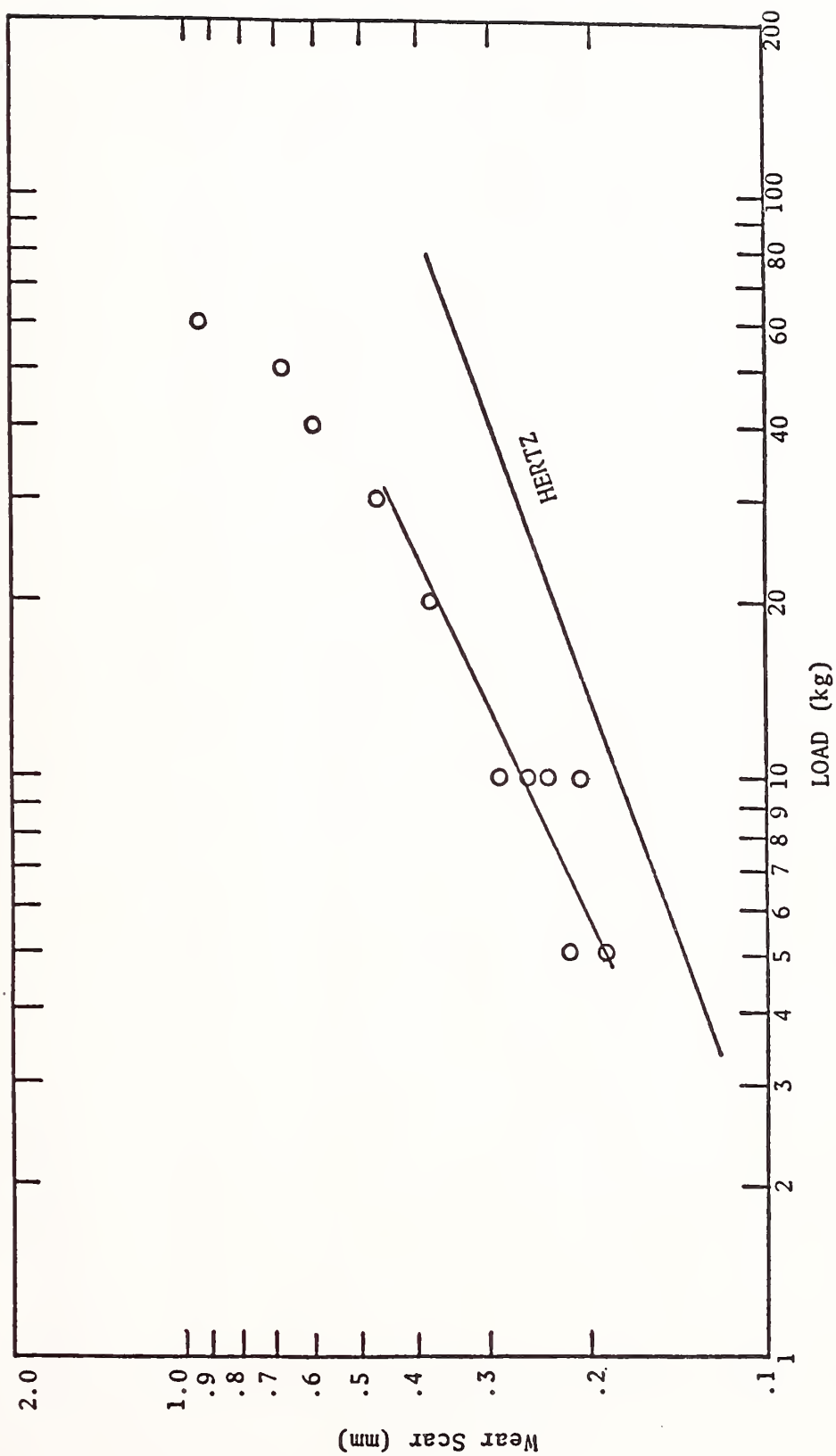
Figure 90. Four-ball wear scar diameter versus load for 0.5% TMPTH at 370°C with air as the carrier gas, M-50 steel balls, 600 rpm.
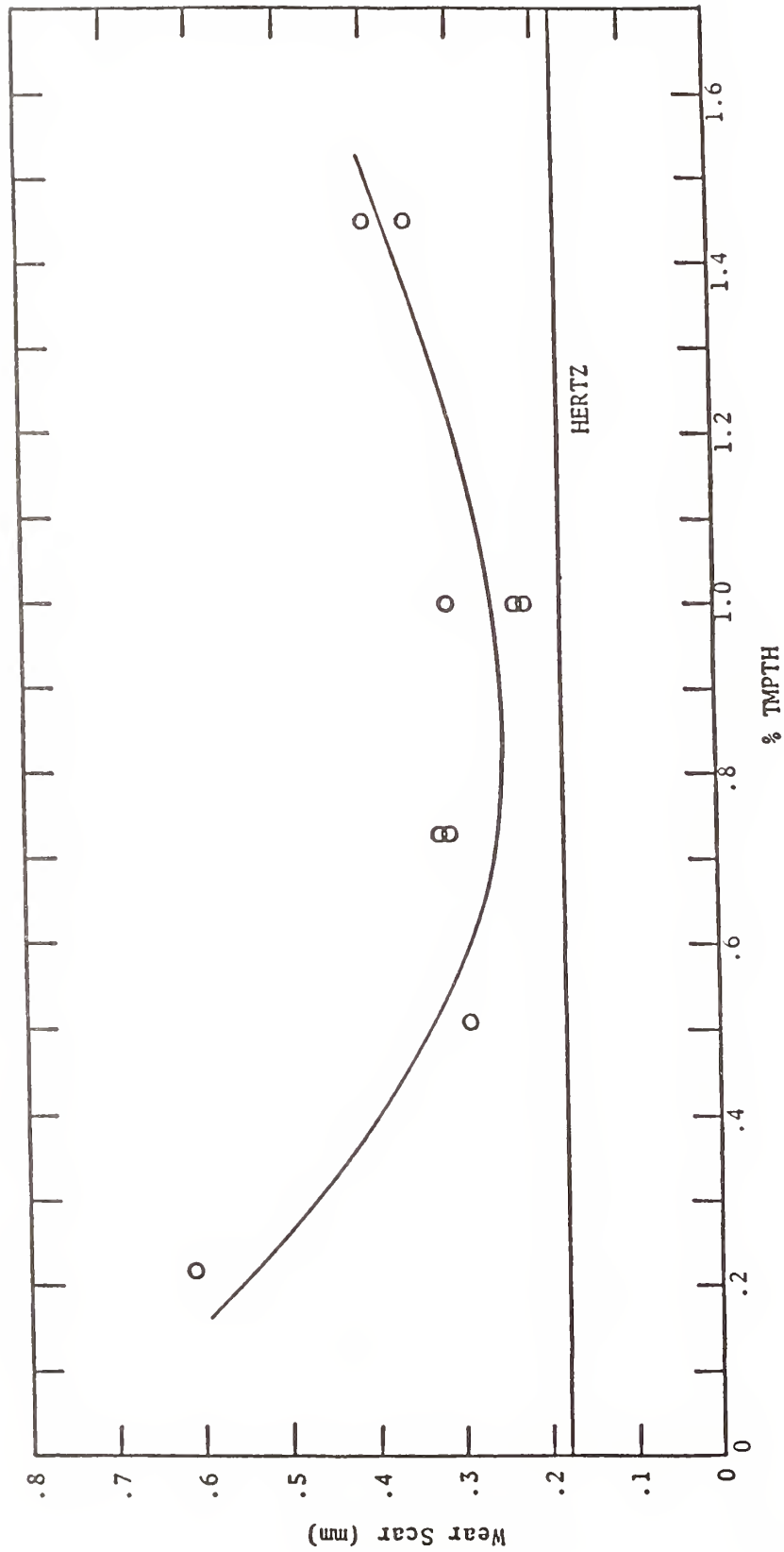
Figure 91.   Four-ball wear scar diameter versus % TMPTH in air at 370°C, 10 kg load, M-50 steel balls, 600 rpm.

84
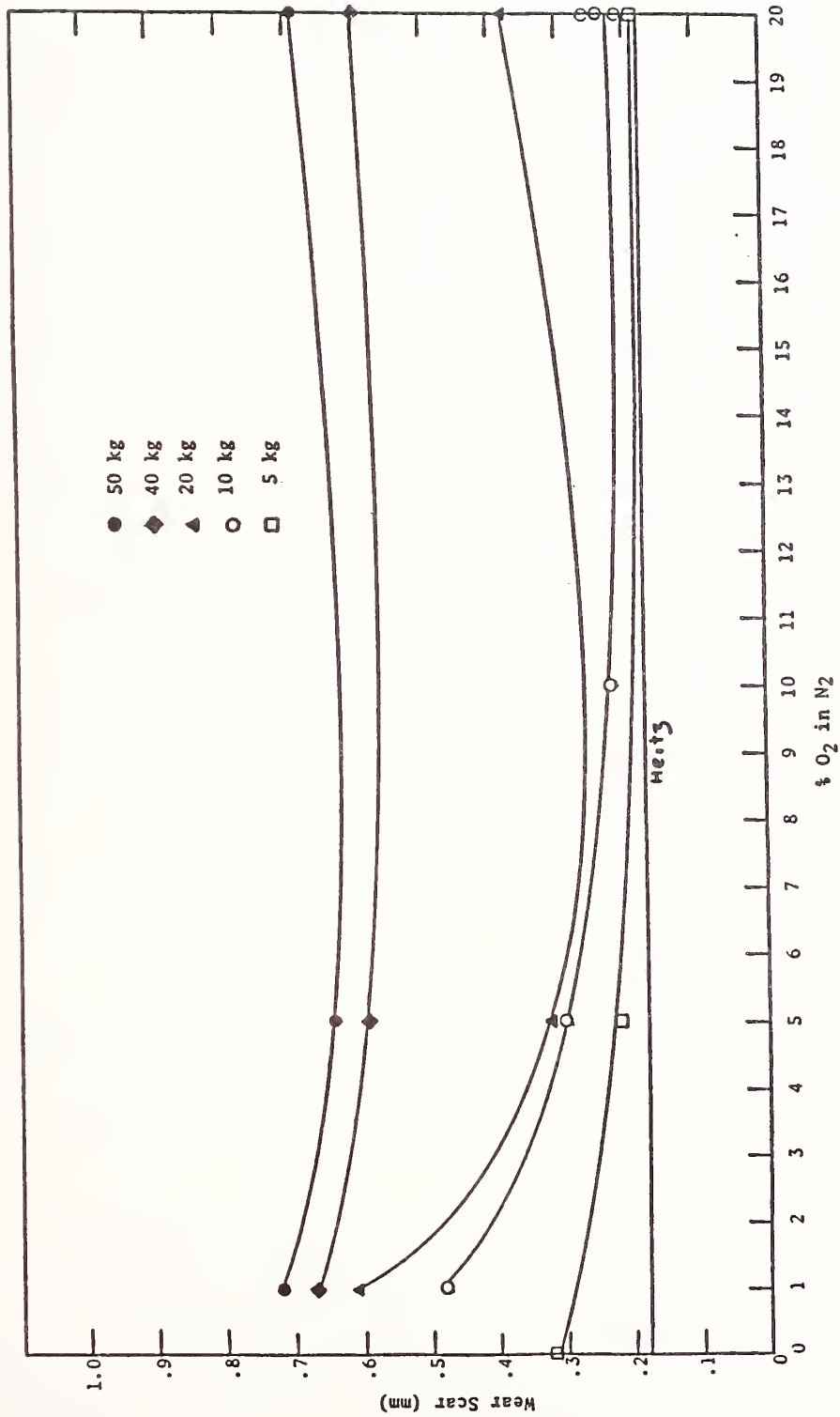
Figure 92. Four-ball wear scar diameter versus percent O_2 in nitrogen at various loads, with 0.5% TMPTH, 370°C, M-50 steel balls, 600 rpm.

85

V. CONCLUSIONS

The vapor-phase lubrication studies discussed in this report have shown that lubricating films of substantial thickness can be formed by vaporizing a liquid lubricant in a carrier gas and depositing thermal and/or thermal-oxidation products of the vaporized lubricant on the substrate surfaces at elevated temperatures. These vapor-deposited lubricating films exhibited excellent anti-wear characteristics. The formation of these lubricating films was found to be dependent on lubricant type, substrate material, temperature, lubricant vapor concentration, and carrier gas composition. Tests conducted using phosphate esters, organic acid esters, polyphenyl ether, and mineral oils demonstrated that these conventional lubricants, when delivered from the vapor phase at temperatures from 370 to 850°C, formed deposits with good lubrication characteristics. An increase in temperature generally caused an increase in deposition rate. Deposition rates were metal specific; i.e., some metals had a significant catalytic effect on the rate of deposition. Iron had a strong catalytic effect for both phosphate esters and non-phosphate hydrocarbons. Copper was catalytic with phosphate esters but essentially inert with respect to non-phosphate hydrocarbons. Nickel was catalytic with non-phosphate hydrocarbons but was essentially inert with phosphate esters. Stainless steel showed catalytic activity that diminished rapidly with increasing coating thickness. All of the metals lost their catalytic effect after a sufficient coating thickness was achieved. The coating thickness needed for this decrease in metal catalytic effect was dependent on type of metal, type of lubricant, temperature, lubricant vapor concentration, and carrier gas composition. The ranking of catalytic activity of metal substrates for deposition of non-phosphate hydrocarbons closely followed the order observed in hydrogenation-dehydrogenation and hydrogenolysis reactions of hydrocarbons. The decrease in catalytic effect with increasing coating thickness was attributed to a decrease in the availability of metal or metal organic product in the coating. With thicker coatings, there may have been a diffusion barrier for metal-lubricant interaction.

Increasing lubricant vapor concentration or oxygen concentration in carrier gas increases the rate of deposition. The level of increase is dependent on lubricant type, metal substrate, and temperature. Increases in rate of deposition are dependent on coating thickness. With thicker coatings, the effect of increasing lubricant vapor concentration or oxygen concentration on rate of deposition decreases.

SEM studies of the surface morphology of the vapor-deposited films show that the structure of the deposits can vary with lubricant type, metal substrate, and coating thickness. With phosphate esters and PPE, the deposits appear to have a granular structure. These granules appear smaller for thin coatings and larger for thick coatings. These larger granules with thicker coatings could be acting as a diffusion barrier for metal-lubricant interaction. The coating appears to be more porous near the metal surface and less porous away from the surface. TMPTH deposits, unlike phosphate esters and PPE, have a filamentous structure. These

filaments appear more dense with thicker coatings. EDAX analysis of the coating shows that there is a substantial concentration of metal in the coating. The metal concentration is higher in the coating next to the metal surface compared to coating away from the surface. This further indicates that the coating is acting as a diffusion barrier for lubricant-metal interaction. Four-ball wear tests show that the vapor-deposited lubricant films exhibit excellent anti-wear characteristics. The wear characteristics were dependent on parameters that had an effect on coating rate such as lubricant type, temperature, lubricant vapor concentration, and carrier gas composition. At the temperatures and lubricant vapor concentrations used in this study, very thin coatings would be expected. Even at these thin coating levels, good lubrication was achieved. When the coating thickness becomes too small, there is a lack of lubricant at the contact and wear can increase. When the coating thickness becomes too large, wear can increase also. With thicker coatings, excess deposit can trap or collect wear particles and cause abrasive three-body wear. There exists an optimum coating thickness for optimum wear. Both phosphate esters and non-phosphate hydrocarbons, when delivered to the contact from the vapor phase, form lubricant films that exhibit excellent anti-wear characteristics.

VI. REFERENCES

[1]. Pinkus, O. and D. E. Wilcock, "Strategy for Energy Conservation Through Tribology," 174 pages, The American Society of Mechanical Engineers, N.Y., 1977.

[2]. Kamo, R., "The Adiabatic Diesel," Tribology Workshop, February 1977, Washington, DC.

[3]. Archard, J.F., "The Temperature of Rubbing Surfaces," Wear 2, p. 455 (1959).

[4]. Fein, R.S., "Transition Temperatures With Four-Ball Machine," ASLE Trans. 3, p. 34 (1960).

[5]. Francis, H.A., "Interfacial Temperature Distribution Within a Sliding Hertzian Contact," ASLE Trans. 14, p. 41 (1970).

[6]. Bos, A., "The Temperature at the Wear Scars of the Four-Ball Apparatus," Wear 31, p. 17 (1975).

[7]. Hsu, S.M. and E.E. Klaus, "Estimation of Molecular Junction Temperatures in Four-Ball Contacts by Chemical Reaction Rate Studies," ASLE Trans. 21 (3), p. 201 (1978).

[8]. Turchina, V., D.M. Sanborn and W.O. Winer, "Temperature Measurements in Sliding Elastohydrodynamic Point Contacts," J. Lub. Tech. 96, p. 464 (1974) D, p. 909.

[9]. Ausherman, V.K., H.S. Nagaraj, D. M. Sanborn, and W.O. Winer, "Infrared Temperature Mapping in Elastohydrodynamic Lubrication," J. of Lub. Tech. 98 F(2), p. 236 (1976).

[10]. Klaus, E.E. and E.J. Tewksbury, "Microcorrosion Studies With Functional Fluids," ASLE Trans. 29 (5), p. 205 (1973).

[11]. Diamond, H., H.C. Kennedy and R.G. Larsen, "Oxidation Characteristics of Lubricating Oils at High Temperatures," Ind. and Eng. Chem. 44, p. 1834 (1952).

[12]. Brook, J.H.T., "A Circulatory Oxidation Test," J. Inst. Petrol. 48 (457), p. 7 (1962).

[13]. Oberright, E.A., S.J. Leonard and H.L. Hepplewhite "Deposit-Forming Tendencies of High-Temperature Lubricants," ASLE Trans. 7 (1), p. 64 (1964).

[14]. Cvitkovic, E., E.E. Klaus and F.E. Lockwood, "A Thin Film Test for Measurement of the Oxidation and Evaporation of Ester Type Lubricants," ASLE Trans. 22, p. 395 (1979).

[15]. Cho, L. and E.E. Klaus, "Oxidative Degradation of Phosphate Esters," ASLE Trans. <u>24</u>, p. 119 (1981).

[16]. Lahijani, J., F.E. Lockwood, and E. E. Klaus, "The Influence of Metals on Sludge Formation," ASLE Preprint No. 80-LC-1C-4 (1980).

[17]. Sinfelt, J.H., Progress in Solid State Chemistry <u>10</u>(2), p. 55 (1975).

[18]. Gunsel, S., "Development and Evaluation of a High-Temperature Lubrication System," Ph.D. Thesis, The Pennsylvania State University (1986).

[19]. Marek, J.C., L.F. Albright, "Surface Phenomena During Pyrolysis," Coke Formation on Metal Surfaces, ACS Symposium Series 202 (1982).

[20]. Marek, J.C., L.F. Albright, "Formation and Removal of Coke Deposited on Stainless Steel and Vycor Surfaces from Acetylene and Ethylene," ACS Symposium Series 202 (1982).

[21]. Lacava, A. I., et al., "Effect of H2 on the Iron and Nickel Catalyzed Formation of Carbon from Benzene," ACS Symposium Series 202 (1982).

[22]. Baker, R.T.K., D.J.C. Yates, J.A. Dumesic, "Filamentous Carbon Formation Over Iron Surfaces," ACS Symposium Series 202 (1982).

[23]. Lacava, A. I., et al., "Mechanism of Surface C-Formation During the Pyrolysis of Benzene in the Presence of Hydrogen," ACS Symposium Series 202 (1982).

Appendix A.   COOPERATIVE EFFORTS

Cooperation between Pennsylvania State University (PSU) and industry has been expanded as a result of the present studies on vapor phase lubrication. A second year of a project supported by ALCOA has begun. The graduate students involved in that project do part of their research at PSU and part at the ALCOA Research Center. The two graduate students involved in this program thus far have conducted vapor-delivered wear tests on the ALCOA high-temperature tests in the range of 300 to 600°C. This tester has been described in the literature by Dr. Robert Bruce. Surface analytical facilities are also available for evaluation of coatings of the wear specimens before and after the wear tests. Results from that work can be compared with four-ball wear tests at 371°C and static deposition tests up to 850°C as used in the present report. Tests using steel-on-steel specimens in the ALCOA (Bruce) wear tester have shown that vapor-phase pre-lubrication on only one of the specimens provides good high-temperature wear and friction values for the four classes of lubricants evaluated thus far. The lubricants include alkyl and aryl phosphate esters, polyphenyl ethers, and organic acid esters.

A proposal was prepared jointly by PSU and Martin-Marietta to develop a vapor-phase lubricated forging system. The feasibility phase of this proposal was completed successfully with EPA and Forging Council sponsorship. Support funding for the next phase of this program is not available at this time. The program has demonstrated the lubricating ability of vapor-delivered phosphate esters as well as the reduced amount of lubricant used and the significant reduction of pollution.

The Chemical Engineering Department of PSU and the Ceramics Division of the National Bureau of Standards have begun the third year of a cooperative program. Graduate students from PSU are conducting thesis research at NBS under the guidance and supervision of Dr. S. M. Hsu. This work includes a high-temperature wear tester developed at NBS for the study of metal and ceramic specimens at high temperatures and for vapor-delivered or more conventional liquid lubrication.

The Gas Research Institute has recently established a Center for Advanced Materials (CAM) at PSU. The CAM is an engineering center for research in ceramics including high-temperature tribology. Research sponsored by CAM is focused on the specific effects that result from the use of natural gas as a fuel. Current plans call for research to be conducted at PSU, NBS, and the University of Illinois.

Appendix B. PUBLICATIONS, THESES, AND PRESENTATIONS

Publications:

1. Klaus, E. E. and C. W. Lai, "VAPOR-DEPOSITED LUBRICANTS FOR EXTREME CONDITIONS," ASLE Special Publication 15, "Solid and Liquid Lubricants for Extreme Environments," pp. 75-79 (1983).

2. Pinto, N. D. G., J. L. Duda, E. E. Graham and E. E. Klaus, "IN SITU FORMATION OF SOLID LUBRICATING FILMS FROM CONVENTIONAL MINERAL OIL AND ESTER BASE LUBRICANTS," ASLE Proceedings, 3rd International Conference on Solid Lubrication, ASLE Pub. 14, pp. 98-104 (1984).

3. Graham, E. E. and E. E. Klaus, "Lubrication from the Vapor Phase at High Temperatures," ASLE Preprint No. 85AM1B1, May (1985).

Theses:

1. Gunsel, S., "Development and Evaluation of a High-Temperature Lubrication System," Ph.D. Thesis, The Pennsylvania State University, University Park, PA 1986.

2. Jeng, G. S., "Interaction at High Temperatures of Phosphate Esters in the Vapor Phase With Metal Surfaces," Ph.D. Thesis, The Pennsylvania State University, University Park, PA (1986).

Presentations:

1. Klaus, E. E., "Vapor-Phase Lubrication in Engines," Gas Research Institute Workshop, June 5 (1986).

U.S. DEPT. OF COMM. **BIBLIOGRAPHIC DATA** **SHEET** (See instructions)	1. PUBLICATION OR REPORT NO. NIST/SP-744	2. Performing Organ. Report No.	3. Publication Date September 1988

4. TITLE AND SUBTITLE

Formation of Lubricating Films at Elevated Temperatures
From the Gas Phase

5. AUTHOR(S)
E. E. Klaus, J. L. Duda, and S. K. Naidu

6. PERFORMING ORGANIZATION (If joint or other than NBS, see instructions) **NATIONAL INSTITUTE OF STANDARDS AND TECHNOLOGY** (formerly NATIONAL BUREAU OF STANDARDS) **U.S. DEPARTMENT OF COMMERCE** **GAITHERSBURG, MD 20899**	7. Contract/Grant No. 60NANB5D0548
	8. Type of Report & Period Covered Topical

9. SPONSORING ORGANIZATION NAME AND COMPLETE ADDRESS (Street, City, State, ZIP)

SAME AS ITEM #6 ABOVE.   and   Department of Energy
                                                      Washington, DC   20585

10. SUPPLEMENTARY NOTES

Library of Congress Catalog Card Number: 88-600554

☐ Document describes a computer program; SF-185, FIPS Software Summary, is attached.

11. ABSTRACT (A 200-word or less factual summary of most significant information. If document includes a significant bibliography or literature survey, mention it here)

Conventional liquid lubricants, when subjected to temperatures of 250°C and above for extended time in an air atmosphere, degrade rapidly to make large amounts of solid sludge and deposits. Based on boundary lubrication of bearings, these same lubricants, when subjected to 250°C to the melting point of the bearing metal, produce in the micro- to milli-second residence time in the bearing contact enough "friction polymer" to result in good lubrication. This report describes the use of these conventional liquid lubricants delivered in a homogeneous vapor phase where the carrier gas is nitrogen, air or mixtures of these two gases. The lubricants studied include alkyl and aryl phosphate esters, organic acid esters, polyphenyl ethers, and mineral oil.

12. KEY WORDS (Six to twelve entries; alphabetical order; capitalize only proper names; and separate key words by semicolons)
Boundary lubrication; gas phase; high temperature; tribology.

13. AVAILABILITY ☒ Unlimited ☐ For Official Distribution. Do Not Release to NTIS ☒ Order From Superintendent of Documents, U.S. Government Printing Office, Washington, D.C. 20402. ☒ Order From National Technical Information Service (NTIS), Springfield, VA. 22161	14. NO. OF PRINTED PAGES 97
	15. Price